LA-UR-15-29524
Approved for public release; distribution is unlimited.

Title: Production of Energetic Heavy Clusters in CEM and MCNP6

Author(s): Kerby, Leslie Marie
Mashnik, Stepan Georgievich
Gudima, Konstantin K.
Sierk, Arnold John
Bull, Jeffrey S.
James, Michael R.

Intended for: Reviews of Modern Physics

Issued: 2015-12-14

Production of Energetic Heavy Clusters in CEM and MCNP6

Leslie M. Kerby,[1,*] Stepan G. Mashnik,[1] Konstantin K. Gudima,[2] Arnold J. Sierk,[1] Jeffrey S. Bull,[1] and Michael R. James[1]
[1] *Los Alamos National Laboratory, Los Alamos, NM 87545, USA*
[2] *Institute of Applied Physics, Academy of Science of Moldova, Chișinău, Moldova*

(Dated: December 14, 2015)

The emission of heavy clusters, or light fragments (LF), also known as intermediate-mass fragments (IMF), produced in nuclear reactions is an open question. Different reaction mechanisms contribute to their production; the relative roles of each, and how they change with incident energy, mass number of the target, and the type and emission energy of the clusters is not completely understood.
None of the available models are able to accurately predict emission of LF from arbitrary reactions. However, the ability to describe production of LF (especially at energies $\gtrsim$ 30 MeV) from many reactions is important for many applications, such as cosmic-ray-induced single event upsets (SEUs), radiation protection, and cancer therapy with proton, neutron, and heavy-ion beams, to name just a few. The cascade-exciton model (CEM), version 03.03, and the Los Alamos version of the quark-gluon string model (LAQGSM), version 03.03, event generators in the Monte-Carlo N-Particle Transport Code, version 6 (MCNP6) describe quite well the spectra of fragments with sizes up to ^{4}He across a broad range of target masses and incident energies (up to $\sim$ 5 GeV for CEM and up to $\sim$ 1 TeV/A for LAQGSM). However, they do not predict the high-energy tails of LF spectra heavier than ^{4}He well. Most LF with energies above several tens of MeV are emitted during the precompound stage of a reaction; the 03.03 versions of CEM and LAQGSM do not account for precompound emission of LF larger than ^{4}He. The aim of this work is to extend the precompound model in these event generators to include such processes, with the aim of increasing the predictive power of MCNP6 for LF production. This entails upgrading the modified exciton model currently used at the preequilibrium stage in CEM and LAQGSM. It also includes extending the coalescence and Fermi breakup models used in the precompound stages of spallation reactions within CEM and LAQGSM. Extending the models to include emission of fragments heavier than ^{4}He at the precompound stage has indeed provided results that have much better agreement with experimental data.

CONTENTS

* leslie31415@gmail.com

I. INTRODUCTION

The Monte Carlo Methods, Codes, and Applications group within the Computational Physics Division at Los Alamos National Laboratory (LANL) has led the development of the transport code MCNP6 (Monte Carlo N-Particle transport code, version 6) (Goorley *et al.*, 2012). MCNP6 is a general-purpose, continuous-energy, generalized-geometry, time-dependent, Monte-Carlo radiation-transport code designed to track many particle types over broad ranges of energies. It is used around the world in applications ranging from radiation protection and dosimetry, nuclear-reactor design, nuclear criticality safety, detector design and analysis, decontamination and decommissioning, accelerator applications, medical physics, space research, and beyond. At lower energies, the code uses tables of evaluated nuclear data, while for energies ($>$ 150 MeV), MCNP6 uses the cascade-exciton model, version 03.03 (CEM03.03) (Gudima *et al.*, 1983; Mashnik *et al.*, 2008), and the Los Alamos quark-gluon string model, version 03.03 (LAQGSM03.03) (Gudima *et al.*, 2001; Mashnik *et al.*, 2008) to model nuclear reactions.

Emission of energetic heavy clusters heavier than ^{4}He from nuclear reactions play a critical role in several applications, including electronics performance in space, human radiation dosages in space or other extreme radiation environments, proton- and hadron-therapy in medical physics, accelerator and shielding applications, and more. Understanding the production of LF is still an open question. Different reaction mechanisms contribute to their production; the relative roles of each, and how they change with incident energy, mass number of the target, and the type and emission energy of the fragments is not completely understood.

None of the available models are able to accurately predict emission of LF from arbitrary reactions. The CEM and LAQGSM event generators in MCNP6 describe quite well the spectra of fragments with sizes up to ^{4}He across a broad range of target masses and incident energies (up to $\sim$ 5 GeV for CEM and up to $\sim$ 1 TeV/A for LAQGSM). However, they do not predict the high-energy tails of LF spectra heavier than ^{4}He well. Most LF with energies above several tens of MeV are emitted during the precompound stage of a reaction. The 03.03 versions of CEM and LAQGSM do not account for precompound emission of LF larger than ^{4}He.

The aim of this study is to extend the precompound model in these event generators to include such processes, leading to an increase of predictive power for LF production in MCNP6. This entails upgrading the modified exciton model currently used at the preequilibrium stage in CEM and LAQGSM. It also includes verifying and extending the coalescence and Fermi break-up models used in the precompound stages of spallation reactions within CEM and LAQGSM. We will demonstate an improved agreement with experimental data achieved by extending these models to include emission of fragments heavier than ^{4}He at the precompound stage.

A. Why This Research Is Needed

In October 2008, an Airbus commercial airplane was struck by a cosmic ray en route from Perth to Singapore. One of its inertial reference computer units failed, and it sharply lost altitude (Cooper, 2012). It did land safely, but the occupants of the plane sustained significant injuries and the plane sustained significant damage.

These SEUs are not rare, and can wreak significant havoc. For example, in a typical space shuttle mission the craft's computers typically receive hundreds of SEUs (Singleterry, 2012). In addition, even though the airplane incident was serious, even more serious incidents can occur: during the Cold War, a U. S. satellite was hit by cosmic rays, subsequently malfunctioning and triggering false alarms of nuclear attacks (Borning, 1987). Understanding how high-energy fragments interact with matter is critical to preventing such malfunctions.

Accurate simulation of LF spectra is also important in the field of radiation shielding, especially for extreme environments like accelerators. An even larger problem is radiation shielding for the humans exposed to these extreme environments, such as astronauts in space (Singleterry, 2012).

This research is also important to several medical fields, such as cancer treatment with proton or heavy-ion beams. Proton and heavy-ion therapy has been shown to be more effective than x-ray therapy, and have many fewer side effects (MacReady, 2012). However, challenges remain in ensuring energy is deposted only in the desired target (tumor) (Polf and Parodi, 2015).

Another indication of the importance of this research

is the recommendation of the IAEA following an international evaluation and comparison, the 2008-2010 International Atomic Energy Agency (IAEA) Benchmark of Spallation Models, that we make this change in the code (Leray *et al.*, 2011; Mashnik *et al.*, 2010). While no other spallation model can generally predict high-energy light-fragment emission from arbitrary reactions, it is a goal of several international model-development groups.

On a more pragmatic level, MCNP6's GENXS option presently does not produce tallies of spectra for particles heavier than ^{4}He. This limitation is serious for some MCNP6 interest groups.

Finally, we anticipate that this research will help us to understand better the mechanisms of nuclear reactions at intermediate energies.

1. Comparison with Experimental Data

Figure 1 shows the double-differential cross sections for the reaction 200 MeV p + ^{27}Al→ ^{6}Li, comparing the experimental data from Machner et al. (Machner *et al.*, 2006) (open symbols) to the unmodified CEM03.03 (solid red lines).

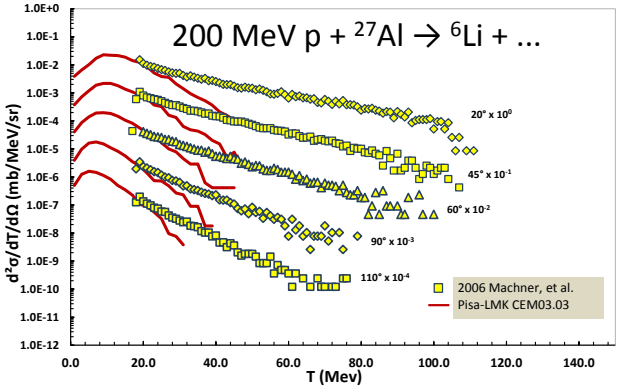

FIG. 1 Comparison of results calculated by CEM03.03 (solid red lines) to experimental data on 200 MeV p + ^{27}Al → ^{6}Li, measured by Machner et al. (Machner *et al.*, 2006) (open symbols).

The vertical axis presents the double differential cross sections. The horizontal axis shows the kinetic energy of the emitted ^{6}Li particles in MeV. The different data bands represent ^{6}Li detected (or simulated) at different angles, and are separated by multiplying each band by a different power of 10. The current version of CEM does not predict the observed high-energy tails of ^{6}Li well. This is true across other reaction energies and target mass numbers for all fragments heavier than ^{4}He, for higher energies. At lower energies ($\lesssim$ 25 MeV) CEM matches well, but as we enter intermediate energies ($\gtrsim$ 25 MeV) CEM falls off sharply. This is because the only mechanism for producing ^{6}Li fragments is evaporation, which does consider emission of LF (up to ^{28}Mg) (Furihata *et al.*, 2001). At higher energies ($\gtrsim$ 25 MeV), the fragments should largely be produced at the preequilibrium stage, while a smaller, but still significant, contribution will come from the coalescence of nucleons produced in the INC. Neither the MEM nor the coalescence model presently considers fragments heavier than ^{4}He.

B. CEM and LAQGSM Physics

Details, examples of results, and useful references to different versions of CEM and LAQGSM may be found in a recent lecture (Mashnik *et al.*, 2008).

The cascade-exciton model (CEM) of nuclear reactions was proposed more than 30 years ago at the Laboratory of Theoretical Physics, JINR, Dubna, USSR by Gudima, Mashnik, and Toneev (Gudima *et al.*, 1983). It is based on the standard (non time-dependent) Dubna intranuclear cascade (INC) model (Barashenkov *et al.*, 1973; Barashenkov and Toneev, 1972) and the modified exciton model (MEM) (Gudima *et al.*, 1975; Mashnik and Toneev, 1974). The code LAQGSM03.03 is the latest modification (Mashnik *et al.*, 2007a) of LAQGSM (Gudima *et al.*, 2001), which in its turn is an improvement of the quark-gluon string model (QGSM) (Amelin *et al.*, 1990). It describes reactions induced by both particles and nuclei at incident energies up to about 1 TeV/nucleon.

The basic versions of both the CEM and LAQGSM event generators are the so-called '03.03' versions, namely CEM03.03 (Mashnik *et al.*, 2008, 2005b; Mashnik and Sierk, 2012) and LAQGSM03.03 (Mashnik *et al.*, 2005a, 2007a, 2008). The CEM code calculates nuclear reactions induced by nucleons, pions, and photons. It assumes that the reactions occur generally in three stages (see Fig. 2). The first stage is the INC, in which primary particles can be re-scattered and produce secondary particles several times prior to absorption by, or escape from, the nucleus. When the cascade stage of a reaction is completed, CEM uses the coalescence model to create high-energy d, t, ^{3}He, and ^{4}He by final-state interactions among emitted cascade nucleons outside the target. The emission of the cascade particles determines the particle-hole configuration, Z, A, and the excitation energy that comprise the starting conditions for the second, preequilibrium stage of the reaction. The subsequent relaxation of the nuclear excitation is treated in terms of an improved version of the modified exciton model of preequilibrium decay, followed by the equilibrium evaporation/fission stage.

Generally, all three components may contribute to experimentally measured particle spectra and other distributions. But if the residual nuclei after the INC have atomic numbers with $A \leq A_{Fermi} = 12$, CEM uses the Fermi breakup model to calculate their further disintegration instead of using the preequilibrium and evapora-

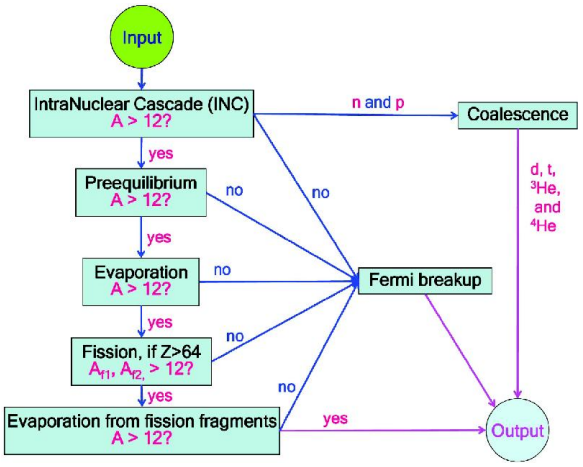

FIG. 2 Flow chart of nuclear-reaction calculations by CEM03.03 and LAQGSM03.03.

tion models. Fermi breakup, which estimates the probabilities of various final states by calculating the approximate phase space available for each configuration, is much faster to calculate and gives results very similar to using the continuation of the more detailed models for lighter nuclei. LAQGSM also describes nuclear reactions, as a three-stage process: INC, followed by preequilibrium emission of particles during the equilibration of the excited residual nuclei formed after the INC, followed by evaporation of particles from and/or fission of the compound nuclei. LAQGSM was developed with a primary focus on describing reactions induced by nuclei, as well as induced by most elementary particles, at high energies, up to about 1 TeV/nucleon. The INC of LAQGSM is completely different from that in CEM. LAQGSM also considers Fermi breakup of nuclei with $A \leq 12$ produced after the cascade, and the coalescence model to produce high-energy d, t, ^{3}He, and ^{4}He from nucleons emitted during the INC.

Many people participated in the CEM and LAQGSM code development over their more than 40-year history. Contributors to the '03.03' versions are S. G. Mashnik, K. K. Gudima, A. J. Sierk, R. E. Prael, M. I. Baznat, and N. V. Mokhov. L. M. Kerby has joined these efforts recently to extend the precompound models of CEM and LAQGSM by accounting for possible emission of light fragments heavier than ^{4}He, specifically up to ^{28}Mg.

For more details on the physics of CEM and LAQGSM, see Ref. (Mashnik and Kerby, 2014).

1. Comments on the Emission of Energetic LF

The goal of this research is to enable MCNP6 to produce high-energy light fragments. Energetic light fragments can only be emitted through precompound processes, because by the time the reaction reaches compound-stage processes (evaporation and fission), there is not enough energy left in the thermally-equilibrated system to emit a high-energy light fragment. Therefore, energetic light fragments may be emitted through one of three processes:

- Fermi breakup
- Preequilibrium
- Coalescence

We explore the emission of light fragments through each of these mechanisms.

C. Emission of High-Energy LF in Other Models

The bulk of this research focuses on the emission of high-energy LF at the preequilibrium stage of nuclear reactions, as considered by our models. However, high-energy LF can be produced at other precompound stages of reactions. Cugnon et al. have modified their Liège IntraNuclear Cascade (INCL) code to consider emission of light fragments heavier than ^{4}He during the cascade stage of reactions via coalescence of several nucleons at the nuclear periphery (David *et al.*, 2011). These modifications have not yet been generalized across all types of reactions. In addition, the INCL+ABLA model is limited to relatively light incident projectiles (particles and light ions, typically, up to oxygen) (Mancusi *et al.*, 2014). Several previous papers by the same group discuss the production of light fragments up to $A = 10$ (see, e.g., (Cugnon *et al.*, 2011a,b)). A 2013 paper by the same authors presents satisfactory results for emission spectra of ^{6}He, ^{6}Li, ^{7}Li, and ^{7}Be in the reaction $p + ^{197}Au \rightarrow ...$ and discusses emission of clusters up to $A = 12$ (Boudard *et al.*, 2013).

Emission of ^{7}Be at the preequilibrium stage (described by a hybrid exciton model and coalescence pick-up model) was studied by A. Yu. Konobeyev and Yu. A. Korovin two decades ago (Konobeyev and Korovin, 1995). Additionally, preequilibrium emission of helium and lithium ions and the necessary adjustments to the Kalbach systematics was discussed in Ref. (Uozumi *et al.*, 2007). Preequilibrium emission of light fragments was also studied within the CEM in 2002 (Mashnik *et al.*, 2006), but that project was never completed.

Finally, energetic fragments can be produced via Fermi breakup (Fermi, 1950) and multifragmentation processes, as described, e.g., by the statistical multifragmentation model (SMM) (Bondorf *et al.*, 1995); (see a comparison of the Fermi breakup model with SMM in the recent paper by Souza et al. (Souza *et al.*, 2013)).

Light fragments can also be emitted during the compound stage of reactions. GEM2, the evaporation model used in CEM and LAQGSM, evaporates light fragments up to ^{28}Mg (Furihata *et al.*, 2001). In addition, light fragments can be produced via very asymmetric binary

fission, as described, e.g., by the fission-like binary decay code GEMINI by Charity et al. (Charity *et al.*, 2001), and also via ternary fission. For more information, see Ref. (Ronen, 2012) wherein Y. Ronen discusses the physics of how light fragments are products seen in ternary fission. However, neither evaporation nor any fission processes can produce high-energy fragments, the focus of this study.

Finally, we mention that, as a rule, the authors of most of the recent measurements of LF spectra analyze their experimental data using a variety of simplified approaches assuming emission of LF from different moving sources (see, e.g., Refs. (Bubak *et al.*, 2007; Budzanowski *et al.*, 2008, 2010; Machner *et al.*, 2006)). Such simplified moving-source prescriptions are fitted to describe as well as possible only their own measured LF spectra, and have not been developed further to become universal models with predictive power for spectra of LF from arbitrary reactions. In addition, such approaches cannot describe at all many other characteristics of nuclear reactions, like the yields and energies of spallation products, fission-fragment production, etc., and therefore are not general enough to be useful as event generators in transport codes.

For detailed information on spallation reactions and research, see the book *Handbook of Spallation Research*, by D. Filges and F. Goldenbaum (Filges and Goldenbaum, 2009). A useful summary paper by J.-C. David, on spallation models, is available in Ref. (David, 2015).

II. FERMI BREAKUP

One of the ways energetic heavy clusters can be produced is via Fermi breakup. The Fermi breakup model is used in CEM and LAQGSM for residual nuclei with atomic mass number $A \leq 12$, making it particularly important for reactions with light target nuclei. It is impossible to measure all nuclear data needed for such applications; therefore, Monte-Carlo transport codes are usually used to simulate impacts associated with fragmentation reactions. It is important that available transport codes simulate such reactions as well as possible. For this reason, during recent years, efforts have been made to investigate the validity and performance of, and to improve where possible, nuclear reaction models simulating fragmentation of light nuclei in GEANT4 (Pshenichnov *et al.*, 2010), SHIELD-HIT (Hansen *et al.*, 2012; Hultqvist *et al.*, 2012; Lühr *et al.*, 2012), and PHITS (Ogawa *et al.*, 2013; Sato *et al.*, 2013).

The Los Alamos Monte-Carlo transport code MCNP6 uses CEM03.03 to simulate fragmentation of light nuclei at intermediate energies for reactions induced by nucleons, pions, and photons, and LAQGSM03.03 to simulate fragmentation reactions induced by nuclei and by elementary particles at higher energies, up to about 1 TeV/nucleon. In recent years, MCNP6, with its CEM and LAQGSM event generators, has been extensively validated and verified (V&V) against a large variety of nuclear-reaction data on both thin and thick targets (see, e.g., Refs. (Mashnik, 2011a,b,c, 2013) and references therein), and was recently specifically tested on fragmentation of light nuclei at intermediate energies (Mashnik and Kerby, 2014).

A. Investigation of Fermi Breakup Cut-off

De-excitation of light nuclei with $A \leq A_{\rm Fermi}$ remaining after the INC is described in CEM and LAQGSM only with the Fermi breakup model, where $A_{\rm Fermi}$ is a 'cut-off value' fixed in the models. The value of $A_{\rm Fermi}$ is a model parameter, not a physical characteristic of nuclear reactions. Actually, the initial version of the Fermi breakup model incorporated into CEM and LAQGSM (Mashnik *et al.*, 2005a,b) used $A \leq A_{\rm Fermi} = 16$, just as $A_{\rm Fermi} = 16$ is used currently in GEANT4 (see (Pshenichnov *et al.*, 2010)) and in SHIELD-HIT (see (Hansen *et al.*, 2012; Hultqvist *et al.*, 2012; Lühr *et al.*, 2012)). But that initial version of the Fermi breakup model had some problems and code crashes in some cases. To avoid unphysical results and code crashes, we chose the expedient of using $A_{\rm Fermi} = 12$ in both CEM and LAQGSM. Later, the problems in the Fermi breakup model were fixed, but the value of $A_{\rm Fermi}$ was not changed at that time, nor was how its value affects the final results of these codes studied. We will address this, calculating spectra of emitted particles and light fragments, and yields of all possible products from various reactions using different values for $A_{\rm Fermi}$. We discuss separately production cross sections (Section II.B) and spectra of particles and light fragments (Section II.C). See Ref. (Mashnik and Kerby, 2014) for more complete results.

B. Fragment Production Cross Sections

One of the most difficult tasks for any theoretical model is to predict cross sections of arbitrary products as functions of the incident energy of the projectiles initiating the reactions, i.e., excitation functions. Therefore, we start the study by comparing the available experimental data on excitation functions of products from several proton-induced reactions on light nuclei at intermediate energies with predictions by MCNP6 using its default event generator for such reactions, CEM03.03, as well as with results calculated by CEM03.03 used as a standalone code.

We show only a few excitation functions, for proton-induced reactions on ^{16}O. Many more results can be found in Ref. (Mashnik and Kerby, 2014). Fig. 3 presents results for the reaction p + ^{16}O. Most of the experimental

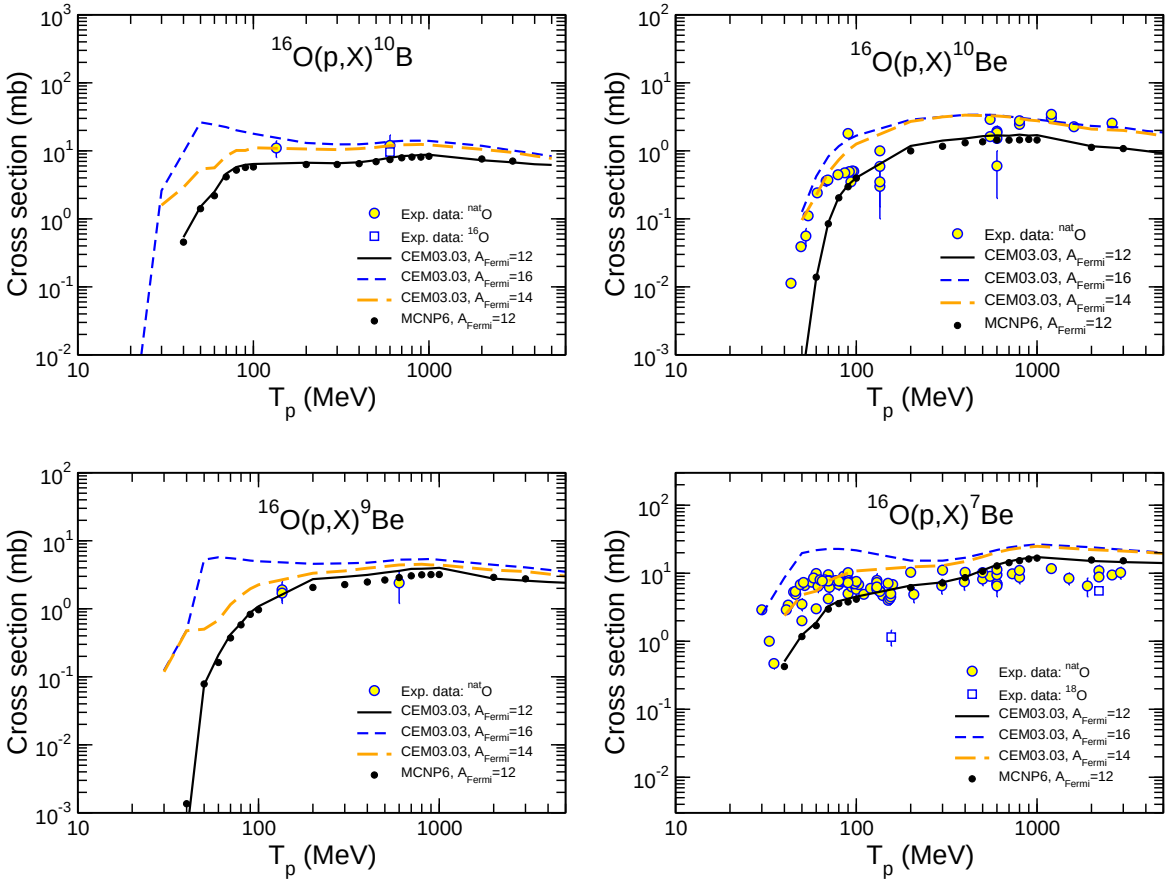

FIG. 3

Excitation functions for the production of ^{10}B, ^{10}Be, ^{9}Be, and ^{7}Be, calculated with CEM03.03 using the 'standard' version of the Fermi breakup model ($A_{\rm Fermi} = 12$) and with cut-off values $A_{\rm Fermi}$ of 16 and 14, as well as with MCNP6 using CEM03.03 ($A_{\rm Fermi} = 12$) compared with experimental data, as indicated. Experimental data are from the T16 Lib compilation (Mashnik *et al.*, 1998b).

data for these reactions were measured on ^{nat}O targets, with only a few data points obtained for ^{16}O; all the calculations use ^{16}O. For these reactions, we perform three sets of calculations, using $A_{\rm Fermi}$ = 12, 14, and 16 in CEM03.03. The general agreement/disagreement of the results with available measured data for oxygen is very similar to what we displayed in Ref. (Mashnik and Kerby, 2014) for p + ^{14}N, ^{27}Al, or ^{nat}Si.

The results demonstrate very good agreement between the excitation functions simulated by MCNP6 using CEM03.03 and calculations by the stand-alone CEM03.03, and a reasonable agreement with most of the available experimental data. This serves as a (V&V) of MCNP6 and shows no problems with the imcorporation of CEM03.03 into MCNP6 or with the simulations of these reactions by either code.

The observed discrepancies between some calculated excitation functions and measured data at energies below 20 MeV are not of concern. As its default, MCNP6 uses data libraries at such low energies and never uses CEM03.03 or other event generators, when data libraries are available, as is the case for the reactions studied here. By contrast, CEM uses its INC to simulate the first stage of nuclear reactions, and the INC is not expected to work properly at such low energies (see details in (Mashnik *et al.*, 2008; Mashnik and Sierk, 2012)).

Results calculated both with $A_{\rm Fermi} = 12$ and 16 agree reasonably well with available data, taking into account that all calculations, at all nergies and for all reactions are done with the fixed versions of these codes, without any tuning or changing of any parameters. However, in some cases, there are significant differences between excitation functions calculated with $A_{\rm Fermi} = 12$ and 16.

For many cases, a better description of the heavy fragments occurs for $A_{\rm Fermi} = 16$ or 14, and usually the light fragments are better described using $A_{Fermi} = 12$. However, the model with any of these values agrees quite well with the measured data, especially for LF with $Z \leq 4$ (See Ref. (Mashnik and Kerby, 2014)). For LF with $Z > 4$, it is difficult to determine which value agrees

better with the data: $A_{\rm Fermi} = 12$ or $A_{\rm Fermi} = 16$. Light fragments with $Z = 3$ and 4 are described a little better with $A_{\rm Fermi} = 12$. As discussed at the end of the next Section, preequilibrium emission described with an extended version of the MEM (not accounted for in the calculations shown in Fig. 3), can be important and may change the final CEM results for this reaction; therefore, we are not ready to make a final decision about which value of the Fermi-breakup cut-off works better for this system.

C. Fragment Spectra

This section presents several examples of particle and LF spectra from p + ^{9}Be at 300 MeV. Many more examples are shown in Ref. (Mashnik and Kerby, 2014), some of which address different reaction mechanisms for fragment production, with some involving more than one mechanism in the production of the same LF in a given reaction.

Fig. 4 shows examples of measured particle and LF double- differential spectra from p + ^{9}Be at 300 MeV (Green *et al.*, 1987), compared to CEM results. Because ^{9}Be has a mass number $A < A_{\rm Fermi} = 12$, all the LF from these reactions are calculated by CEM either as fragments from the Fermi breakup of the excited nuclei remaining after the initial INC stage, or as residual nuclei after emission of several particles from the ^{9}Be target nucleus during the INC. No preequilibrium or evaporation mechanisms are considered for these reactions by CEM. There is quite a good agreement of the CEM predictions with the measured spectra from p + ^{9}Be for all products shown in this example: protons, complex particles (t), and heavier nuclides ^{6}He to ^{7}Be.

D. Limiting Fragmentation

The limiting-fragmentation hypothesis, first proposed by Benecke, et al. (Benecke *et al.*, 1969), suggests that fragmentation cross sections reach asymptotic values at sufficiently high incident-projectile energies. That is to say that, above a given bombarding energy, both the differential and total production cross sections remain constant. Figs. 5 and 6 validate the limiting-fragmentation hypothesis.

Fig. 5 displays the double differential cross sections for the production of ^{4}He from the reaction 1.2/1.9/2.5 GeV p + ^{12}C. Fig. 6 shows the total production cross sections by isotope, from protons to ^{12}N, from the same reactions. The fragmentation differential cross sections for ^{4}He are approximately constant across the bombarding energy range of 1.2, 1.9, and 2.5 GeV. Limiting fragmentation predicts this constancy. From Fig. 2.1 of M. Fidelus' Ph.D. thesis (Fidelus, 2010), we expect that, for the production of ^{7}Be, limiting fragmentation will begin at $\sim$ 200 MeV bombarding energy; for this case of protons incident on ^{12}C. ^{4}He is lighter than ^{7}Be, and the bombarding energies are all well above 200 MeV; therefore, we expect constancy in differential and total production cross sections. Fig. 6 demonstrates constancy of total production cross sections. There are small differences in total production cross sections for the heavier clusters (i.e., ^{10,11}C), which is also in agreement with the limiting-fragmentation hypothesis, as heavier emitted fragments should have a higher bombarding energy at which limiting fragmentation occurs.

E. Conclusion

Energetic LF can be produced with Fermi breakup, especially for light targets. On the whole, MCNP6 and its CEM and LAQGSM event generators describe quite well all the reactions we tested, providing good enough agreement with available experimental data. This is especially important for calculations of cross sections of arbitrary products as functions of incident projectile energies, i.e., excitation functions, one of the most difficult tasks for any nuclear reaction model. We find good predictions by both MCNP6 and CEM03.03 used as a stand-alone code, of a large variety of excitation functions for products from proton-induced reactions (see (Mashnik and Kerby, 2014) for more results of excitation functions). An older version of CEM, CEM95, was able to predict reasonably well most excitation functions for medium and heavy nuclear targets, but had big problems in calculating some excitation functions for light nuclei (Mashnik *et al.*, 1998a).

CEM and LAQGSM assume that intermediate-energy fragmentation reactions on light nuclei occur generally in two stages. The first stage is the (INC), followed by the second, Fermi breakup disintegration of light excited residual nuclei produced after the INC. Both CEM and LAQGSM also account for coalescence of light fragments (complex particles) up to ^{4}He from energetic nucleons emitted during the INC.

We investigated the validity and performance of MCNP6, CEM, and LAQGSM in simulating fragmentation reactions at intermediate energies for targets with $A < 13$ (see (Mashnik and Kerby, 2014) for more results). We find that while the fixed default versions of CEM03.03 and LAQGSM03.03 in MCNP6 provide reasonably good predictions for all reactions tested, a fine-tuning of the A_{Fermi} cut-off parameter in the Fermi breakup model might provide a better description of some experimental data.

An independent test of the Fermi Breakup model used in CEM03.03 and LAQGSM03.03 was performed recently by Konobeyev and Fischer (Konobeyev and Fischer, 2014) for the Fall 2014 Nuclear Data Week. These authors calculated with MCNP6 using its Bertini (Bertini,

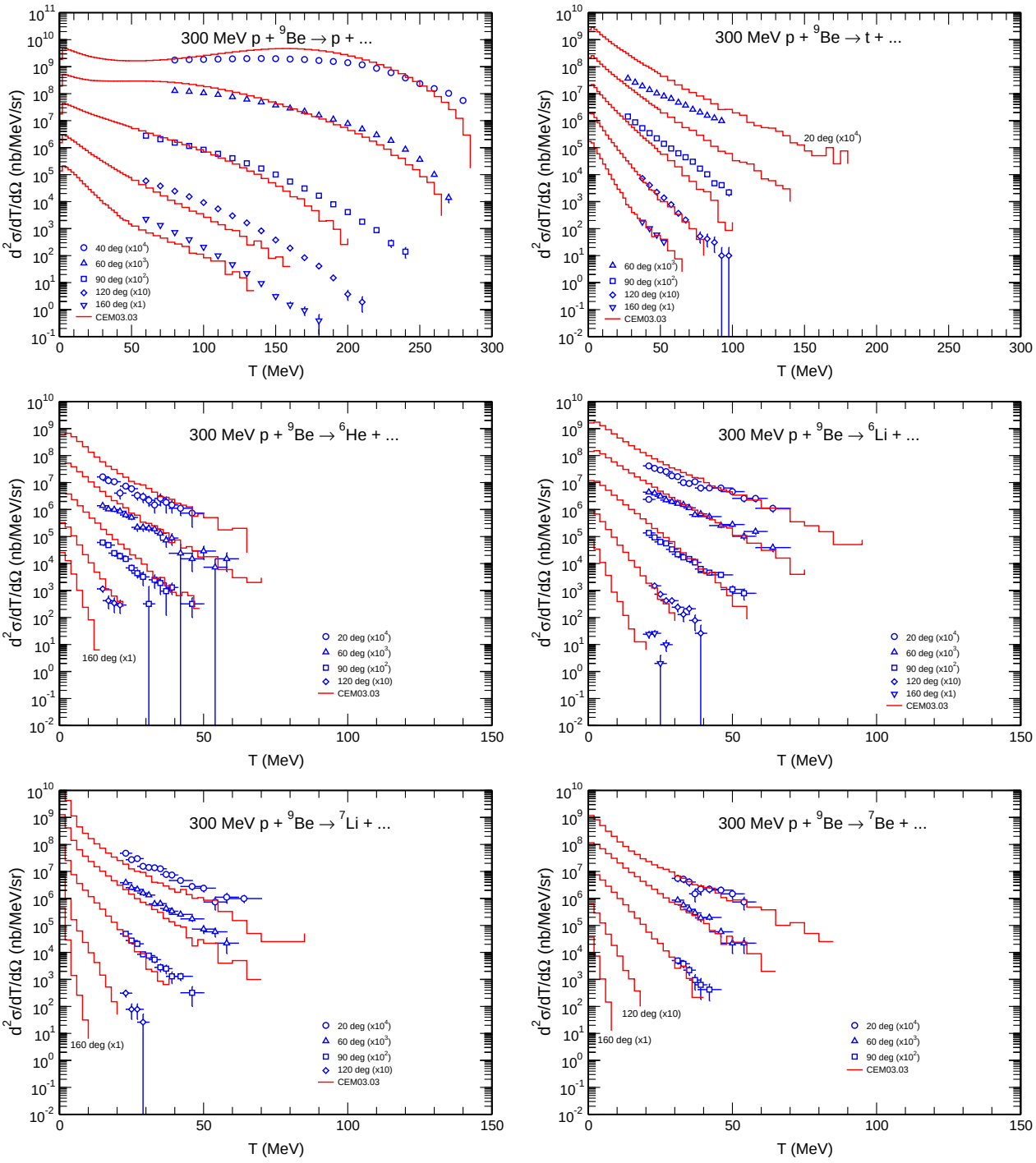

FIG. 4 Examples of measured particle and LF double-differential spectra from p + ^{9}Be at 300 MeV (Green *et al.*, 1987) (open symbols), compared to CEM results (histograms).

1963, 1969), ISABEL (Yariv, 2008; Yariv and Frankel, 1979, 1981), INCL+ABLA (Boudard *et al.*, 2002; Cugnon *et al.*, 1997; Junghans *et al.*, 1998), and CEM03.03 event generators (Mashnik and Sierk, 2012), as well as with the TALYS code (Koning *et al.*, 2004), all the experimental spectra of ^{3}He and ^{4}He measured in Ref. (Green *et al.*, 1987) from the reaction 190 MeV p + ^{9}Be; all spectra of p, d, t, ^{3}He, and ^{4}He from the reaction of 300 MeV p + ^{9}Be (Green *et al.*, 1987), as well as all neutron spectra from interactions of 113 MeV protons with ^{9}Be (Meier *et al.*, 1989) and from 256 MeV p + ^{9}Be (Meier *et al.*, 1992). As is often done in the literature, to get quan-

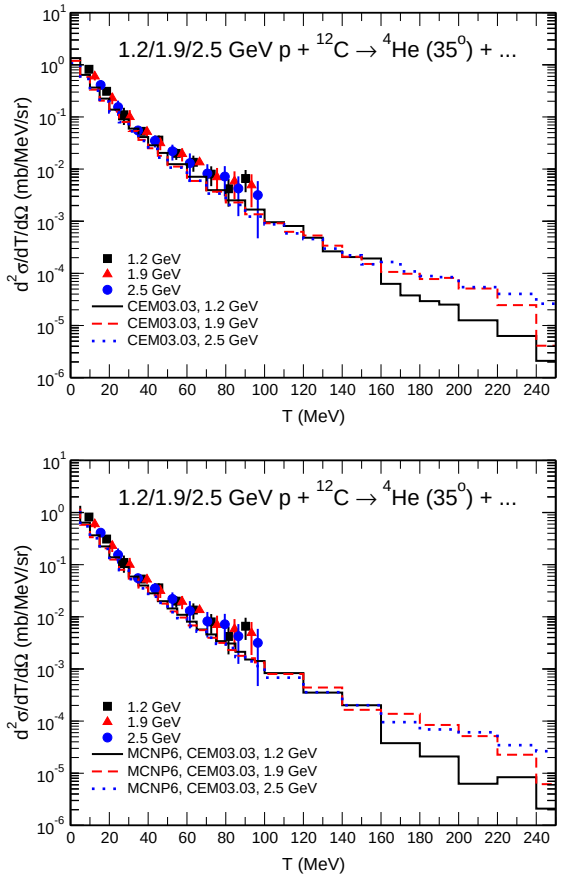

FIG. 5 ^{4}He spectra at 35°for 1.2/1.9/2.5 GeV p + ^{12}C measured by M. Fidelus of the PISA collaboration (Fidelus, 2010) (solid symbols) with calculations by CEM03.03 (top) and MCNP6 (bottom) (lines).

titative estimations of the agreement or disagreement of the spectra calculated by different models with the measured ones, the authors performed a detailed statistical analysis using nine different 'deviation factors,' namely, H, R^{CE}, R^{EC}, $< F >$, S, L, $P_{2.0}$, $P_{10.0}$, and N_x. The definition of each can be found in the Konobeyev and Fischer paper.

Konobeyev and Fischer found that results by CEM03.03 for these particular reactions agree better with the experimental data than all the other models tested. As ^{9}Be has a mass number of 9, all these reactions are calculated using only the INC followed by the Fermi Breakup model. The better results from CEM03.03 in comparison with the other models prove that the Fermi breakup model used in CEM03.03 (and in LAQGSM03.03) in MCNP6 is reliable and can be used with confidence as a good predictive tool for various nuclear applications.

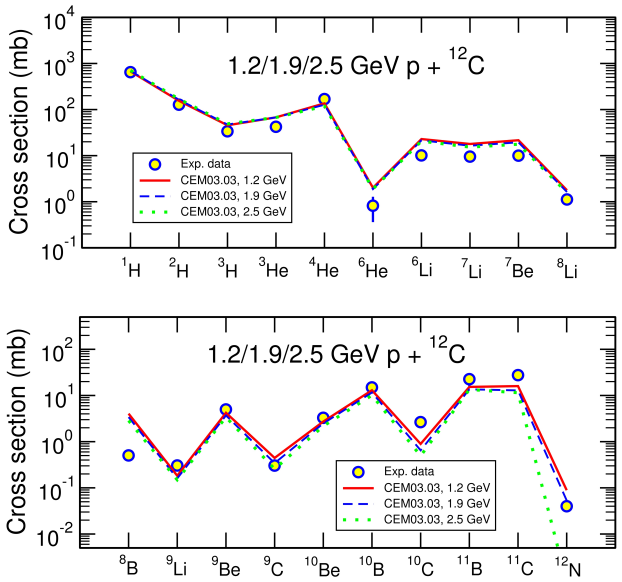

FIG. 6 Total production cross sections by isotope, from protons to ^{12}N, for 1.2/1.9/2.5 GeV p + ^{12}C measured by M. Fidelus of the PISA collaboration (Fidelus, 2010) (open symbols) with calculations by CEM03.03 (lines).

III. EXTENDING THE PREEQUILIBRIUM MODEL

The preequilibrium interaction stage of nuclear reactions is considered by the current CEM and LAQGSM in the framework of the latest version of the modified exciton model (MEM) (Gudima *et al.*, 1975; Mashnik and Toneev, 1974), as described in Ref. (Mashnik *et al.*, 2005b). At the preequilibrium stage of a reaction, CEM03.03 and LAQGSM03.03 take into account all possible nuclear transitions changing the number of excitons n with Δ_n = +2, -2, and 0, as well as all possible multiple subsequent emissions of n, p, d, t, ^{3}He, and ^{4}He. The corresponding system of master equations describing the behavior of a nucleus at the preequilibrium stage is solved by the Monte-Carlo technique (Gudima *et al.*, 1983). This section investigates the impact of extending the MEM to include the possibility of emitting heavy clusters, with $A > 4$, up to ^{28}Mg.

A. The Modified Exciton Model (MEM)

The probability of finding the system at the time moment t in the $E\alpha$ state, $P(E, \alpha, t)$, is given by the differential equation:

$$\frac{\delta P(E,\alpha,t)}{\delta t} = \sum_{\alpha \neq \alpha'} [\lambda(E\alpha, E\alpha')P(E,\alpha',t) - \lambda(E\alpha', E\alpha)P(E,\alpha,t)]. \quad (1)$$

Here $\lambda(E\alpha, E\alpha')$ is the energy-conserving probability rate, defined in first-order time-dependent perturbation

theory as

$$\lambda(E\alpha, E\alpha') = \frac{2\pi}{h}| < E\alpha|V|E\alpha' > |^2 \omega_\alpha(E). \quad (2)$$

The matrix element $< E\alpha|V|E\alpha' >$ is believed to be a smooth function of energy, and $\omega_\alpha(E)$ is the density of the final state of the system. We note that Eq. (1) is derived assuming that the memory time τ_{mem} of the system is small compared to the characteristic time for intranuclear transitions $\hbar/\lambda(E\alpha, E\alpha')$ but, on the other hand, Eq. (1) itself is applicable for the time moments $t \gg \hbar/\lambda(E\alpha, E\alpha')$. Due to the condition $\tau_{mem} \gg \hbar/\lambda(E\alpha, E\alpha')$, being described by Eq. (1), the random process is a Markovian one.

The modified exciton model (Gudima *et al.*, 1983, 1975; Mashnik and Toneev, 1974) utilized by CEM and LAQGSM uses effectively the relationship of the master equation (1) with Markovian random processes. Indeed, an attainment of the statistical equilibration described by Eq. (1) is an example of a discontinuous Markovian process: the temporal variable changes continuously and at a random moment the state of the system changes by a discontinuous jump, the behavior of the system at the next moment being completely defined by its present state. As long as the transition probabilities $\lambda(E\alpha, E\alpha')$ are time-independent, the waiting time for the system in the $E\alpha$ state has an exponential distribution (Poisson flow) with the average lifetime $\hbar/\Lambda(\alpha, E) = \hbar/\sum'_\alpha \lambda(E\alpha, E\alpha')$. This prompts a simple method of solving the related system of Eq. (1): simulation of the random process by the Monte-Carlo technique. In this treatment, it is possible to generalize the exciton model to all nuclear transitions with $\Delta n = 0, \pm 2$, and the multiple emission of particles and to depletion of nuclear states due to particle emission. In this case the system (1) becomes (Mashnik and Smolyansky, 1996):

$$\begin{aligned}\frac{\delta P(E,\alpha,t)}{\delta t} &= -\Lambda(n,E)P(E,n,t)+ \\ &+ \lambda_+(n-2,E)P(E,n-2,t)+ \\ &+ \lambda_0(n,E)P(E,n,t)+ \\ &+ \lambda_-(n+2,E)P(E,n+2,t)+ \\ &+ \sum_j \int dT \int dE' \lambda_j(n,E,T) \\ &\times P(E', n+n_j, t)\delta(E'-E-B_j-T).\end{aligned} \quad (3)$$

With the master equation (3), we can find the particle emission rates λ_j and the exciton transition rates λ_+, λ_0, and λ_-.

1. Particle Emission

According to the detailed balance principle, the emission width Γ_j, (or probability of emitting particle fragment j), is estimated as

$$\Gamma_j(p,h,E) = \int_{V_j^c}^{E-B_j} \lambda_j(p,h,E,T)dT, \quad (4)$$

where the partial transmission probabilities, λ_j, are equal to

$$\begin{aligned}\lambda_j(p,h,E,T) =& \frac{2s_j+1}{\pi^2\hbar^3}\mu_j \frac{\omega(p-1,h,E-B_j-T)}{\omega(p,h,E)} \\ &\times \Re(p,h)T\sigma_j^{inv}(T);\end{aligned} \quad (5)$$

: p: number of particle excitons;
: h: number of hole excitons;
: E: internal energy of the excited nucleus (sometimes referred to as U);
: s_j: spin of the emitted particle j;
: μ_j: reduced mass of the emitted particle j;
: ω: level density of the n-exciton state;
: B_j: binding energy;
: V_j^c: Coulomb barrier;
: T: kinetic energy of the emitted particle j;
: σ_j^{inv}: inverse cross section;
: $\Re$: creates zero probability of emission if the number of particle excitons is less than the number nucleons of particle j.

Equation (5) describes the emission of neutrons and protons. For complex particles, the level density formula ω becomes more complicated and an extra factor γ_j must be introduced:

$$\gamma_j \approx p_j^3 (\frac{p_j}{A})^{p_j-1}. \quad (6)$$

In reality Equation (6) for γ_j is a preliminary rough estimation that is refined by parameterizing it over a mesh of residual nuclear energy and mass number (Mashnik and Sierk, 2012). As the MEM uses a Monte-Carlo technique to solve the master equations describing the behavior of the nucleus at the preequilibrium stage (see details in (Gudima *et al.*, 1983)), it is relatively easy to extend the number of types of possible LF that can be emitted during this stage. However, adding the possibility of LF emission alters the previous γ_j parameterization, effectively requiring new parameters. The task of parameterizing γ_j is the focus of Section VI.

Assuming an equidistant level scheme with the single-particle density g, the level density of the n-exciton state is (Ericson, 1960)

$$\omega(p,h,E) = \frac{g(gE)^{p+h-1}}{p!h!(p+h-1)!}\ . \quad (7)$$

This expression should be substituted into Eq. 5 to obtain the transmission rates λ_j.

2. Exciton Transitions

According to Equation (2), for a preequilibrium nucleus with excitation energy E and number of excitons $n = p + h$, the partial transition probabilities changing the exciton number by Δn are

$$\lambda_{\Delta n}(p,h,E) = \frac{2\pi}{\hbar}|M_{\Delta n}|^2 \omega_{\Delta n}(p,h,E) \ . \tag{8}$$

For these transition rates, one needs the number of states, ω, taking into account the selection rules for intranuclear exciton-exciton scattering. The appropriate formulae have been derived by Williams (F. Williams Jr., 1970) and later corrected for the exclusion principle and indistinguishability of identical excitons in Refs. (F. Williams Jr., 1971; Ribansky *et al.*, 1973):

$$\begin{aligned}
\omega_+(p,h,E) =& \frac{1}{2} g \frac{[gE - \mathcal{A}(p+1,h+1)]^2}{n+1} \\
& \times \left[\frac{gE - \mathcal{A}(p+1,h+1)}{gE - \mathcal{A}(p,h)}\right]^{n-1} \ , \\
\omega_0(p,h,E) =& \frac{1}{2} g \frac{[gE - \mathcal{A}(p,h)]}{n} \\
& \times [p(p-1) + 4ph + h(h-1)] \ , \\
\omega_-(p,h,E) =& \frac{1}{2} gph(n-2) \ ,
\end{aligned} \tag{9}$$

where $\mathcal{A}(p,h) = (p^2 + h^2 + p - h)/4 - h/2$. By neglecting the difference of matrix elements with different Δn, $M_+ = M_- = M_0 = M$, we estimate the value of M for a given nuclear state by associating the $\lambda_+(p,h,E)$ transitions with the probability for quasi-free scattering of a nucleon above the Fermi level on a nucleon of the target nucleus. Therefore, we have

$$\begin{aligned}
\frac{< \sigma(v_{rel}) v_{rel} >}{V_{int}} =& \frac{\pi}{\hbar}|M|^2 \frac{g[gE - \mathcal{A}(p+1,h+1)]}{n+1} \\
& \left[\frac{gE - \mathcal{A}(p+1,h+1)}{gE - \mathcal{A}(p,h)}\right]^{n-1} \ ,
\end{aligned} \tag{10}$$

where V_{int} is the interaction volume estimated as $V_{int} = \frac{4}{3}\pi(2r_c + \lambda/2\pi)^3$, with the de Broglie wave length $\lambda/2\pi$ corresponding to the relative velocity $v_{rel} = \sqrt{2T_{rel}/m_N}$. A value of the order of the nucleon radius is used for r_c in the CEM: $r_c = 0.6$ fm.

The averaging on the left-hand side of Eq. (10) is carried out over all excited states, taking into account the exclusion principle. Combining (8), (9), and (10) we finally get for the transition rates:

$$\begin{aligned}
\lambda_+(p,h,E) =& \frac{< \sigma(v_{rel}) v_{rel} >}{V_{int}} \ , \\
\lambda_0(p,h,E) =& \frac{< \sigma(v_{rel}) v_{rel} >}{V_{int}} \left[\frac{gE - \mathcal{A}(p,h)}{gE - \mathcal{A}(p+1,h+1)}\right]^{n+1} \\
& \times \frac{n+1}{n} \frac{p(p-1) + 4ph + h(h-1)}{gE - \mathcal{A}(p,h)} \ , \\
\lambda_-(p,h,E) =& \frac{< \sigma(v_{rel}) v_{rel} >}{V_{int}} \left[\frac{gE - \mathcal{A}(p,h)}{gE - \mathcal{A}(p+1,h+1)}\right]^{n+1} \\
& \frac{ph(n+1)(n-2)}{[gE - \mathcal{A}(p,h)]^2} \ .
\end{aligned} \tag{11}$$

3. Angular Distributions

The CEM predicts angular distributions for preequilibrium particles that are forward-peaked in the laboratory system. For instance, CEM03.03 assumes that a nuclear state with a given excitation energy E^* should be specified not only by the exciton number n but also by the momentum direction Ω. Following Ref. (Mantzouranis *et al.*, 1976), the master equation (Eq. (3)) can be generalized for this case provided that the angular dependence for the transition rates λ_+, λ_0, and λ_- (Eq. (11)) may be factorized. In accordance with Eq. 10, in the CEM it is assumed that

$$< \sigma > \rightarrow < \sigma > F(\Omega) \ , \tag{12}$$

where

$$F(\Omega) = \frac{d\sigma^{free}/d\Omega}{\int d\Omega' d\sigma^{free}/d\Omega'} \ . \tag{13}$$

The scattering cross section $d\sigma^{free}/d\Omega$ is assumed to be isotropic in the reference frame of the interacting excitons, thus resulting in an asymmetry in both the nucleus center-of-mass and laboratory frames. The angular distributions of preequilibrium complex particles are assumed to be similar to those for the nucleons in each nuclear state (Gudima *et al.*, 1983).

This calculational scheme is easily realized by the Monte-Carlo technique. It provides a good description of double-differential spectra of preequilibrium nucleons and a not-so-good but still reasonable description of complex-particle spectra from different types of nuclear reactions at incident energies from tens of MeV to several GeV. For incident energies below about 200 MeV, Kalbach (Kalbach, 1988) has developed a phenomenological systematics for preequilibrium-particle angular distributions by fitting available measured spectra of nucleons and complex particles. As the Kalbach systematics are based on measured spectra, they describe very

well the double-differential spectra of preequilibrium particles and generally provide a better agreement of calculated preequilibrium complex-particle spectra with data than does the CEM approach based on Eqs. (12, 13). Therefore, CEM03.03 incorporates the Kalbach systematics (Kalbach, 1988) to describe angular distributions of both preequilibrium nucleons and complex particles at incident energies up to 210 MeV. At higher energies, CEM03.03 uses the CEM approach based on Eqs. (12, 13).

B. Extension of the MEM

CEM03.03 does not have the capability to output cross sections for fragments larger than ^{4}He. Therefore, one of the first things done was to add this capability. We also created the capability to output by isotope, Z number, or mass number. For more details of this work, see Ref. (Kerby *et al.*, 2012).

Extending the MEM to produce the 66 fragments listed in Table I involves extending Eq. (4) to calculate emission widths for all 66 fragment types. This entails calculating Coulomb barriers, binding energies, reduced masses, inverse cross sections, and condensation probabilities for all 66 fragment types.

TABLE I The emitted fragments included in the modified MEM.

Z_j	Ejectiles						
0	n						
1	p	d	t				
2	^{3}He	^{4}He	^{6}He	^{8}He			
3	^{6}Li	^{7}Li	^{8}Li	^{9}Li			
4	^{7}Be	^{9}Be	^{10}Be	^{11}Be	^{12}Be		
5	^{8}B	^{10}B	^{11}B	^{12}B	^{13}B		
6	^{10}C	^{11}C	^{12}C	^{13}C	^{14}C	^{15}C	^{16}C
7	^{12}N	^{13}N	^{14}N	^{15}N	^{16}N	^{17}N	
8	^{14}O	^{15}O	^{16}O	^{17}O	^{18}O	^{19}O	^{20}O
9	^{17}F	^{18}F	^{19}F	^{20}F	^{21}F		
10	^{18}Ne	^{19}Ne	^{20}Ne	^{21}Ne	^{22}Ne	^{23}Ne	^{24}Ne
11	^{21}Na	^{22}Na	^{23}Na	^{24}Na	^{25}Na		
12	^{22}Mg	^{23}Mg	^{24}Mg	^{25}Mg	^{26}Mg	^{27}Mg	^{28}Mg

The upgraded MEM provides a dramatically improved ability to describe light-fragment production at intermediate to high energies across most reactions tested. Furthermore, we evaluated the energy spectra of nucleons and complex fragments, to verify that the modified-MEM code predicts the high-energy tails of fragment spectra without destroying the spectra of established particles and fragments; i.e., the good results for fragments $\leq^4$He are not degraded. The bulk of these preliminary results are not shown here because we modified the inverse-cross-section model. However, some results are shown in Fig. 13, with further results to be found in Ref. (Kerby *et al.*, 2012).

A number of programming improvements to the revised CEM code have made it more robust than the original CEM03.03.

IV. PREEQUILIBRIUM —INVERSE CROSS SECTIONS

Total-reaction-cross-section models have a significant impact on the predictions and accuracy of spallation and transport codes. CEM03.03 and LAQGSM03.03 use such cross-section models for different purposes than does MCNP6. While total reaction cross sections are used throughout the transport and spallation models, there are two main uses. MCNP6 uses total reaction cross sections to determine where a reaction occurs (through the mean-free-path length), then with what nucleus the projectile interacts, and what type of interaction it is (inelastic or elastic). CEM uses total reaction cross sections as *inverse* cross sections to calculate the probabilities for the emission of the possible nucleons and fragments. Phenomenological approximations of total reaction cross sections are also used by CEM03.03 as the default option for normalization of all results in the case of reactions induced by protons and neutrons, in its stand-alone mode; see details in Refs. (Mashnik *et al.*, 2008; Mashnik and Sierk, 2012).

Having accurate total-reaction-cross-section models in the intermediate-energy region (∼50 MeV to ∼5 GeV) is important for many applications. Space applications include astronaut radiation dosage, electronics-malfunction analysis, structural-material analysis, and galactic-cosmic-ray (GCR) shielding. Medical applications include hadron therapy for cancer (MacReady, 2012), radiation shielding, medical isotope production, and high-radiation environment dosimetry. Other applications include accelerator design and simulation. In addition, implementing better inverse cross sections in CEM should provide more reliable predictions; that is, this current work should be useful also from an academic point of view, allowing us to better understand the mechanisms of nuclear reactions. Finally, the 2008–2010 IAEA Benchmark of Spallation Models recommended an improvement to CEM's ability to predict the production of energetic light fragments (Leray *et al.*, 2011; Mashnik *et al.*, 2010). The improvement of the inverse cross sections used by CEM03.03 directly addresses this point, both for a better description of light fragments, but also of nucleons.

The current inverse cross sections used in the preequilibrium and evaporation stages of CEM are based on the Dostrovsky et al. model, published in 1959 (Dostrovsky *et al.*, 1959). Better total reaction (*inverse*)-cross-section models are now available (Barashenkov and Polanski,

1994; Iida *et al.*, 2007; Ingemarsson and Lantz, 2003; Kalbach, 1998; Kox *et al.*, 1987; Shen *et al.*, 1989; Takechi *et al.*, 2009; Townsend and Wilson, 1988; Tripathi *et al.*, 1996, 1997, 1999; Tsang *et al.*, 1990).

MCNP6 uses an update of the Barashenkov and Polanski (BP) cross-section model (Barashenkov and Polanski, 1994) as described briefly in (Barashenkov *et al.*, 1990; Prael *et al.*, 1998a) to calculate the mean-free-path length for neutrons, protons, and light fragments up to ^{4}He. It uses a parameterization based on a geometric cross section for light fragments above ^{4}He. Implementing better cross-section models in CEM, LAQGSM, and MCNP6 should yield improved results of particle spectra and total production cross sections, among other quantities. We demonstrate in the following sections that improving the inverse-cross-section model in the preequilibrium stage of CEM, does indeed lead to the expected improvements.

As discussed in the prior section, the extension of the preequilibrium model to produce heavier clusters up to ^{28}Mg yields good results for most reactions tested, with dramatically improved ability to produce energetic LF. However, for some reactions, while the results are improved, they are not as good as we wished. We chose to upgrade the inverse-cross-section models used in CEM to calculate the emission widths (probabilities) in the preequilibrium stage, in an attempt to further improve these results. As CEM is the default event generator in MCNP6 in the intermediate-energy range, once these changes are implemented into MCNP6, we see a corresponding improvement in its results as well.

A. Background

The current inverse cross sections in CEM are taken from the Dostrovsky et al. model (Dostrovsky *et al.*, 1959). It is based on the strong-absorption model and its general form is as shown in Eq. (14).

$$\sigma_{Dost.} = \pi r_0^2 A^{2/3} \alpha_j (1 - \frac{V_j}{T}). \quad (14)$$

The Dostrovsky model was not intended for use above about 50 MeV/nucleon, and is not very suitable for emission of fragments heavier than ^{4}He. Better total-reaction-cross-section models are available today, most notably the NASA model (Tripathi *et al.*, 1996, 1997, 1999). The NASA (or Tripathi et al.) model is also based on the strong absorption model and its general form is shown in Eq. (15). The NASA cross section attempts to simulate several quantum-mechanical effects, such as the optical potential for neutrons (with the parameter X_m) and collective effects like Pauli blocking (through the quantity δ_T). (For more details, see Refs. (Tripathi *et al.*, 1996, 1997, 1999).)

$$\sigma_{NASA} = \pi r_0^2 (A_P^{1/3} + A_T^{1/3} + \delta_T)^2 (1 - R_c \frac{B_T}{T_{cm}}) X_m \ , \quad (15)$$

where

: r_0: a constant related to the radius of a nucleus;
: A_P: the mass number of the projectile nucleus;
: A_T: the mass number of the target nucleus;
: δ_T: an energy-dependent parameter;
: R_c: a system-dependent Coulomb multiplier;
: B_T: the energy-dependent Coulomb barrier;
: T_{cm}: the colliding system center-of-momentum energy;
: X_m: an optical model multiplier used for neutron-induced reactions.

There are other total-reaction-cross-section models, such as those by Shen, et al. (Shen *et al.*, 1989), and Takechi, et al. (Takechi *et al.*, 2009), among others (Barashenkov and Polanski, 1994; Iida *et al.*, 2007; Ingemarsson and Lantz, 2003; Kalbach, 1998; Kox *et al.*, 1987; Townsend and Wilson, 1988; Tsang *et al.*, 1990). Both the Shen model and the Kox model have projectile-target asymmetry, as discussed in Ref. (Sihver *et al.*, 2014b). Sihver et al. (Sihver *et al.*, 2014a) explore a new total reaction cross section used in PHITS: the hybrid Kurotama model. This model is a combination of the black-sphere model (Iida *et al.*, 2007) and the NASA model (Tripathi *et al.*, 1996, 1997, 1999). Ref. (Sihver *et al.*, 2012b) compares a number of different total-reaction-cross-section models, most notably those in FLUKA, NASA, and several other recently developed models.

PHITS uses the NASA model as its default, but the Shen model can be specified as an option (Sihver *et al.*, 2012b). FLUKA uses a modified version of the NASA model (Andersen *et al.*, 2004). GEANT4 has the option to use NASA, or a number of other models such as those of Shen (Shen *et al.*, 1989) or Sihver (Sihver *et al.*, 1993), or the Axen-Wellisch (Wellisch and Axen, 1996) parameterizations for high-energy hadronic interactions. See Refs. (Koi and Wright, 2013; Sihver *et al.*, 2012a) for more details on the total-reaction- cross-section models used in PHITS, FLUKA, and GEANT4.

Krylov et al. (Krylov *et al.*, 2014) compare proton spectra as calculated by GEANT4, SHIELD, and MCNPX 2.6 for relativistic heavy-ion collisions. A better version of MCNP is now available, but these results demonstrate the need for updated cross-section models within CEM, LAQGSM, and MCNP6.

Mashnik et al. (Mashnik *et al.*, 2007b, 2002) and Prael et al. (Prael *et al.*, 1998a,b) previously conducted an extensive comparison of the NASA (Tripathi *et al.*, 1996, 1997, 1999), Tsang et al. (Tsang *et al.*, 1990), Dostrovsky et al. (Dostrovsky *et al.*, 1959), Barashenkov and Polanski (Barashenkov and Polanski, 1994), and Kalbach (Kalbach, 1998) systematics for total reaction (*inverse*) cross sections. These authors found that the NASA

model was superior, in general, to the other available models. See Ref. (Kerby and Mashnik, 2014; Mashnik *et al.*, 2007b, 2002; Prael *et al.*, 1998a,b) for details of these findings.

B. Comparison of Total-Reaction-Cross-Section Models

In the original version of CEM03.03, we include the NASA model (Tripathi *et al.*, 1996, 1997, 1999) to define the total reaction cross section, and use the Dostrovsky model (Dostrovsky *et al.*, 1959) as inverse cross sections to calculate the preequilibrium decay. For the evaporation model (described with the code GEM2 by Furihata (Furihata, 2003), there is still a third set of inverse cross sections used. We compare these approximations, and the original Barashenkov and Polanski systematics (BP) (Barashenkov and Polanski, 1994) to experimental data and to total cross sections used in the MCNP6 code to calculate mean-free-path lengths, in the following two figures. The MCNP6 total cross sections are based on an updated version of the BP model (Barashenkov *et al.*, 1990; Prael *et al.*, 1998a).

1. Neutron-Induced Reactions

Fig. 7 displays the total reaction cross section for n + ^{208}Pb, as calculated by the NASA, Dostrovsky, GEM2, and BP, and MCNP6 models, compared to experimental data (Beghian *et al.*, 1966; Beyster *et al.*, 1955, 1956; Bonner and Slattery, 1959; Degtjarev, 1966; Morrison, 1956; Pasechnik, 1955; Poze and Glazkov, 1956; Strizhak, 1957; Taylor and O. Lönsjö and T. Bonner, 1955; Walt and Beyster, 1955).

We observe: 1) the Dostrovsky and GEM2 (also a Dostrovsky-like model) both approach asymptotic values at very low energies—thus they are not as useful at their constant values for neutrons with energies much above 10 MeV, and 2) the NASA model, while much better at predicting the total reaction cross section throughout the energy region of the data, falls to zero at low energies in the case of neutrons, which have no Coulomb barrier. For this reason, we cannot use the NASA model as an approximation for inverse cross sections in the case of low-energy neutrons: neutrons are emitted with low energies, too. In the case of low energy neutrons, we use the Kalbach systematics (Kalbach, 1998), which prove to be a very good approximation for the inverse cross section of low-energy neutrons, as discussed in Ref. (Mashnik *et al.*, 2002) and in subsection IV.C.1.

This problem of neutron cross sections was addressed first for the code CEM2k in Ref. (Mashnik *et al.*, 2002), by combining the NASA systematics by Tripathi, Cucinota, and Wilson (Tripathi *et al.*, 1996, 1997, 1999) and the Kalbach parameterization (Kalbach, 1998) into a FORTRAN routine called hybrid. We address this problem for the improved CEM03.03 code, which we call CEM03.03F, in a very similar way (see Ref. (Kerby and Mashnik, 2014), which also shows other neutron-induced reactions.)

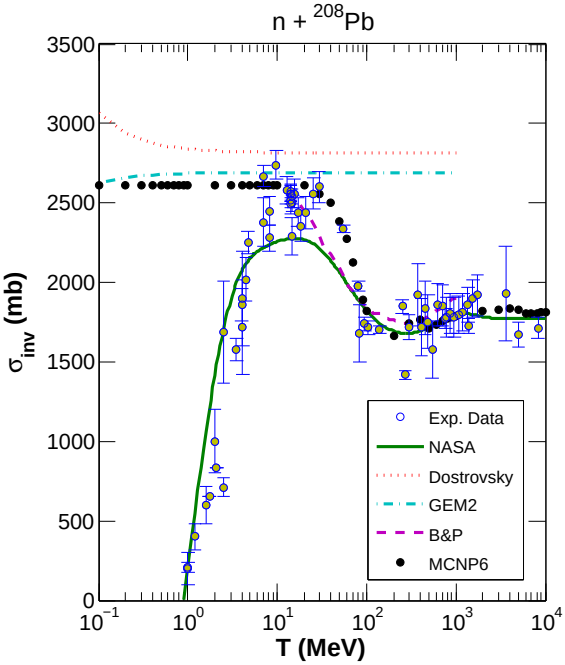

FIG. 7 Reaction cross sections as a function of neutron energy for n + ^{208}Pb, as calculated by the NASA, Dostrovsky, GEM2, and BP models. The black dots are cross sections calculated in MCNP6, and the yellow circles are experimental data (see the text for references).

2. Proton-Induced Reactions

Fig. 8 illustrates calculated total reaction cross sections using the NASA, Dostrovsky, GEM2, and BP models, compared to calculations by MCNP6 and experimental data. The NASA model appears to be superior to the Dostrovsky-like models.

Figs. 7 and 8, similar results on complex particles and fragments heavier than ^{4}He in Figs. 9 and 10, as well as numerous figures published in Refs. (Kerby and Mashnik, 2015d; Mashnik *et al.*, 2007b, 2002; Prael *et al.*, 1998a,b), suggest the BP approximations also agree well with available data. For this reason, the BP parametrization was chosen to be used for the calculation of the total reaction cross sections in the transport code MCNP6. However, the numerous current comparisons for various reactions, as well as the voluminous results published in Refs. (Mashnik *et al.*, 2007b, 2002; Prael *et al.*, 1998a,b), show that generally the NASA approximation agrees a

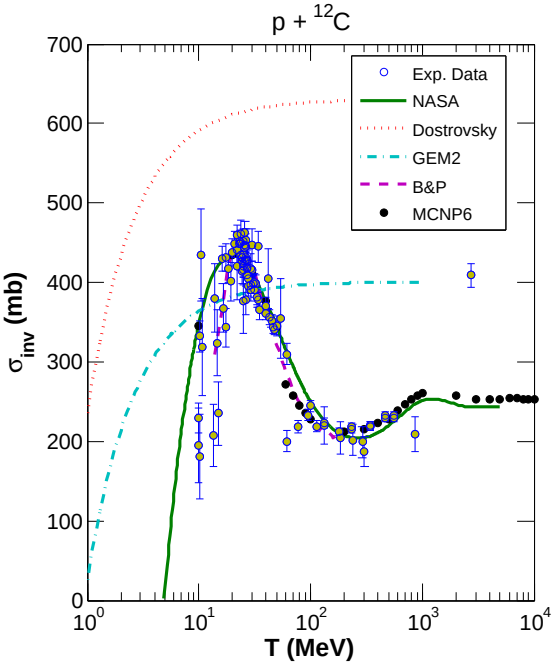

FIG. 8 Reaction cross section for p + ^{12}C, as calculated by the NASA, Dostrovsky, GEM2, and BP models. The black dots are cross sections calculated by MCNP6, and the yellow circles are experimental data (Carlson, 1996).

little better with most of the available experimental data than does the BP systematics. Ref. (Kerby and Mashnik, 2014) presents results of other proton-induced reactions.

3. Heavy-Ion Induced Reactions

We had not previously tested how CEM03.03 calculates inverse cross sections for LF heavier than ^{4}He. We now address this. Fig. 9 illustrates calculated total reaction cross sections by the NASA, Dostrovsky, GEM2, and BP models for the reactions α + ^{28}Si and ^{6}Li + ^{208}Pb, compared to experimental data.

Fig. 10 displays the total reaction cross section for ^{12}C + ^{12}C, as calculated by the NASA, Dostrovsky, GEM2, and BP models and compared to experimental data and to measured total charge-changing (TCC) cross sections. TCC cross sections should be 5% – 10% less than total reaction cross sections, as TCC cross sections do not include neutron removal.

The NASA cross-section model fits the experimentally measured data, in general, better than the other models tested. See Ref. (Kerby and Mashnik, 2014) for results of other heavy-ion-induced reactions.

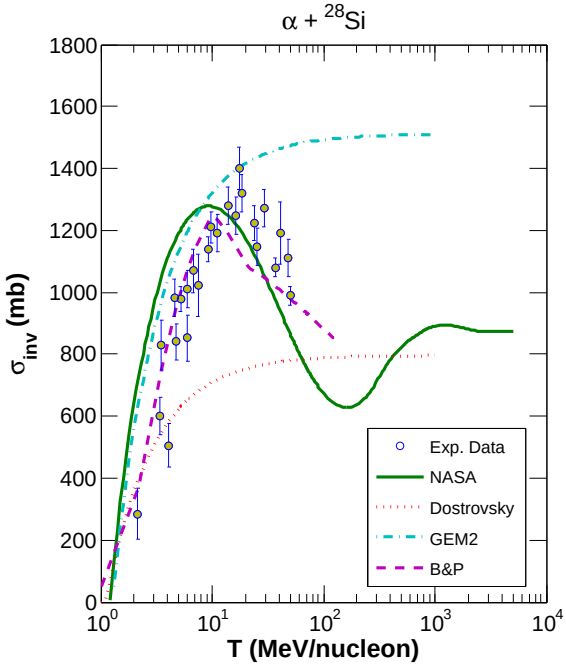

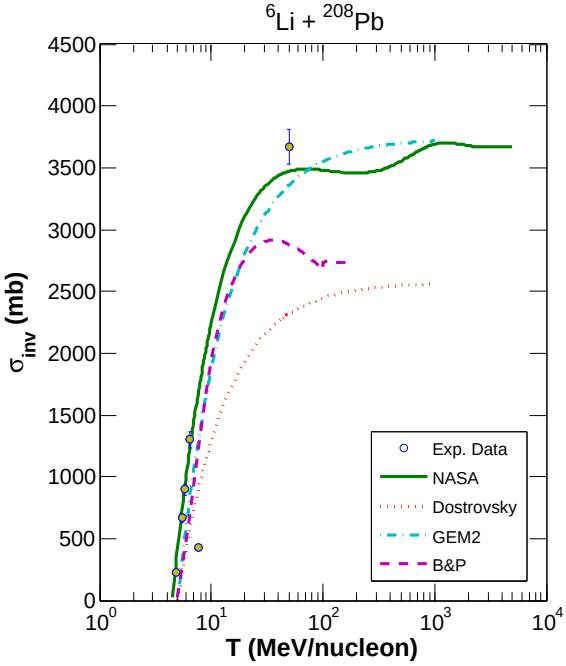

FIG. 9 Reaction cross sections for α + ^{28}Si and ^{6}Li + ^{208}Pb, as calculated by the NASA, Dostrovsky, GEM2, and BP models. The yellow circles are experimental data (Baktybaev *et al.*, 2003; Ingemarsson *et al.*, 2000; Ugryumov *et al.*, 2004, 2005; Warner *et al.*, 1996).

C. Implementation of the NASA Cross Section Model into CEM03.03F

The implementation of the NASA cross section model into CEM involved adding Kalbach systematics for low-energy neutrons, updating the emission width calcula-

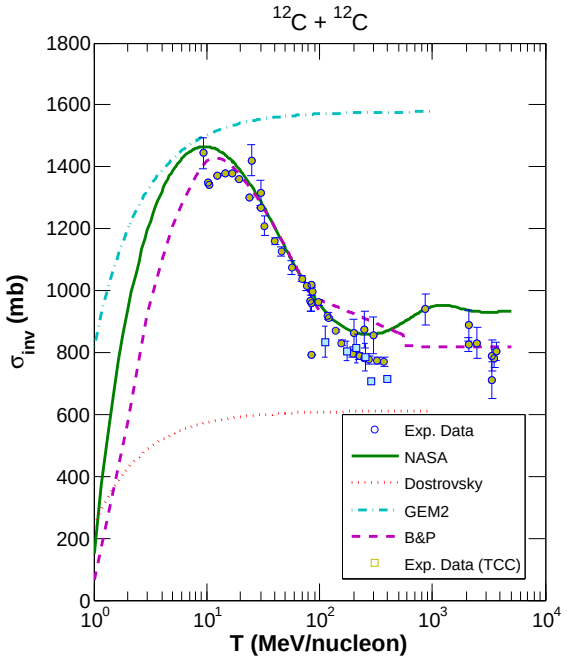

FIG. 10 Reaction cross section for $^{12}C + ^{12}C$, as calculated by the NASA, Dostrovsky, GEM2, and BP models. The yellow circles are experimental data (Barashenkov, 1993; Mazarakis and Stephens, 1973; Takechi *et al.*, 2009) and the blue squares are total charge-changing cross section (TCC) measurements (Golovchenko *et al.*, 2002; Zeitlin *et al.*, 2007).

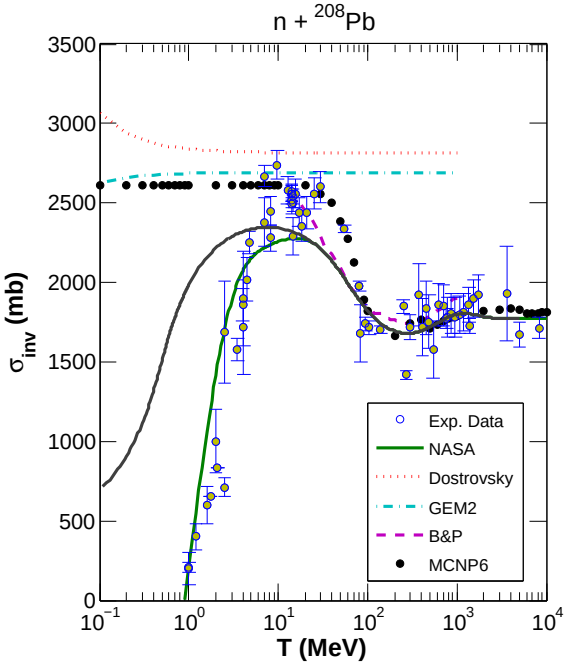

FIG. 11 Reaction cross section for n + ^{208}Pb, as calculated by the NASA, NASA-Kalbach hybrid (black line), Dostrovsky, GEM2, and BP models, as indicated. The black dots are cross sections calculations by MCNP6, and the yellow circles are experimental data from Refs. (Beghian *et al.*, 1966; Beyster *et al.*, 1955, 1956; Bonner and Slattery, 1959; Degtjarev, 1966; Morrison, 1956; Pasechnik, 1955; Poze and Glazkov, 1956; Strizhak, 1957; Taylor and O. Lönsjö and T. Bonner, 1955; Walt and Beyster, 1955).

tion, and upgrading the emitted-fragment kinetic energy simulation.

1. Kalbach Systematics

We added in CEM03.03F the Kalbach systematics (Kalbach, 1998) to replace the NASA inverse cross sections (Tripathi *et al.*, 1996, 1997, 1999) for low-energy neutrons, similar to what was suggested and done in Ref. (Mashnik *et al.*, 2002) for the code CEM2k. Fig. 11 displays the Kalbach systematics implementation for the cross section n + ^{208}Pb. For around 24 MeV and below, the calculation uses Kalbach systematics, and switches to the NASA model for the rest of the neutron-energy range. The Kalbach systematics are scaled to match the NASA model results at the transition point so as not to have a discontinuity.

As part of the Kalbach systematics implementation, transition points and scaling factors must be obtained for all possible residual nuclei, by mass number. Ref. (Kerby and Mashnik, 2014) provides tables of these.

2. Calculation of the Emission Width, Γ_j

CEM uses the inverse cross section, σ_j^{inv}, in determining what particles and/or fragments are emitted from the excited nucleus. We use the total reaction cross section as the best approximation for this inverse cross section. The emission width Γ_j, or the probability of emitting fragment type j, is calculated according to Eqs. (4 and 5) for nucleons. It is dependent upon σ_j^{inv} (see more details in Refs. (Gudima *et al.*, 1983; Mashnik *et al.*, 2008; Mashnik and Sierk, 2012)).

The partial transmission probability λ_j, or the probability that a particle or a fragment of the type j will be emitted with kinetic energy T, as shown in Eq. (5) is written in its simplest form, as is valid for neutrons and protons only. An extension of Eq. (5) for the case of complex particles and light fragments (LF) is (see Ref. (Gudima *et al.*, 1983)):

$$\lambda_j(p,h,E,T) = \gamma_j \frac{2s_j+1}{\pi^2\hbar^3}\mu_j \Re(p,h)\frac{\omega(p_j,0,T+B_j)}{g_j} \times \frac{\omega(p-p_j,h,E-B_j-T)}{\omega(p,h,E)} T\sigma_j^{inv}(T) \ , \quad (16)$$

where

$$g_j = \frac{V(2\mu_j)^{3/2}}{4\pi^2\hbar^3}(2s_j+1)(T+B_j)^{1/2} \ . \quad (17)$$

See Ref. (Wu and Chang, 1978) for details on Eq. (17). γ_j is the probability that the proper number of particle excitons will coalesce to form a type j fragment (also called γ_β in a number of our earlier publications; see, e.g., Refs. (Betak, 1976; Blideanu *et al.*, 2004; Wu and Chang, 1978)). It is the subject of Section VI.

In the standard CEM03.03, the Dostrovsky form of the inverse cross section is simple enough so that for neutrons and protons this integral can be done analytically. However, for complex particles, the level density, ω, becomes too complicated (see details in Refs. (Gudima *et al.*, 1983; Mashnik *et al.*, 2008; Mashnik and Sierk, 2012)); therefore, the integral is evaluated numerically. In this case, a 6-point Gaussian quadrature is used when the exciton number is 15 or less, and a 6-point Gauss-Laguerre quadrature is used when the number of excitons is greater than 15.

We adopt for CEM03.03F the NASA form of the cross section for nucleons which is too complicated for analytic integration, so the integral is always calculated numerically. We use an 8-point Gaussian quadrature when the number of excitons is 15 or less, and an 8-point Gauss-Laguerre quadrature when the number of excitons is greater than 15. See Ref. (Kerby and Mashnik, 2015d) for details.

Better integration methods could be investigated at a later time. However, these integration methods are sufficient because individual Γ_j precision is not extremely important for choosing what type of particle/LF j will be emitted. In contrast to analytical preequilibrium models, the Monte-Carlo method employed by CEM uses the ratios of Γ_j to the sum of Γ_j over all j. That is, if we estimate all Γ_j with the same percentage error, the final choice of the type j of particle/LF to be emitted as simulated by CEM would be the same as if we would calculate all Γ_j exactly. We think that this is the main reason why CEM provides quite reasonable results using the old Dostrovsky approximation for inverse cross sections, in spite of the significant difference of the Dostrovsky inverse cross sections from those now used. The ratios of the individual widths to the total width were approximated better than each individual width, because the errors in each channel have the same sign. This is illustrated in Figs. 8– 11.

3. Kinetic-Energy Simulation

Once a fragment type j has been randomly chosen for emission, the kinetic energy of this fragment needs to be determined. This is done by sampling the kinetic energy from the λ_j distribution, Eq. (16), using the NASA cross section as the σ_j^{inv}.

The details of the NASA cross section can be found in (Tripathi *et al.*, 1999). The NASA inverse cross sections contain dependences on both the lab-reference-frame kinetic energy (T) and the center-of-momentum-reference-frame kinetic energy (T_{cm}). The relativistic transformation between the two is not trivial. The level density, ω, also contains T-dependences. Finally, as noted above, for neutrons we use a NASA-Kalbach hybrid inverse cross section in place of the pure NASA approximation. To conclude, the energy-dependence of λ_j for the new inverse cross sections is very complicated, as compared to that arising from the simple Dostrovsky form used in the original CEM03.03. This affects the method we choose to appropriately sample T_j.

To sample T_j uniformly from the λ_j distribution using the Monte-Carlo method, we must first find the maximum of λ_j. In CEM03.03, this is done analytically using the derivative of λ_j with respect to T_j, due to the simple nature of the energy-dependence in the Dostrovsky systematics. The NASA cross section energy dependence is complicated; therefore, we find the maximum of λ_j numerically using the Golden-Section method. This also provides us the flexibility to modify the cross-section model in the future without needing to modify the kinetic energy algorithm.

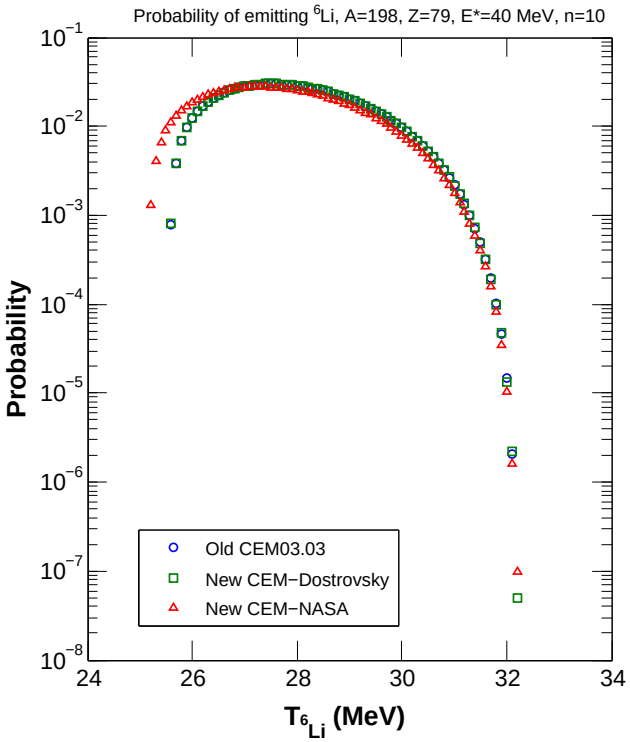

FIG. 12 The normalized probability of emitting a ^{6}Li with a given kinetic energy T_{Li}, simulated using the Monte-Carlo method according to Eq. (16) in the preequilibrium stage. The circles are results from the old kinetic energy subroutine, the squares are results from the new kinetic energy subroutine using the Dostrovsky inverse cross sections, and the triangles are from the new kinetic-energy subroutine using the NASA inverse cross sections.

After finding the maximum value of λ_j, the kinetic energy of the emitted fragment j is uniformly sampled

from the λ_j distribution using the rejection technique from a Gamma distribution (shape parameter $\alpha = 2$) as the comparison function. Fig. 12 illustrates results for the probability of emitting ^{6}Li with a given kinetic energy T_{Li}. Probabilities from the λ_j distributions with the NASA inverse cross sections differ slightly from those with the Dostrovsky inverse cross sections primarily because the NASA Coulomb barriers are strongly based on T_{cm}, as opposed to T.

D. Results

The results from the improved code are promising. Fig. 13 shows the double differential cross section for the production of ^{6}Li and ^{7}Be from the reaction of 200-MeV protons on ^{59}Co.

The blue dashed lines are the extended preequilibrium (Section III) results with the Dostrovsky inverse cross sections, and the red solid lines are results by CEM03.03F with the upgraded NASA-Kalbach hybrid inverse cross sections. The green circles are experimental data from Ref. (Machner *et al.*, 2006). There is improved agreement with data in the high-energy tails. This figure also highlights the importance of eventually upgrading the inverse cross sections used in the evaporation stage of CEM as well. The evaporation stage produces the peak of the spectra, which for this reaction is too low, especially for ^{7}Be. With the implementation of the NASA inverse cross sections into the preequilibrium model we see improved high-energy tails, but in order to achieve improved agreement in the thermal region we need to implement the NASA inverse cross sections into the evaporation stage. We plan to do this in the future.

E. Conclusion

The inverse-cross-section approximation in the preequilibrium and evaporation stages of CEM03.03 is based on the Dostrovsky inverse cross sections. Better cross-section systematics are now available. We compare several inverse-cross-section models and find that the NASA (Tripathi, et al.) (Tripathi *et al.*, 1996, 1997, 1999) approximation is generally the most accurate when compared with experimental data.

We implemented the NASA inverse-cross-section model into the extended MEM; the upgraded code is called CEM03.03F. These results are promising and show improved agreement with experimental data using the NASA inverse-cross-section model compared to the original Dostrovsky approximation.

There are several implications of this work for MCNP6. CEM03.03 is the default event generator in MCNP6 for high-energy collisions induced by nucleons, pions, and gamma rays at energies up to several GeV. Improvements to the CEM inverse cross sections should, therefore, result in improved predictions of particle spectra and total production cross sections, especially above ∼100 MeV and for fragments heavier than ^{4}He.

MCNP6 uses the updated Barashenkov and Polanski total-reaction-cross-section systematics to simulate the mean-free path of neutrons, protons, and light fragments up to ^{4}He. It uses a parameterization based on a geometric cross section for fragments heavier than ^{4}He. It is possible further improvement of MCNP6 could be obtained by replacing the Barashenkov and Polanski model with the NASA systematics and by replacing the geometric cross section approach with the better NASA model. We hope to investigate this in the future.

Other recommendations include investigating adaptive quadrature and upgrading the inverse-cross-section model used in the evaporation stage from the Dostrovsky/GEM2 approximations to the NASA-Kalbach hybrid cross sections.

V. COALESCENCE

In CEM there are three ways high-energy heavy clusters can be produced: via coalescence, preequilibrium, and Fermi breakup. In this section we study the impact of extending the coalescence model to heavy cluster emission. CEM03.03, the event generator in MCNP6 for intermediate-energy nuclear reactions, is capable of producing light fragments up to ^{4}He in its coalescence model. We extend the coalescence model to be able to produce up to ^{7}Be in CEM03.03F and up to ^{12}C in LAQGSM03.03F.

A. Background

When the cascade stage of a reaction is completed, CEM uses the coalescence model described in Ref. (Schulz *et al.*, 1983; Toneev and Gudima, 1983) to create high-energy d, t, ^{3}He, and ^{4}He fragments by final-state interactions among emitted cascade nucleons outside of the target nucleus. The coalescence model used in CEM is similar to other coalescence models for heavy-ion-induced reactions. The main difference is that instead of complex-particle spectra being estimated by simply convolving the measured or calculated inclusive spectra of nucleons with corresponding fitted coefficients, CEM03.03 uses the calculated information about all emitted cascade nucleons and does not use integrated spectra. (Coalescence was introduced recently into the Liège intranuclear cascade (INCL) (Boudard *et al.*, 2013; Cugnon *et al.*, 2011a; Leray *et al.*, 2014; Mancusi *et al.*, 2014); it is in a way similar to the coalescence considered by CEM as proposed in Ref. (Schulz *et al.*, 1983; Toneev and Gudima, 1983), with the main contrast be-

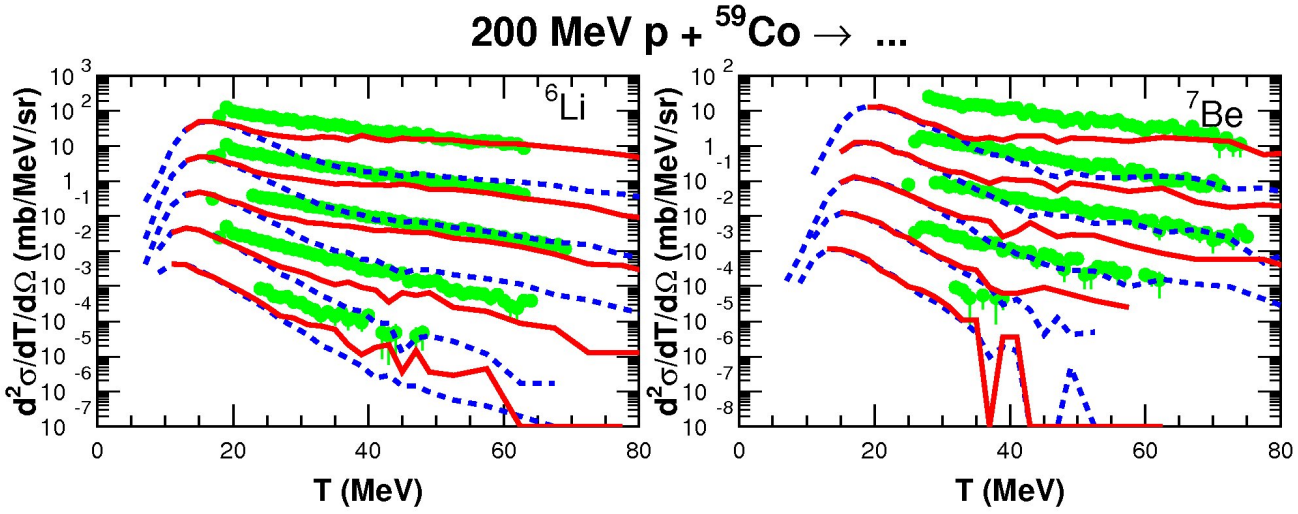

FIG. 13 Double differential cross section for the production of ^{6}Li and ^{7}Be from the reaction of 200-MeV protons + ^{59}Co, for the angles of 20°, 45°, 60°, 90°, and 110°. The 110° spectra (the lowest sets) are shown unscaled, while the 90°, 60°, 45°, and 20° spectra are scaled up by successive powers of 10, respectively. The blue dashed lines are the extended-MEM (CEM03.03F) results with the Dostrovsky inverse cross sections, and the red solid lines are results by CEM03.03F with the NASA inverse cross sections. The green circles are experimental data by Machner, et al (Machner *et al.*, 2006).

ing that INCL considers coalescence of INC nucleons on the border of a nucleus, inside the target nucleus, while CEM coalesces INC nucleons outside the nucleus.) We assume that all the cascade nucleons having differences in their momenta smaller than p_c and with the correct isotopic content form an appropriate composite particle. Each complex particle has its own empirical coalescence radius p_c, whose values in CEM03.03 are:
Incident energy, T, < 300 MeV or > 1000 MeV

$$\begin{aligned} p_c(d) &= 90 \text{ MeV/c} ; \\ p_c(t) &= p_c(^3He) = 108 \text{ MeV/cvector} ; \\ p_c(^4He) &= 115 \text{ MeV/c} . \end{aligned} \quad (18)$$

$300 \text{ MeV} < T < 1000 \text{ MeV}$

$$\begin{aligned} p_c(d) &= 150 \text{ MeV/c} ; \\ p_c(t) &= p_c(^3He) = 175 \text{ MeV/c} ; \\ p_c(^4He) &= 175 \text{ MeV/c} . \end{aligned} \quad (19)$$

When several cascade nucleons coalesce into composite particles, they are removed from the distributions of nucleons and do not contribute further to such nucleon characteristics as spectra, multiplicities, etc.

B. Coalescence Model Extension

The magnitude of the momentum, p, of each nucleon is calculated relativistically from its kinetic energy, T:

$$p^2c^2 = KE(KE + 2m_0c^2), \quad (20)$$

where m_0 is the rest mass of the nucleon. The momentum vector is defined from the magnitude of the momentum and its spatial direction. Coalescence occurs if each nucleon in the group has $|\Delta\mathbf{p}| \leq p_c$, where $\Delta\mathbf{p}$ is defined as the vector difference between the nucleon momentum and the average momentum of all nucleons in the group.

The coalescence model first checks all nucleons to form 2-nucleon pairs, their momenta permitting. It then checks if an alpha particle can be formed from two 2-nucleon pairs (either from two n-p pairs or from an n-n and a p-p pair). After this it checks to see if any of the two-nucleon pairs left can combine with another nucleon to form either tritium or ^{3}He. And lastly, it checks to see if any of these three-nucleon groups (tritium or ^{3}He) can coalesce with another nucleon to form ^{4}He.

The extended coalescence model takes these two-nucleon pairs, three-nucleon (tritium or ^{3}He only) groups, and ^{4}He to see if they can coalesce to form heavier clusters. ^{4}He can coalesce with a 3-nucleon group to form either ^{7}Be or ^{7}Li. Two 3-nucleon groups can coalesce to form either ^{6}Li or ^{6}He. And ^{4}He can coalesce with a 2-nucleon pair to form either ^{6}Li or ^{6}He. All coalesced nucleons are removed from the distributions of nucleons so that the coalescence model conserves both atomic and mass numbers.

For additional details of the extended coalescence model, see Ref. (Kerby and Mashnik, 2015a).

1. Coalescence Parameter p_c

As mentioned in Section V.A, p_c determines how dissimilar the momenta of nucleons can be and still coalesce. p_c was extended to also include a value for heavy clusters, or light fragments (LF): $p_c(LF)$. The new p_c's for incident energies, T, less than 300 MeV or greater than 1000 MeV are:

$$\begin{aligned} p_c(d) &= 90 \text{ MeV/c} ; \\ p_c(t) &= p_c(^3He) = 108 \text{ MeV/c} ; \\ p_c(^4\text{He}) &= 130 \text{ MeV/c} . \\ p_c(LF) &= 175 \text{ MeV/c} . \end{aligned} \tag{21}$$

For 300 MeV $< T <$ 1000 MeV they are:

$$\begin{aligned} p_c(d) &= 150 \text{ MeV/c} ; \\ p_c(t) &= p_c(^3He) = 175 \text{ MeV/c} ; \\ p_c(^4\text{He}) &= 205 \text{ MeV/c} . \\ p_c(LF) &= 250 \text{ MeV/c} . \end{aligned} \tag{22}$$

The $p_c(^4He)$ was increased compared to the original p_c values. Too many alpha particles were lost (coalesced into heavy clusters); therefore, we compensated by coalescing more ^{4}He.

C. Results and Analysis

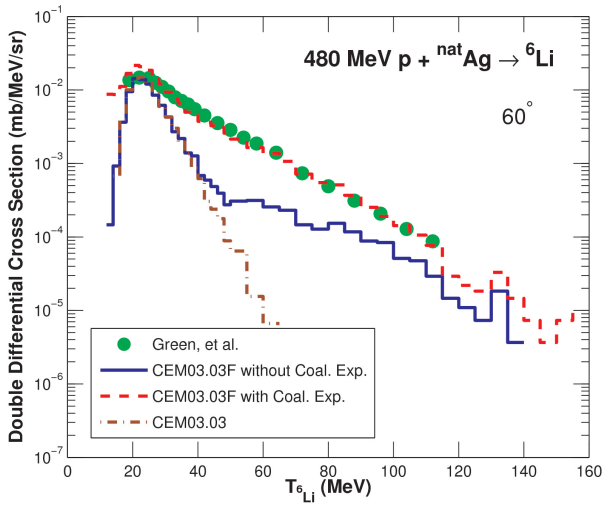

FIG. 14 Comparison of experimental measurements of the reaction 480 MeV p + ^{nat}Ag → ^{6}Li at 60° by Green et al. (Green *et al.*, 1984) (green circles), with simulations from the original CEM03.03 (brown dashed-dotted lines), CEM03.03F without the coalescence extension (blue solid lines) and CEM03.03F with the coalescence extension (red dashed lines).

Fig. 14 displays experimental measurements of the reaction 480 MeV p + ^{nat}Ag → ^{6}Li by Green et al. (Green *et al.*, 1984) (green circles), compared with simulations from CEM03.03F without the coalescence extension (blue solid lines), CEM03.03F with the coalescence extension (red dashed lines), and the original CEM03.03 (brown dashed-dotted lines). Even without the coalescence extension, CEM03.03F (which contains the extended preequilibrium model and the total-reaction-cross-section improvement) yields much better results than CEM03.03 without these improvements. Adding the coalescence extension produces even better results.

This reaction also highlights how coalescence can produce heavy clusters not just at high energies, but also at low and moderate energies, thus improving agreement with experimental data in all these energy regions.

Similar results for many other reactions induced by protons, neutrons, and heavy ions, where the last are simulated with a similarly extended LAQGSM03.03F, are described in Ref. (Mashnik *et al.*, 2015) and further discussed in Refs. (Kerby, 2015b; Kerby and Mashnik, 2015a,c; Mashnik and Kerby, 2015; Mashnik *et al.*, 2015).

D. LAQGSM

LAQGSM is a powerful predictive tool for heavy-ion-induced reactions and/or nuclear reactions at very high energies (> several GeV/nucleon). Several results of LAQGSM03.03, the default event generator in MCNP6 for these types of reactions, are shown in Figs. 15 and 16.

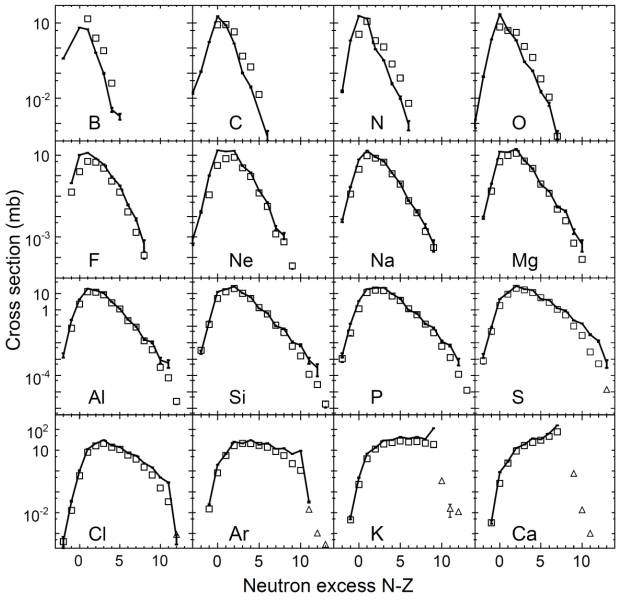

FIG. 15 Measured cross sections for ^{48}Ca fragmentation on ^{9}Be at 140 MeV/A (Mocko, 2006; Mocko *et al.*, 2006) (open circles) compared to LAQGSM03.03 predictions solid lines.

Fig. 15 shows an example of product yields measured by Mocko, et al. (Mocko, 2006; Mocko *et al.*, 2006) from

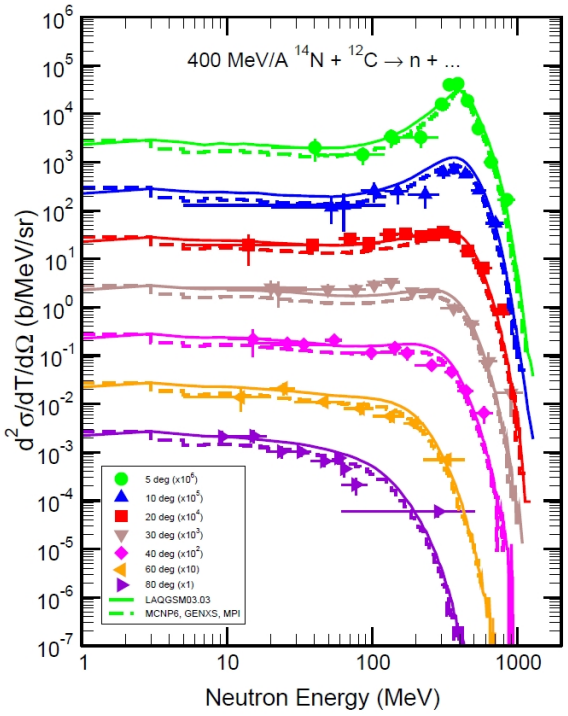

FIG. 16 Experimental (Heilbronn *et al.*, 2007; Nakamura and Heilbronn, 2006) neutron spectra from 400 MeV/A ^{14}N + ^{12}C (solid symbols), compared with calculations by the production version of MCNP6 (dashed lines) and by the LAQGSM03.03 event generator used as a stand-alone code (solid lines).

the fragmentation of ^{48}Ca on ^{9}Be at 140 MeV/nucleon. Many more similar results for other reactions can be found in (Mashnik *et al.*, 2007a).

Fig. 16 displays experimental (Heilbronn *et al.*, 2007; Nakamura and Heilbronn, 2006) neutron spectra from 400 MeV/A ^{14}N + ^{12}C, compared with calculations by the production version of MCNP6 and the LAQGSM03.03 event generator used as a stand-alone code. Such data are of significant interest for applications related to cancer treatment with carbon beams, and most of the neutron spectra from such reactions were measured at the Heavy-Ion Medical Accelerator in the Chiba (HIMAC) facility of the Japanese National Institute of Radiological Science (NIRS). We obtained similar agreement by LAQGSM and by MCNP6 using LAQGSM for many other similar reactions, at different incident energies and for different projectile- target nuclear combinations (see Ref. (Mashnik, 2014)).

In CEM03.03F we extended the coalescence model to account for heavier fragments up to ^{7}Be. As CEM is restricted to simulate only particle-induced reactions, and only at energies below about 5 GeV, such an extension of the coalescence model may be good enough. But as LAQGSM is used to calculate also reactions induced by heavy ions, and at much higher incident energies, where the mean multiplicities of the secondary nucleons and LF are much higher than for reactions simulated with CEM, we need to extend the coalescence model in LAQGSM for even heavier LF up to ^{12}C. Table II shows the LF we produce via coalescence in LAQGSM03.03F, and the real channels (modes) we consider to form each LF.

Fig. 17 provides an example of some preliminary results for the case of fragment-production cross sections as functions of mass number, measured by Jacak, et al., at the LBL BEVALAC (Jacak *et al.*, 1987), for 137 MeV/nucleon beams of ^{40}Ar bombarding ^{197}Au targets, compared to LAQGSM03.03F results obtained with the extended coalescence model (green stars). There is reasonable agreement with experimental data for mass numbers up to $A = 12$, except for $A = 9$. The LAQGSM03.03F coalescence extension is still a work in progress.

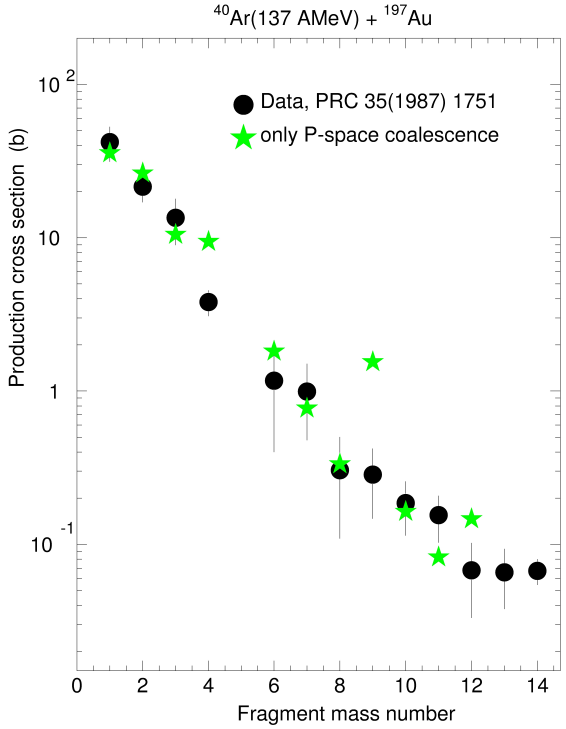

FIG. 17 Measured cross sections for fragments produced in 137 MeV/A ^{40}A + ^{197}Au reactions (Jacak *et al.*, 1987) (black circles) compared to LAQGSM03.03F predictions (green stars).

E. Conclusion

Extending the coalescence model within the CEM yields increased production of heavy clusters in nuclear spallation reactions, particularly in the high-energy region, but also in the low- and moderate-energy regions. Results indicate this coalescence extension yields improved agreement with experimental data. These upgrades were recently implemented into and tested in

TABLE II Coalescence channels (modes) for LF produced in the extended coalescence model in LAQGSM03.03F.

Name	A	Z	p_c (MeV/c/A)	Channels (Modes)				
d	2	1	90	$p+n$				
t	3	1	108	$d+n$				
^{3}He	3	2	108	$d+p$				
^{4}He	4	2	115	^{3}He+n	$t+p$	$d+d$		
^{6}He	6	2	150	$t+t$				
^{6}Li	6	3	150	t+^{3}He	^{4}He+d			
^{7}Li	7	3	150	t+^{4}He	^{6}Li+n			
^{8}Li	8	3	150	^{7}Li+n	^{6}He+d			
^{9}Li	9	3	150	^{8}Li+n	^{6}He+t			
^{7}Be	7	4	150	^{3}He+^{4}He	^{6}Li+p			
^{9}Be	9	4	150	^{8}Li+p	^{7}Li+d			
^{10}Be	10	4	150	^{9}Be+n	^{8}Li+d			
^{10}B	10	5	150	^{9}Be+p	^{7}Li+^{3}He	^{6}Li+^{4}He		
^{11}B	11	5	150	^{10}B+n	^{9}Be+d	^{7}Li+^{4}He		
^{12}B	12	5	150	^{11}B+n	^{10}Be+d	^{8}Li+^{4}He		
^{11}C	11	6	150	^{10}B+p	^{7}Be+^{4}He			
^{12}C	12	6	150	^{11}C+n	^{11}B+p	^{10}B+d	^{9}Be+^{3}He	^{6}Li+^{6}Li

MCNP6 and will be described in a later section. Preliminary results from extending the coalescence model in LAQGSM03.03F also yield promising results.

We recommend further improvement of the coalescence model in the CEM, to include more heavy clusters, such as ^{8}Li and ^{9}Li, etc. The coalescence model favors the formation of neutron-rich heavy clusters for heavy targets, due to the presence of more neutrons than protons produced in the INC. We expect that the predictions for the spectra for these neutron-rich heavy clusters could be improved by such a coalescence extension. In this further improvement of the coalescence model, we also recommend including the Coulomb barrier, now ignored, to limit low-energy production.

VI. PREEQUILIBRIUM —γ_j MODEL

After the extension of the preequilibrium model to allow emission of light fragments up to ^{28}Mg, the implementation of the NASA-Kalbach total reaction cross sections into the preequilibrium stage as inverse cross sections, and the extension of the coalescence model, we turned our attention to recalibrating γ_j. This involves the re-fitting of all available reliable experimental data. We have concluded this process for most available proton-induced and neutron-induced reactions.

The condensation probability, γ_j, is an important quantity in the preequilibrium stage of nuclear spallation reactions. It represents the probability that p_j excited nucleons (excitons) will condense to form a complex particle of type j in the excited residual nucleus. It has a significant impact on the emission width, or probability of emitting a fragment of type j from the residual nucleus (Betak, 1976; Cline, 1972; Ribansky *et al.*, 1973). In this section we explore the formulation of a new model for γ_j, one which is energy-dependent, and which provides improved fits compared to experimental fragment spectra.

A. Background

CEM03.03F considers the possibility of fast heavy cluster emission at the preequilibrium stage of a reaction, in addition to the emission of nucleons and light fragments up to ^{4}He, according to Eqs. (4) and (16). We assume that in the course of a reaction p_j excited nucleons (excitons) are able to condense with probability γ_j forming a complex particle which can be emitted during the preequilibrium stage. The condensation probability γ_j could be calculated from first principles, but such a calculation is not feasible given practical Monte-Carlo computational time limitations. γ_j is, therefore, estimated as the overlap integral of the wave function of independent nucleons with that of the complex particle (see details in (Gudima *et al.*, 1983)), as shown in Eq. (6) and repeated here:

$$\gamma_j \simeq p_j^3 (p_j/A)^{p_j-1} \ . \tag{23}$$

This is a rather crude estimate. As is frequently done (see e.g., Refs. (Blideanu *et al.*, 2004; Wu and Chang, 1978)), the values of γ_j are taken from fitting the theoretical preequilibrium spectra to the experimental ones.

In CEM, to improve the description of preequilibrium complex-particle emission, we estimate γ_j by multiplying the estimate provided by Eq. (23) by empirical coefficients $F_j(A, Z, T_0)$, whose values are fitted to available nucleon-induced experimental complex-particle spectra. Therefore, the new equation for γ_j using this empirical coefficient is

$$\gamma_j = F_j p_j^3 \left(\frac{p_j}{A}\right)^{p_j - 1}. \quad (24)$$

Values of F_j for d, t, ^{3}He, and ^{4}He need to be re-fit after the upgrades to the inverse-cross-section and coalescence models, and values of F_j need to be obtained for heavy clusters up to ^{28}Mg, once the model is extended to emit these heavy clusters.

Previously, γ_j had been formulated with no energy dependence (Betak, 1976; Cline, 1972; Ribansky and Oblozinsky, 1973). However, we expect energy to be the largest effect on the model for F_j. The importance of γ_j can be seen in the calculation of the emission width, Γ_j, for complex fragments, represented by Eqs. (4) and (16). The value for γ_j directly impacts the emission width, which in turn determines the amount of fragment production.

B. Statistical Analysis

An increase or decrease in F_j generally leads to an increase or decrease in the emission of fragment type j, especially in the high-energy tails. We fit these values of F_j so that CEM03.03F results match experimental data as closely as possible. The F_j values obtained for several hundred reactions, are available in Ref. (Kerby, 2015b). The results for predicted fragment spectra using these fitted F_j values were plotted and compared to experimental data and calculated results from the original CEM03.03, for the several hundred reactions fitted, and are available in (Kerby and Mashnik, 2015b). We do not show them here to conserve space.

We analyze the complete data set with the statistical programming language *R* (Venables *et al.*, 2015). We first look at F_j values for proton-induced reactions. Fig. 18 displays values of F_j as a function of incident proton energy. Two effects are apparent. First, F_j appears to have an exponentially decreasing energy dependence, at least up to very roughly 1 GeV proton energy. This saturating energy dependence for higher energies makes sense, considering the physics of the reactions. This F_j model depends on the incident energy of the incoming proton, not the excitation energy of the residual nucleus at the time of the preequilibrium decay. As the energy increases, eventually most of the additional energy in the system leads to emission of more cascade particles, with the energy remaining in the composite system at the beginning of the preequilibrium decay, apparently reaching

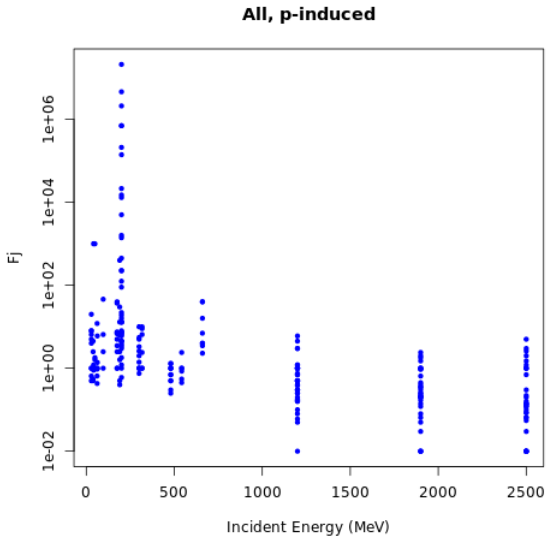

FIG. 18 Values of F_j as functions of incident proton energy (MeV).

a limiting value, as seems to be reflected in the approximate constancy of the values of F_j above about 1–1.5 GeV. This idea is analogous to 'limiting fragmentation' (Benecke *et al.*, 1969; El-Nagdy *et al.*, 2013). In addition, CEM accounts for the INC, preequilibrium, evaporation/fission, Fermi break-up, and coalescence mechanisms of reactions, but does not account for pick-up and knock-out (direct) reactions. Direct-reaction mechanisms are especially important at low energies; therefore, the increase in F_j at lower incident energies can be partially attributed to compensating for this physics missing in CEM. Furthermore, CEM does not include most nuclear-structure effects, also important at low energies for some reactions. Finally, CEM, like any model simple enough to be practical as a nuclear event generator in a transport code, will miss some aspects of the relevant physics. For these reasons, we need to look at the model for γ_j in CEM pragmatically, understanding that in some energy/target-size regions, it will not have exactly the right meaning of the condensation probability, also containing a component approximating physics not directly modeled in CEM.

The second effect in Fig. 18 is the presence of 'stacks' of F_j values at each energy; these correspond to different target sizes and different emitted fragment sizes; this means F_j is also dependent on the target and emitted fragment, in addition to the incident energy.

Fig. 19 displays F_j values as functions of both energy and target mass number. We restricted this plot to F_j values < 1000, as there are some very large values for F_j at low energies, which, if included would make it difficult to see any patterns. Some sense of the target-size dependence F_j appears, but it is still somewhat obscured by

including all different emitted fragment sizes.

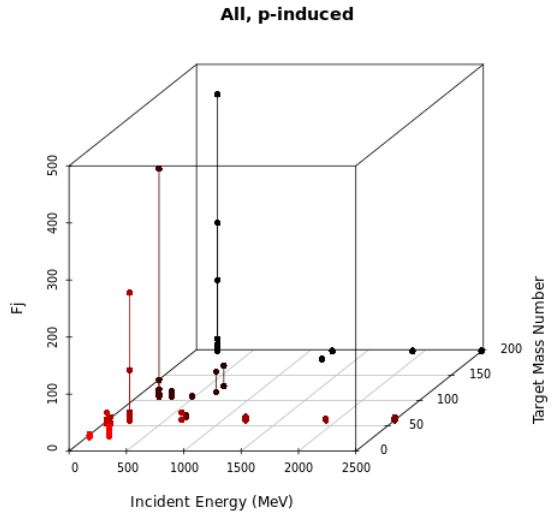

FIG. 19 Values of F_j as a function of the incident proton energy (MeV) and mass number of the target.

We also plot in (Kerby, 2015a) F_j as a function of target size for each emitted fragment type; a sample plot for ^{6}Li is shown in Fig. 20. In these plots, F_j appears to decrease as target size increases. Such a conclusion is due to all different incident energies being included. As we will show, the incident energy is the dominant variable in F_j; therefore, by including all incident energies, we obscure any valid conclusions about variables of secondary importance.

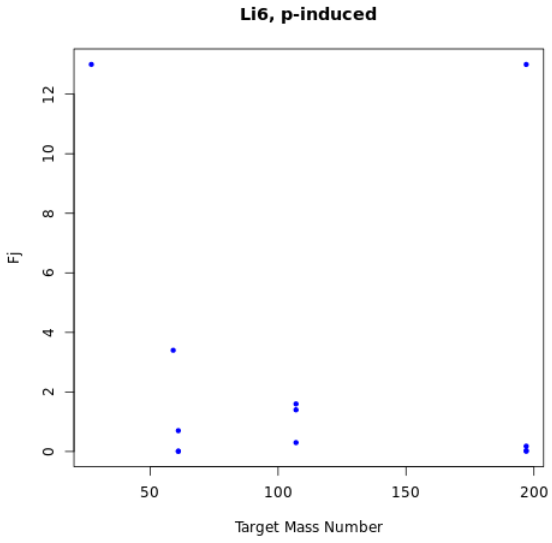

FIG. 20 Values of F_j for the emitted fragment ^{6}Li for all energies as a function of target mass number.

Plotting F_j as a function of both incident energy and target size for each individual emitted fragment leads to the emergence of a different pattern; namely, that F_j increases as target size increases (see Fig. 22, with similar plots for different fragments available in Ref. (Kerby, 2015b)).

We have established that F_j is dependent upon incident energy, target size, and fragment size. We assume for mathematical simplicity that the dependencies on incident energy and target size are separable, and that the target-size dependence is independent of fragment size.

1. Fragment-Specific F_j

We then assume an F_j model which has the form

$$F_j(T_0, A_j, Z_j, A_t) = f(T_0, A_j, Z_j)g(A_t), \qquad (25)$$

where T_0 is the incident energy of the projectile (MeV), A_j is the mass number of the emitted fragment of type j, Z_j is the atomic number of the emitted fragment of type j, and A_t is the mass number of the target nucleus.

A simple exponential decay describes $g(A_t)$ quite well. We define it so that it is valid for all $A_t < 300$. Unsurprisingly, a suitable model for the three-variable function $f(T_0, A_j, Z_j)$ proves more difficult to obtain. All common distributions have been tested and none of them are able to describe both the low-energy and high-energy dependencies of F_j. We therefore used one function (an exponential decay) to describe the energy dependence at low energies, and a $1/T_0^\alpha$ form to describe the dependence at high energies. For the $1/T_0^\alpha$ term, we rather arbitrarily add 100 to the denominator T_0^α to ensure no singularities in the range of conceivable energies. These two different energy dependencies make sense considering the previous discussion about CEM lacking some important physics in the low-energy region, and therefore the F_j model is compensating for missing physics in that region. In the higher-energy region, the CEM is reliable enough. We also find that for lighter LF (^{4}He and below), dependence on target size disappears. Equations for some of the lighter specific fragment types for which there is sufficient data are displayed in Eq. 26.

Examples of fits are shown in Figs. 21 and 22. More results are available in (Kerby, 2015a).

2. Neutron-Induced Reactions

After obtaining a fragment-specific F_j model for proton-induced reactions, we next consider neutron-induced reactions. There is less experimental data available for neutron-induced reactions, due to the difficulty of conducting these experiments. There is also no experimental data on the emission of light fragments heavier than ^{4}He, in an energy range of interest for this paper.

$$
\begin{aligned}
F_d &= -3e^{-T_0/20} + \frac{125}{T_0^{0.2}+100};\\
F_t &= 20e^{-T_0/20} + \frac{175}{T_0^{0.4}+100};\\
F_{^3He} &= 20e^{-T_0/20} + \frac{250}{T_0^{0.6}+100};\\
F_{^4He} &= 100e^{-T_0/20} + \frac{1000}{T_0^{0.8}+100};\\
F_{^6He} &= \left[1.4e5e^{-T_0/20} + \frac{1400}{T_0^{1.2}+100}\right]e^{-\frac{300-A_t}{100}};\\
F_{^6Li} &= \left[4.0e5e^{-T_0/20} + \frac{5000}{T_0^{1.2}+100}\right]e^{-\frac{300-A_t}{100}};\\
F_{^7Li} &= \left[1.0e6e^{-T_0/20} + \frac{2.5e4}{T_0^{1.4}+100}\right]e^{-\frac{300-A_t}{100}};\\
F_{^8Li} &= \left[2.5e6e^{-T_0/20} + \frac{1.0e5}{T_0^{1.6}+100}\right]e^{-\frac{300-A_t}{100}};\\
F_{^9Li} &= \left[6.25e6e^{-T_0/20} + \frac{4.0e5}{T_0^{1.8}+100}\right]e^{-\frac{300-A_t}{100}};\\
F_{^7Be} &= \left[1.0e6e^{-T_0/20} + \frac{5000}{T_0^{1.2}+100}\right]e^{-\frac{300-A_t}{100}};\\
F_{^9Be} &= \left[6.25e6e^{-T_0/20} + \frac{1.0e5}{T_0^{1.6}+100}\right]e^{-\frac{300-A_t}{100}};\\
F_{^{10}Be} &= \left[1.56e7e^{-T_0/20} + \frac{4.0e5}{T_0^{1.8}+100}\right]e^{-\frac{300-A_t}{100}};\\
F_{^{10}B} &= \left[1.56e7e^{-T_0/20} + \frac{1.5e5}{T_0^{1.6}+100}\right]e^{-\frac{300-A_t}{100}};\\
F_{^{11}B} &= \left[3.9e7e^{-T_0/20} + \frac{6.0e5}{T_0^{1.8}+100}\right]e^{-\frac{300-A_t}{100}};\\
F_{^{12}B} &= \left[9.75e7e^{-T_0/20} + \frac{2.4e6}{T_0^{2.0}+100}\right]e^{-\frac{300-A_t}{100}};\\
F_{^{12}C} &= \left[9.75e7e^{-T_0/20} + \frac{6.0e5}{T_0^{1.8}+100}\right]e^{-\frac{300-A_t}{100}};\\
F_{^{13}C} &= \left[2.44e8e^{-T_0/20} + \frac{2.4e6}{T_0^{2.0}+100}\right]e^{-\frac{300-A_t}{100}}.
\end{aligned}
\tag{26}
$$

Therefore, for LF heavier than ^{4}He, we use the fragment-specific F_j model developed for proton-induced reactions as a first guess. The F_j equations for d, t, ^{3}He, and ^{4}He for neutron-induced reactions are presented in Eq. 27, and are similar to the respective F_j equations obtained for these emitted fragments for proton-induced reactions.

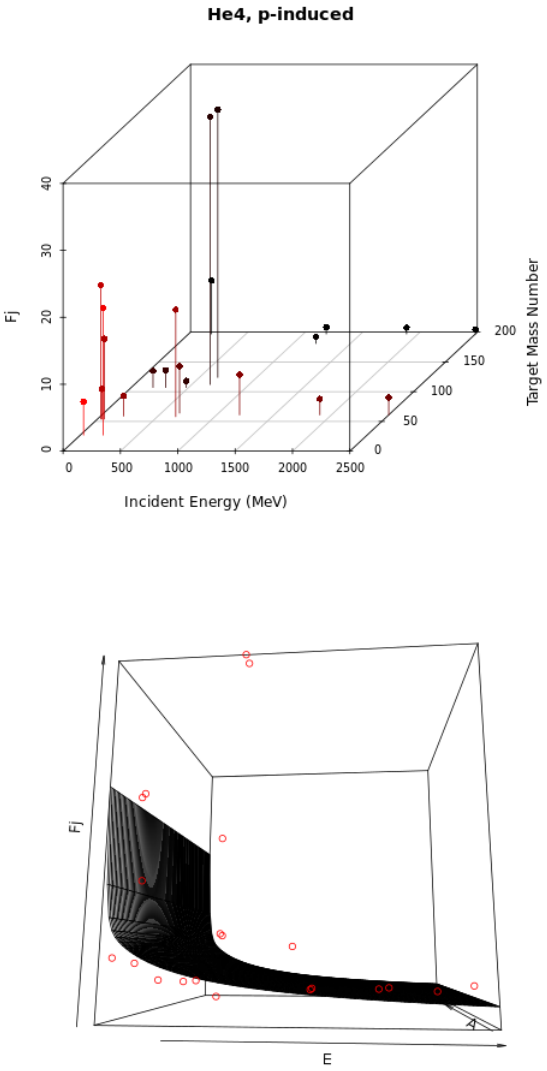

FIG. 21 Fitted values of F_j (upper plot) and the F_j model (lower plot) for ^{4}He fragments, as functions of incident proton energy (MeV) and the target mass number.

$$
\begin{aligned}
F_d &= -4.5e^{-T_0/20} + \frac{187.5}{T_0^{0.2}+100};\\
F_t &= -6.75e^{-T_0/20} + \frac{281}{T_0^{0.2}+100};\\
F_{^3He} &= 30e^{-T_0/20} + \frac{375}{T_0^{0.6}+100};\\
F_{^4He} &= 500e^{-T_0/20} + \frac{5000}{T_0^{0.8}+100}.
\end{aligned}
\tag{27}
$$

Examples of these fits compared to data can be found in Ref. (Kerby, 2015a).

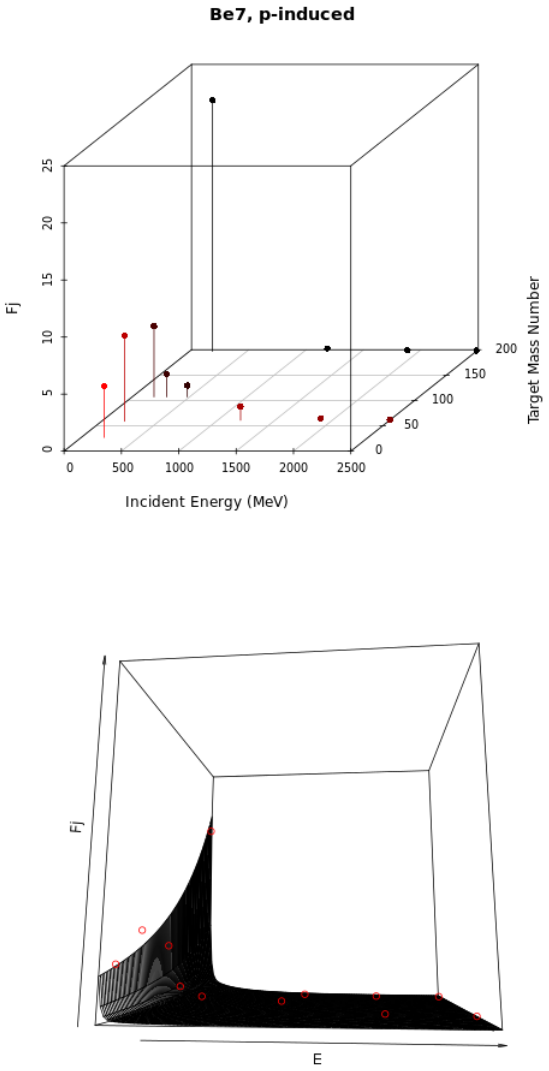

FIG. 22 Fitted values of F_j (upper plot) and the F_j model (lower plot) for ^{7}Be fragments as functions of incident proton energy (MeV) and the target mass number.

3. General F_j Model

In studying the fragment-specific equations for F_j in Eq. 26, a pattern quickly emerges. Heavy clusters can be nicely generalized as approximately Eq. 28:

$$F_j(T_0, A_j, Z_j, A_t) = \left[7800(2.5)^{A_j} e^{-T_0/20} + \frac{2(4)^{\tau}}{T_0^{0.2\tau} + 100}\right] \times e^{-\frac{300-A_t}{100}}, \quad \tau = A_j - (Z_j - 3). \tag{28}$$

This general form is used for heavy clusters for which we do not have sufficient data: ^{8}He, ^{11,12}Be, ^{8,13}B, ^{10,11,14,15,16}C, and all fragments with $Z \geq 7$ (up to ^{28}Mg).

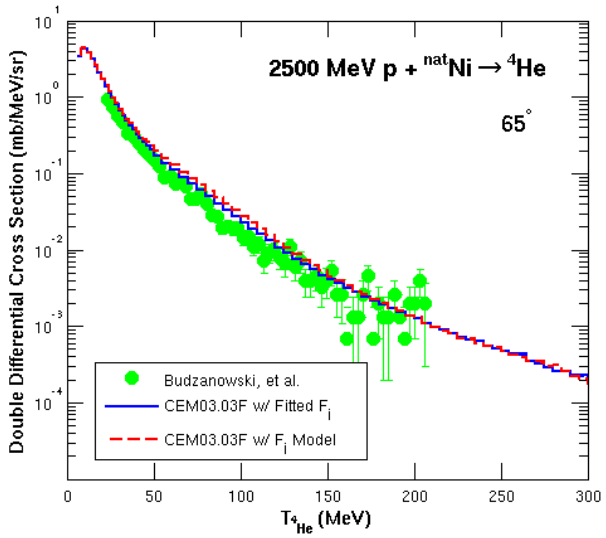

FIG. 23 Comparison of experimental data by Budzanowski, et al. (Budzanowski *et al.*, 2010) (green circles) to results from CEM03.03F with the fitted F_j values (blue solid lines) and to CEM03.03F with the F_j model (red dashed lines) for 2500 MeV p + ^{nat}Ni → ^{4}He,^{7}Be.

Recall that γ_j can theoretically be calculated from first principles, but that this is too computationally time-consuming. We then wish to obtain a γ_j model that is both reasonably accurate and computationally fast. This F_j model (and therefore, γ_j model) accomplishes both of these; it is computationally simple and very fast, and it provides reasonably accurate fragment spectra when compared to experimental results.

C. Spectra with Fitted F_j Compared to Spectra from the F_j Model

For the large majority of reactions tested, the predicted fragment spectra using the F_j model were very similar to the predicted fragment spectra using the fitted F_j values. Fig. 23 gives an example, comparing results from the F_j model to those from the fitted F_j values. Many more comparisons can be found in (Kerby, 2015a; Kerby and Mashnik, 2015b). Oftentimes the F_j model leads to slightly softer spectra; usually giving an improved match to data compared to the model with fitted F_j values.

There were a handful of reactions for which the predicted spectra of a few particular fragment types varied significantly, specifically for the emission of heavier clusters with $A \geq 8$ from reactions with low incident energies and heavy targets. For an example of this, we show the spectra of ^{8}Li in Fig. 24. While the discrepancy is significant, it is not always negative, as sometimes the fitted values were overfit (meaning that the fit compromised accuracy in the high-energy tails to achieve a higher low-energy peak; however, a more productive way to address

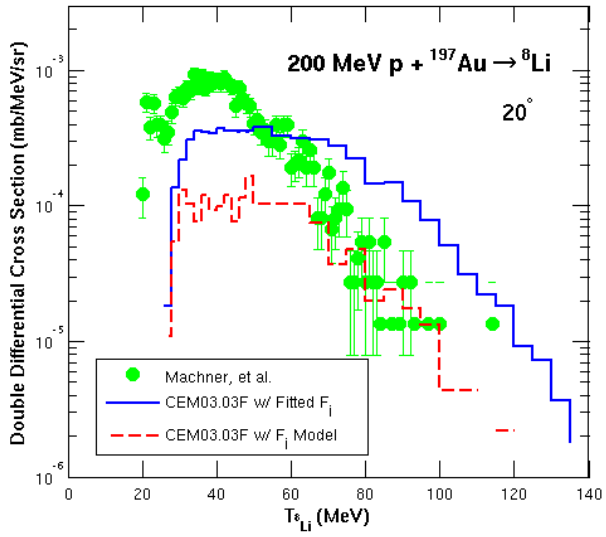

FIG. 24 Comparison of experimental data by Machner, et al. (Machner *et al.*, 2006) (green circles) to results from CEM03.03F using fitted F_j (blue solid lines) and to CEM03.03F using the F_j model (red dashed lines) for 200 MeV p + ^{197}Au → ^{8}Li.

this is to retain accuracy in the high-energy tails and upgrade our evaporation model to attain an improved prediction at the peak). We believe this difference is due to several factors. First, the extended coalescence model emits heavy clusters up to $A = 7$; this leads to a jump in the fitted F_j values for emitted heavy clusters with $A > 7$ as it is compensating for the lack of coalescence emission, compared to those with $A \leq 7$. However, as the F_j model is a smooth model, it cannot completely account for this jump. We expect that extending the coalescence model to larger fragments will reduce this effect. In addition, while we assumed for simplicity that the target-size dependence was independent of the fragment size and the incident energy, this is not strictly the case. The target-size dependence does, in fact, become more pronounced with increasing fragment size. We excluded target-size dependence from emitted ^{4}He and lighter fragments, and included this term for heavier clusters, to partially account for this. However, the greater the fragment size, the less valid this constant-target-size assumption becomes. Lastly, the target-size dependence also does vary with the incident energy (contrary to our assumption), becoming more significant at lower incident energies and less significant at higher incident energies. Thus, for the emission of heavier clusters at low incident energies on heavy targets, we expect a 'perfect storm' of factors to create significant discrepancies between the F_j model and the fitted F_j values. However, since this discrepancy is not always negative, it sometimes leads to either improved fits with experimental data or to more natural spectra. Furthermore, the ^{8}Li spectrum of Fig. 24 demonstrate the need to upgrade the evaporation model, as it primarily produces the peak of the spectrum, which is too low for this reaction. We hope to do this in the future.

D. Conclusion

While γ_j can be theoretically calculated from first principles, this is too computationally time-consuming. We therefore wish to obtain a γ_j model that is both reasonably accurate and computationally fast. The F_j model (and therefore, γ_j model) accomplishes both of these: it is computationally simple and very fast, and it provides reasonably accurate fragment spectra when compared to experimental results.

This γ_j model is specifically designed for use in CEM, taking into account the reaction mechanisms used (or not used) in CEM. However, this model could be useful in other nuclear spallation codes and models, especially for heavy cluster production, with proper readjustment of some parameters.

In conclusion, this γ_j model provides better agreement with experimental data than the old interpolation fits used in CEM03.03, especially for heavy-cluster spectra. We plan to apply this to LAQGSM as well, and discuss implementation into MCNP6 in Section VIII.

VII. TESTING THE PREDICTIVE POWER OF CEM03.03F

Results of the upgraded CEM03.03, called CEM03.03F, are shown in this section and in Section VIII, and are compared to the original CEM03.03 and to experimental results. The most important tests of CEM03.03F are of its predictions for reactions not used in fitting or previously considered in the upgrades. These nonfitted results are shown in Sections VII.C and VII.D. To be clear, the CEM03.03F referred to in this section includes the extended modified exciton model, the upgraded NASA-Kalbach inverse cross sections within the preequilibrium stage, the extended coalesence model, and the new γ_j model. (The cut-off for Fermi breakup was left at $A_{Fermi} = 12$.) For more details on these upgrades, see Refs. (Kerby and Mashnik, 2014, 2015a,b,c,d; Kerby *et al.*, 2014a,b; Mashnik and Kerby, 2014).

A. Fragment Spectra for Proton-Induced Reactions

Double differential cross section spectra for several reactions are plotted in Figs. 25–27, comparing experimental data with results from CEM03.03 and CEM03.03F for proton-induced reactions. Similar results from MCNP6 are presented in Section VIII. Still more extensive results

are found in Ref. (Kerby, 2015b). CEM03.03F, in general, has improved results over the original CEM03.03, especially for heavy-cluster spectra.

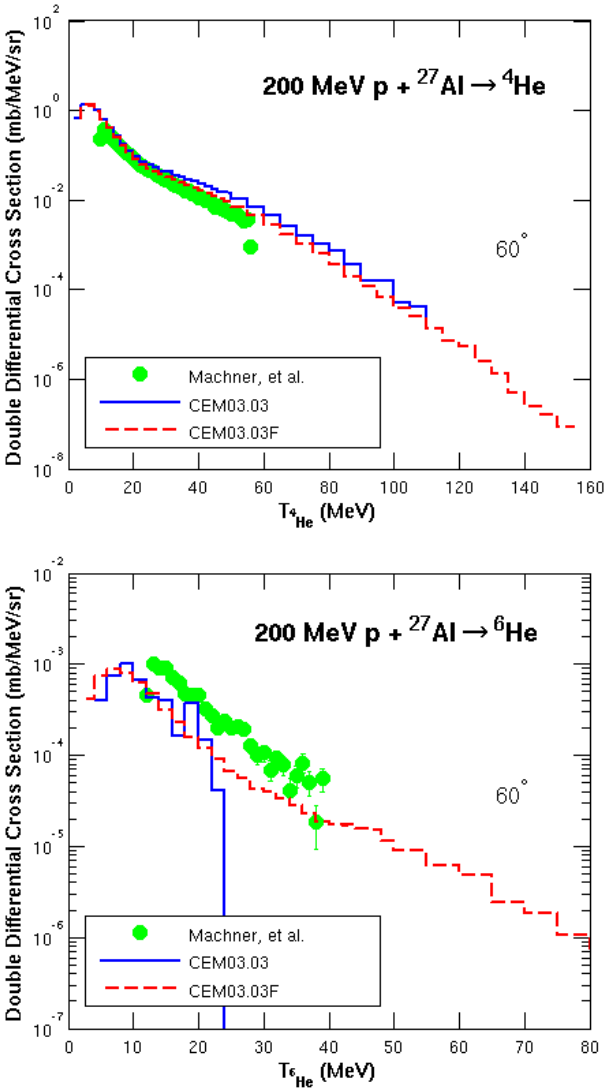

FIG. 25 Comparison of experimental data measured by Machner, et al. (Machner *et al.*, 2006) (green circles) to results from CEM03.03 (blue solid lines) and from CEM03.03F (red dashed lines) for 200 MeV p + ^{27}Al → ^{4,6}He at 60°.

Fig. 25 shows the results for 200 MeV p + ^{27}Al → ^{4,6}He at 60° compared to experimental data by Machner, et al. (Machner *et al.*, 2006). The ^{4}He spectrum demonstrate that CEM03.03F achieves increased production of heavy clusters without destroying the established spectra of nucleons and light fragments up to ^{4}He (in this particular case only ^{4}He), while in some cases it even achieves improved results for nucleons and light fragments up to ^{4}He. The spectrum of ^{6}He from CEM03.03F shows a significant improvement.

Fig. 26 illustrates calculated results for 200 MeV p + ^{59}Co → ^{9}Li at 60°, compared to experimental data

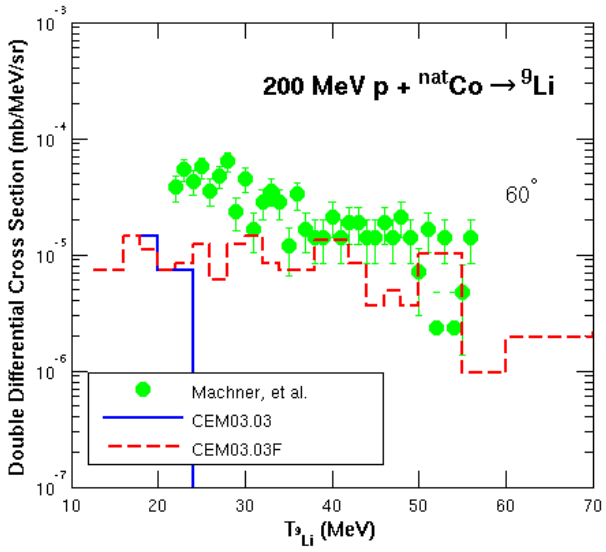

FIG. 26 Comparison of experimental data from 200 MeV p + ^{59}Co → ^{9}Li measured by Machner, et al. (Machner *et al.*, 2006) (green circles) to results from CEM03.03 (blue solid lines) and from CEM03.03F (red dashed lines).

measured by Machner, et al. (Machner *et al.*, 2006). This figure demonstrates results for a rare, neutron-rich lithium isotope. There is dramatic improvement in the production of high-energy ^{9}Li with CEM03.03F. This figure again highlights the need to improve the evaporation model, as the low-energy cross-section peak, produced largely by evaporation, is too low.

Fig. 27 shows calculated results for 1200 MeV p + ^{nat}Ni → ^{7}Li at 15.6°, compared to experimental data measured by Budzanowski, et al. (Budzanowski *et al.*, 2010). CEM03.03F reproduces the experimental data significantly better than does the original CEM03.03.

B. Fragment Spectra for Neutron-Induced Reactions

Figs. 28–30 compare examples of experimental data to results from the unmodified CEM03.03 and from CEM03.03F for neutron-induced reactions. CEM03.03F generally has very similar results for the spectra of emitted fragments up to ^{4}He. Since there are no experimental data for heavier clusters, we cannot evaluate the improved model. However, CEM03.03F gives results that are at least no worse than the current CEM03.03. More results are available in Ref. (Kerby, 2015b).

Fig. 28 displays the calculated results for 96 MeV n + ^{nat}U → p at 20°, compared to experimental data measured by Blideanu, et al. (Blideanu *et al.*, 2004). This figure illustrates the consistency between results from CEM03.03F and CEM03.03 for nucleons, which we also find in other reactions for light fragments no heavier than ^{4}He. Fig. 29 demonstrates this for 317 MeV n + ^{209}Bi →

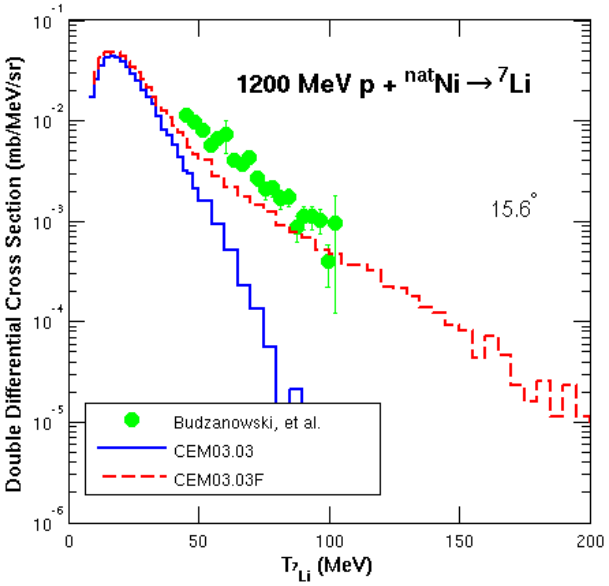

FIG. 27 Comparison of experimental data for 1200 MeV p + ^{nat}Ni → ^{7}Li at 15.6°, measured by Budzanowski, et al. (Budzanowski *et al.*, 2010) (green circles) to results from CEM03.03 (blue solid lines) and to those from CEM03.03F (red dashed lines).

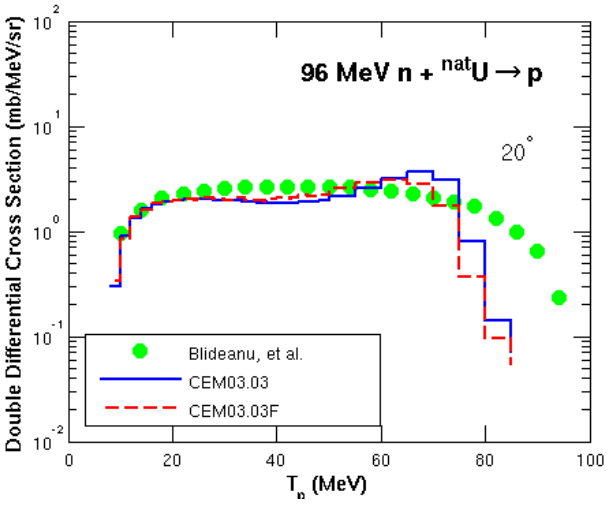

FIG. 28 Comparison of experimental data measured by Blideanu, et al. (Blideanu *et al.*, 2004) (green circles) to results by CEM03.03 (blue solid lines) and to CEM03.03F (red dashed lines) for 96 MeV n + ^{nat}U → p at 20°.

at 54°, with experimental data measured by Franz, et al. (Franz *et al.*, 1990). These two figures illustrate that the improved production of heavy clusters in CEM03.03F has not destroyed the spectra of particles and light fragments of mass 4 and below.

Fig. 30 shows the results for 542 MeV n + ^{nat}Cu → ^{6}Li at 68°. This figure is a first test of the modeling of the production of heavy clusters from neutron-induced

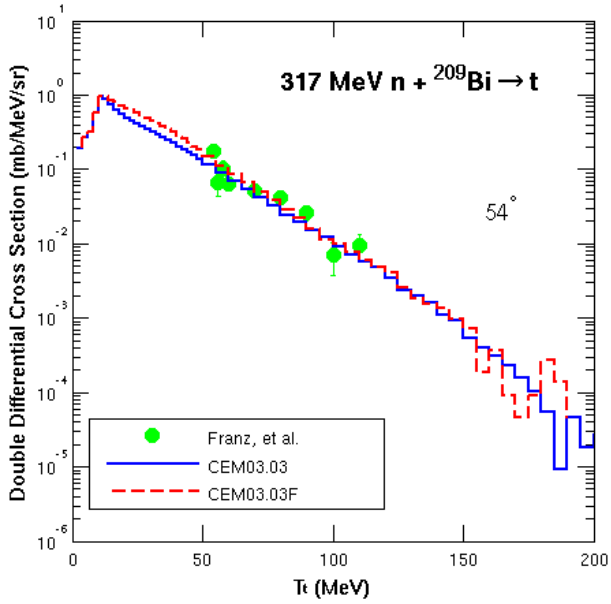

FIG. 29 Comparison of experimental data measured by Franz, et al. (Franz *et al.*, 1990) (green circles) to results from CEM03.03 (blue solid lines) and from CEM03.03F (red dashed lines) for 317 MeV n + ^{209}Bi → t at 54°.

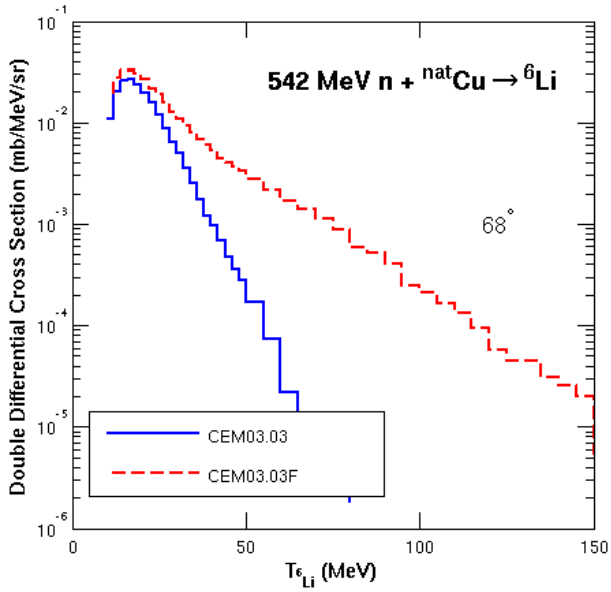

FIG. 30 Comparison of predicted spectra of 542 MeV n + ^{nat}Cu → ^{6}Li at 68° from CEM03.03 (blue solid lines) and from CEM03.03F (red dashed lines).

reactions in CEM03.03F. We hope to be able to compare predictions to other experimental data of heavy-cluster spectra from neutron-induced reactions in the future.

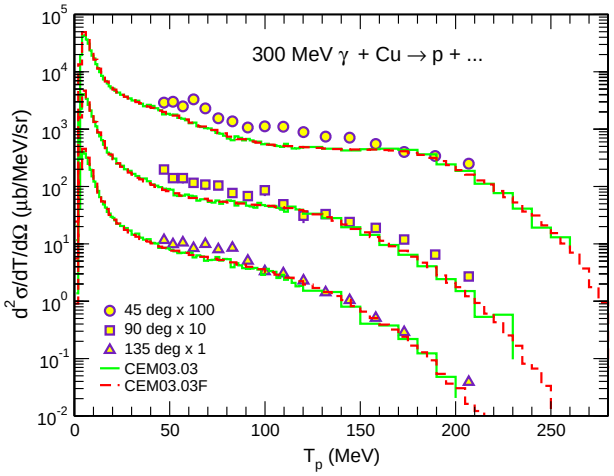

FIG. 31 Comparison of experimental data from Schumacher, et al. (Schumacher *et al.*, 1982) (filled symbols) to results from the unmodified CEM03.03 (green solid lines) and to those from CEM03.03F (red dashed lines) for 300 MeV γ + ^{nat}Cu $\rightarrow$ p at 45°, 90°, and 135°.

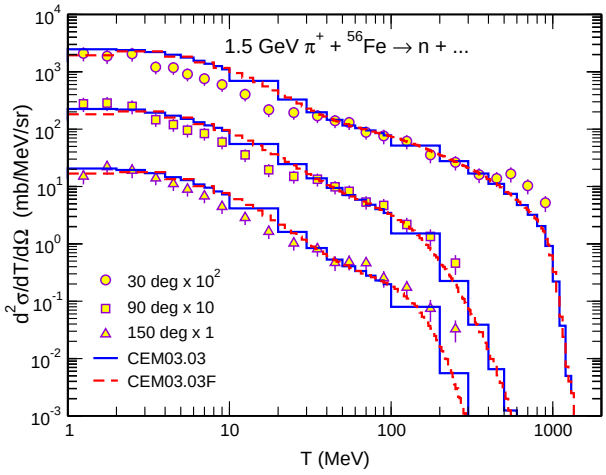

FIG. 32 Comparison of experimental data from Nakamoto, et al. (Nakamoto *et al.*, 1997) (filled symbols) to results from the unmodified CEM03.03 (blue solid lines) and to CEM03.03F (red dashed lines), for 1500 MeV π^+ + ^{nat}Fe $\rightarrow$ n at 30°, 90°, and 150°.

C. Fragment Spectra from γ- and π-Induced Reactions

Figs. 31–32 compare examples of experimental data to results from CEM03.03 and CEM03.03F for γ- and π-induced reactions. CEM03.03F generally is little different from CEM03.03 for the spectra of emitted fragments up to ^{4}He, and as there is no appropriate experimental data for emitted heavier clusters, we cannot evaluate the improved model for heavy clusters for these non-nucleonic projectiles. However, the upgraded code, while now able to predict the emission of the heavier clusters, gives very similar results to the original for nucleons and clusters with fewer than five nucleons.

Fig. 31 shows the results for 300 MeV γ + ^{nat}Cu $\rightarrow$ p at 45°, 90°, and 135°compared to experimental data by Schumacher, et al. (Schumacher *et al.*, 1982). This figure illustrates the consistency of CEM03.03F and CEM03.03 for spectra of ^{4}He and lighter fragments for γ-induced reactions.

Fig. 32 shows the model results for 1500 MeV π^+ + ^{nat}Fe $\rightarrow$ n at 30°, 90°, and 150°, compared to experimental data from Nakamoto, et al. (Nakamoto *et al.*, 1997). This figure provides an example of the consistency between CEM03.03F and CEM03.03 for spectra of ^{4}He and lighter fragments for π-induced reactions.

D. Product Yields

Fig. 33 shows the measured (Benlliure *et al.*, 2001; Rejmund *et al.*, 2001) mass and charge distributions of the product yields from the reaction 800 MeV p + ^{197}Au, and of the mean kinetic energy of these products, and the mass distributions of the cross sections for the production of thirteen elements with atomic number Z from 20 to 80, compared to predicted results from the original CEM03.03 and from CEM03.03F. The results are essentially identical for the two code versions for these observables.

Fig. 34 shows the measured (Bernas *et al.*, 2003; Taieb *et al.*, 2003) mass and charge distributions of the product yields from the reaction 1000 MeV p + ^{nat}U, and of the mean kinetic energies of these products, compared to results from the unmodified CEM03.03 and from CEM03.03F. The results are essentially identical for the two code versions for these observables.

Fig. 35 shows the measured (Fomichev *et al.*, 2005; Tarrío *et al.*, 2011) fission cross sections for n + Bi, compared to results from CEM03.03 and from CEM03.03F. CEM03.03F agrees reasonably well with these new data on n + Bi fission cross sections, and even shows an improvement around energies of 100 MeV. But, because CEM03.03F considers emission of LF at the preequilibrium stage, the mean values of A, Z, and E of the fissioning nuclei differ somewhat from the values in CEM03.03; therefore, to improve the description of fission cross sections, and of the yield of fission fragments, a refitting of the energy-dependent a_f/a_n parameters in CEM03.03F would be desirable. All details on the RAL and GEM2 codes and all formulas used in them to calculate σ_f can be found in Refs. (Atchison, 2007; Furihata, 2000). We mention here only that in the case of subactinide nuclei, the main parameter that determines fission cross sections calculated by GEM2 is the level-density parameter in the fission channel, a_f (or more exactly, the ratio a_f/a_n, where a_n is the level-density parameter for neutron evaporation). The task of improving the fission model of CEM03.03F is outside the scope of this paper,

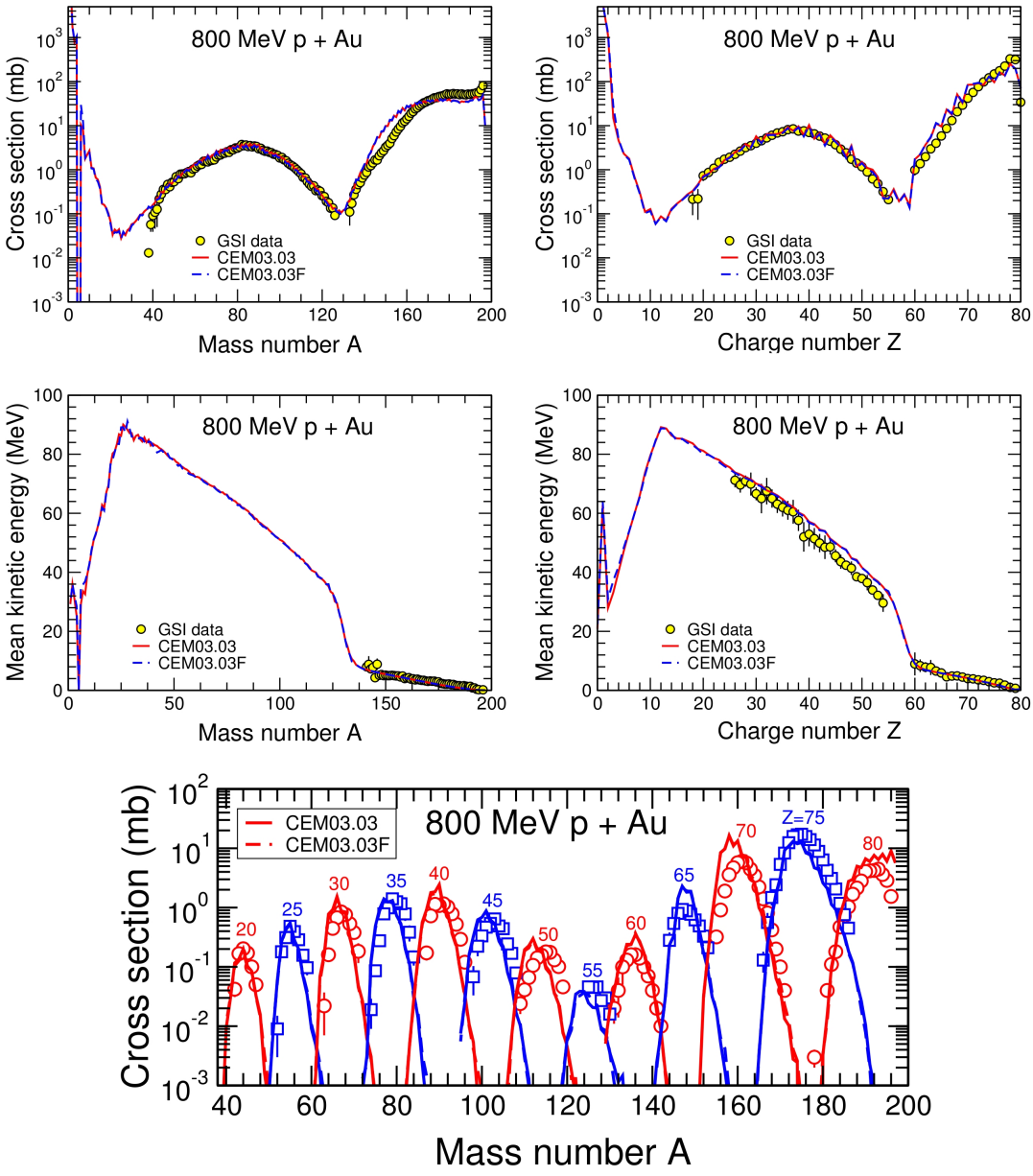

FIG. 33 Comparison of measured (Benlliure *et al.*, 2001; Rejmund *et al.*, 2001) mass and charge distributions of the product yields from the reaction 800 MeV p + ^{197}Au, and of the mean kinetic energies of these products, and the mass distributions of the cross sections for the production of thirteen elements with the atomic number Z ranging from 20 to 80 (open symbols), with predicted results from the original CEM03.03 (solid lines) and from CEM03.03F (dashed lines).

but we hope to perform this effort at a later time, to further improve CEM03.03F.

E. Computational Time Considerations

As CEM03.03 is the default event generator within MCNP6, its ability to run simulations quickly is important. We tested the impact of the upgrades on computation time with each incremental upgrade, and found either no significant increase or only a small increase in computation time. We test the cumulative effect of all of the upgrades on computation time in this section.

Adding all of the upgrades increases the computation time by approximately one-third, depending upon the incident energy and target nucleus. Considering the comprehensive nature of the upgrades, and the dramatic improvements made to the production of heavy clusters, this seems to be a relatively small increase.

If the production of energetic heavy clusters is not

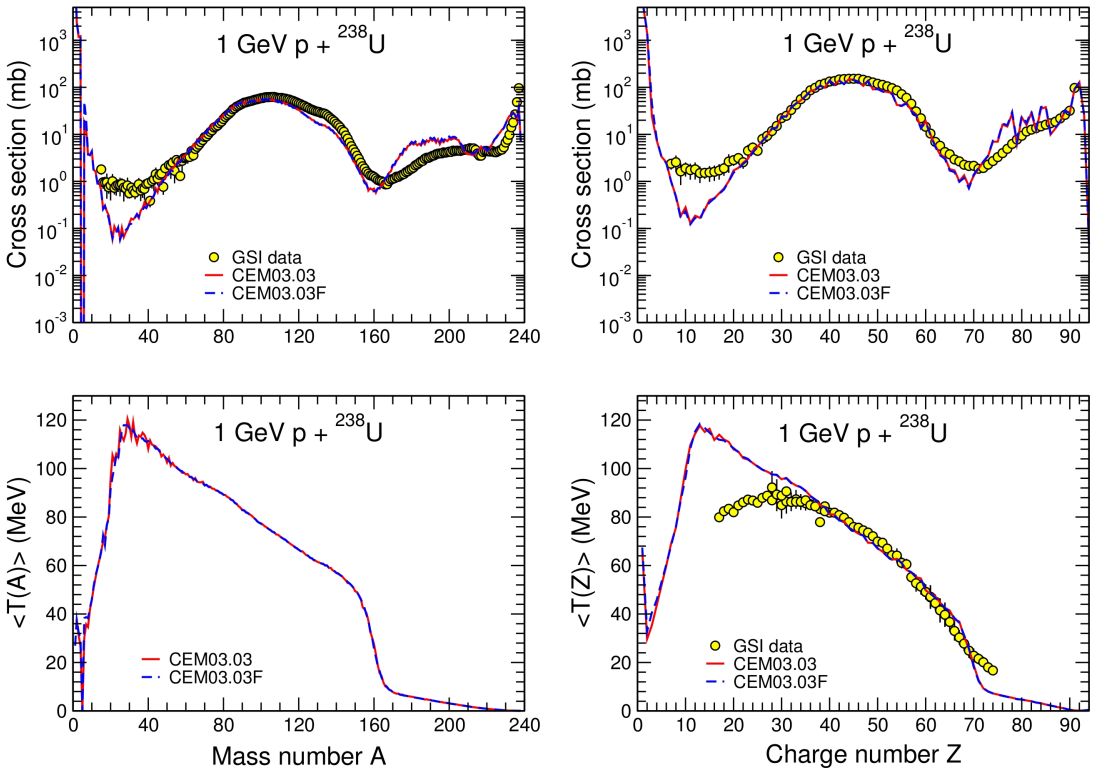

FIG. 34 Comparison of measured (Bernas *et al.*, 2003; Taieb *et al.*, 2003) mass and charge distributions of the products from the reaction 1000 MeV p + ^{nat}U, and of the mean kinetic energies of these products (colored circles), to results by the unmodified CEM03.03 (red solid lines), and to CEM03.03F (blue dashed lines).

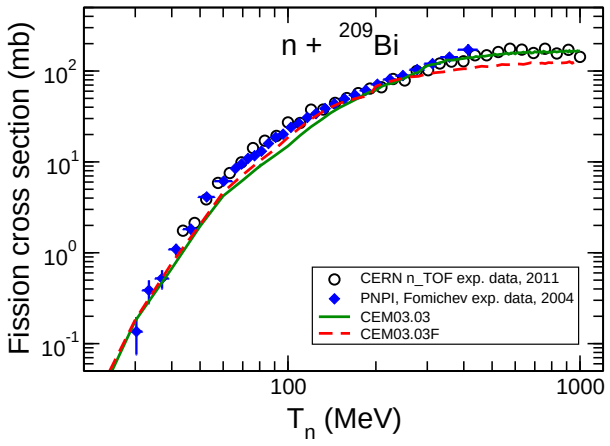

FIG. 35 Comparison of measured (Fomichev *et al.*, 2005; Tarrío *et al.*, 2011) fission cross sections for n + Bi (symbols) to results from the unmodified CEM03.03 (green solid lines) and from CEM03.03F (red dashed lines).

needed, the variable npreqtyp in the CEM03.0F input file can be set to 6 (which means to include only fragments up to ^{4}He) instead of 66 (up to ^{28}Mg). A similar flag could be created to control the use of the extended coalescence model. Such features would eliminate most of the computational-time increase of CEM03.03F, for simulations unconcerned about heavy-fragment production. The upgraded NASA-Kalbach inverse-cross-section model and the revised γ_j model would remain implemented, but these require very little extra computational effort. A similar method of turning off the computationally-expensive extensions has been implemented within MCNP6, as discussed in the next Section.

F. Conclusions

The goal of producing energetic light fragments with a new version of CEM03.03, called CEM03.03F, has been successfully accomplished by extending the modified exciton model and the coalescence model. We further improved the results by upgrading the inverse-cross-section model in the preequilibrium stage to the NASA-Kalbach hybrid model. We also created a model for γ_j which affords greater flexibility and predictability.

CEM03.03F has been tested on proton-, neutron-, gamma-, and pion-induced reactions and in general leads to better or at least no worse results compared to the standard CEM03.03. In the case of heavy-cluster production, CEM03.03F generally far outperforms CEM03.03. The increase in computation time for CEM03.03F is reasonable (about one-third longer).

Goals for future work include upgrading the evaporation model used in CEM, which includes implementing the NASA-Kalbach inverse cross sections into the evaporation stage, extending the coalescence model further to include fragments with $A \geq 8$,and finally, after implementing these changes, to refit the fission level-density parameters, which will need to be modified, after these proposed changes.

VIII. IMPLEMENTATION INTO MCNP6

MCNP6 (Monte Carlo N-Particle transport code, version 6) (Goorley *et al.*, 2012) is a general-purpose, continuous-energy, generalized-geometry, time-dependent, Monte-Carlo radiation-transport code designed to track many particle types over broad ranges of energies. Application areas include, but are not limited to:

- Radiation protection and dosimetry;
- Radiation shielding;
- Radiography;
- Nuclear criticality safety;
- Detector design and analysis;
- Nuclear oil well logging;
- Fission and fusion reactor design;
- Nuclear facility econtamination and decommissioning;
- Design of accelerator spallation targets, particularly for neutron scattering facilities;
- Investigations for accelerator isotope production and destruction programs, including the transmutation of nuclear waste;
- Research into accelerator-driven energy sources;
- Activation of accelerator components and surrounding groundwater and air;
- High-energy dosimetry and neutron detection;
- Medical physics, especially ion, proton, and neutron therapy;
- Investigations of cosmic-ray backgrounds and shielding for high-altitude aircraft and spacecraft;
- Single-event upsets in semiconductors in spacecraft from cosmic rays or from the cosmic-ray-produced neutrons at the earth's surface;
- Analysis of cosmo-chemistry experiments, such as Mars Odyssey;
- Charged-particle propulsion concepts for spaceflight;
- Investigation of fully coupled neutron and charged-particle transport for lower-energy applications;
- Transmutation, activation, and burnup in reactor and other systems;
- Nuclear safeguards;
- Nuclear material detection;
- Design of neutrino experiments.

The culmination of this work is the implementation of the heavy-fragment upgrades to CEM into the MCNP6 transport code.

A. Expanded GENXS Option

The GENXS option allows for various cross sections to be tallied in MCNP6 (see Ref. (Prael, 2011) for details). Previously, production cross sections (i.e., double differential cross sections) were only available for fragments up to ^{4}He. Thus, a necessary first step in implementing the improved CEM03.03F into MCNP6 involves extending the ability to output production cross sections of heavy clusters. This GENXS upgrade accomplishes this and includes the ability to tally and output double differential cross sections for any heavy ion (with a valid ZAID). It also includes the ability to tally and output angle-integrated cross sections as a function of emitted fragment energy and energy-integrated cross sections as a function of emitted angle, for any ZAID.

To output and tally heavy ions in GENXS, simply enter the isotope's ZAID ($1000 * Z + A$) on the 'particle types tracked' line in the GENXS input file. If more than one heavy ion is to be tracked, separate each ZAID with a space. Up to 50 heavy ions can be tracked per simulation. More details on using this GENXS extension can be found in Ref. (Kerby *et al.*, 2015).

Fig. 36 displays an excerpt of the double differential cross section portion of the MCNP6 output file for ^{6}Li (ZAID=3006). Now, instead of showing "mu max" for the emission direction, GENXS now outputs the angles in "degrees+/-spread". We believe this will be easier and more intuitive for users, and help avoid user error and misinterpretation. Angle-integrated spectra and energy-integrated spectra are also calculated, as well as the total angle- and energy-integrated production cross sections.

We tested this GENXS extension in MCNP6 across numerous reactions and find consistency with CEM03.03; for details see Refs. (Kerby, 2015b; Kerby *et al.*, 2015). The MCTAL tallies have also been updated so that angle-integrated cross section spectra of specified heavy ions may be viewed from within mcplot, similar to how specified nucleons and light fragments were viewed in the previous version of GENXS.

3006 production cross section

E(MeV)	167.5deg+/-12.5	150.0deg+/- 5.0	130.0deg+/-15.0	110.0deg+/- 5.0	100.0deg+/- 5.0	90.0deg+/- 5.0	70.0deg+/-15.0
5.000000E+00	0.000E+00 0.000	0.000E+00 0.000	0.000E+00 0.000	0.000E+00 0.000	0.000E+00 0.000	0.000E+00 0.000	0.000E+00 0.000
1.000000E+01	8.301E-06 0.040	9.325E-06 0.039	1.165E-05 0.016	1.442E-05 0.023	1.529E-05 0.022	1.614E-05 0.021	1.803E-05 0.012
1.500000E+01	2.598E-06 0.072	2.822E-06 0.071	3.920E-06 0.028	6.006E-06 0.036	7.040E-06 0.032	8.988E-06 0.028	1.277E-05 0.014
2.000000E+01	6.929E-07 0.139	6.303E-07 0.151	1.011E-06 0.056	1.791E-06 0.065	2.538E-06 0.054	3.180E-06 0.047	5.867E-06 0.021
2.500000E+01	1.999E-07 0.258	1.146E-07 0.354	2.865E-07 0.105	5.259E-07 0.120	6.763E-07 0.104	1.110E-06 0.080	2.287E-06 0.034
3.000000E+01	9.327E-08 0.378	2.865E-08 0.707	1.039E-07 0.174	1.601E-07 0.218	3.200E-07 0.151	3.724E-07 0.139	7.161E-07 0.060
3.500000E+01	0.000E+00 0.000	1.432E-08 1.000	3.463E-08 0.302	3.049E-08 0.500	6.545E-08 0.333	1.003E-07 0.267	2.490E-07 0.102
4.000000E+01	1.332E-08 1.000	0.000E+00 0.000	9.445E-09 0.577	7.622E-09 1.000	1.454E-08 0.707	2.865E-08 0.500	6.673E-08 0.196
4.500000E+01	0.000E+00 0.000	0.000E+00 0.000	0.000E+00 0.000	0.000E+00 0.000	0.000E+00 0.000	7.162E-09 1.000	2.823E-08 0.302
5.000000E+01	0.000E+00 0.000	0.000E+00 0.000	6.297E-09 0.707	0.000E+00 0.000	0.000E+00 0.000	7.162E-09 1.000	1.283E-08 0.447
5.500000E+01	0.000E+00 0.000	0.000E+00 0.000	0.000E+00 0.000	0.000E+00 0.000	0.000E+00 0.000	0.000E+00 0.000	2.567E-09 1.000
6.000000E+01	0.000E+00 0.000	0.000E+00 0.000	0.000E+00 0.000	0.000E+00 0.000	0.000E+00 0.000	0.000E+00 0.000	2.567E-09 1.000
6.500000E+01	0.000E+00 0.000	0.000E+00 0.000	0.000E+00 0.000	0.000E+00 0.000	0.000E+00 0.000	0.000E+00 0.000	2.567E-09 1.000

E(MeV)	50.0deg+/- 5.0	35.0deg+/-10.0	20.0deg+/- 5.0	7.5deg+/- 7.5
5.000000E+00	0.000E+00 0.000	0.000E+00 0.000	0.000E+00 0.000	0.000E+00 0.000
1.000000E+01	1.901E-05 0.022	1.826E-05 0.019	1.853E-05 0.034	1.825E-05 0.045
1.500000E+01	1.709E-05 0.023	1.932E-05 0.018	2.134E-05 0.031	2.213E-05 0.041
2.000000E+01	8.508E-06 0.033	1.070E-05 0.024	1.315E-05 0.040	1.392E-05 0.051
2.500000E+01	3.852E-06 0.049	4.644E-06 0.037	6.638E-06 0.056	6.778E-06 0.074
3.000000E+01	1.683E-06 0.075	2.125E-06 0.054	2.680E-06 0.088	2.528E-06 0.120
3.500000E+01	4.862E-07 0.139	8.711E-07 0.085	1.026E-06 0.143	1.429E-06 0.160
4.000000E+01	2.618E-07 0.189	2.632E-07 0.154	5.863E-07 0.189	5.862E-07 0.250
4.500000E+01	6.544E-08 0.378	1.128E-07 0.236	6.282E-08 0.577	2.198E-07 0.408
5.000000E+01	2.805E-08 0.577	3.134E-08 0.447	6.282E-08 0.577	1.099E-07 0.577
5.500000E+01	0.000E+00 0.000	2.507E-08 0.500	0.000E+00 0.000	0.000E+00 0.000
6.000000E+01	0.000E+00 0.000	0.000E+00 0.000	0.000E+00 0.000	0.000E+00 0.000
6.500000E+01	0.000E+00 0.000	6.267E-09 1.000	0.000E+00 0.000	3.664E-08 1.000

E(MeV)	angle integrated	mu max	deg min	energy integrated
5.000000E+00	0.000E+00 0.000	-0.906307787037	155.0000000	5.949E-05 0.033
1.000000E+01	1.928E-04 0.006	-0.819152044289	145.0000000	6.467E-05 0.033
1.500000E+01	1.267E-04 0.008	-0.422618261741	115.0000000	8.510E-05 0.014
2.000000E+01	5.770E-05 0.012	-0.258819045103	105.0000000	1.147E-04 0.018
2.500000E+01	2.335E-05 0.018	-0.087155742748	95.0000000	1.297E-04 0.017
3.000000E+01	9.052E-06 0.029	0.087155742748	85.0000000	1.496E-04 0.015
3.500000E+01	3.255E-06 0.049	0.573576436351	55.0000000	2.002E-04 0.008
4.000000E+01	1.184E-06 0.081	0.707106781187	45.0000000	2.549E-04 0.014
4.500000E+01	3.608E-07 0.147	0.906307787037	25.0000000	2.818E-04 0.011
5.000000E+01	1.726E-07 0.213	0.965925826289	15.0000000	3.204E-04 0.018
5.500000E+01	3.922E-08 0.447	1.000000000000	0.0000000	3.299E-04 0.024
6.000000E+01	7.844E-09 1.000			
6.500000E+01	2.353E-08 0.577			

total 3006 production cross section = 2.073E-03 0.0045 yield = 5.28630E-03

FIG. 36 Double differential cross section output from MCNP6 using GENXS for the reaction 200 MeV p + ^{27}Al, with angle- and energy-integrated cross sections also calculated.

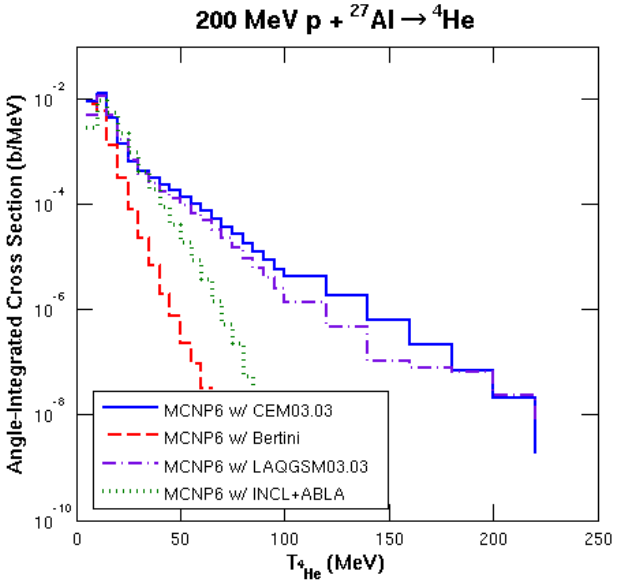

FIG. 37 Comparison of emitted ^{4}He angle-integrated fragment spectra for the reaction 200 MeV p + ^{27}Al, calculated by MCNP6 with CEM03.03 (blue solid lines), with Bertini (red dashed lines), with LAQGSM03.03 (purple dash-dotted lines), and with INCL-ABLA (green dotted lines), all run with the GENXS extension for heavy ions discussed in the text.

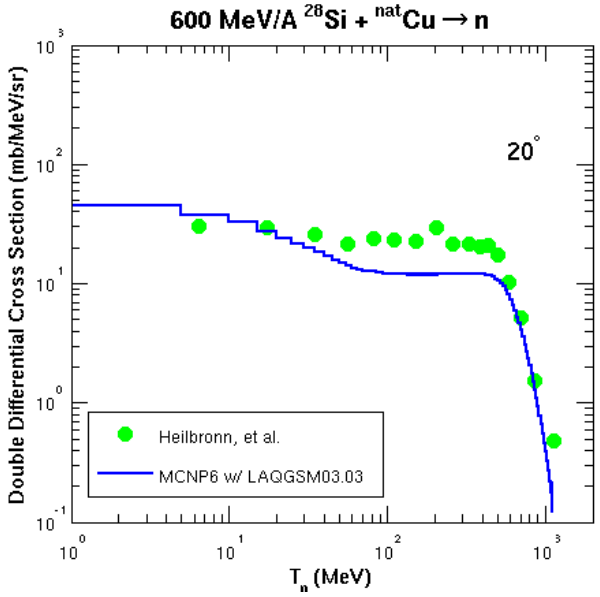

FIG. 38 Comparison of emitted neutron double differential spectra for the reaction 600 MeV/A ^{28}Si + ^{nat}Cu, at an emission angle of 20°, measured by Heilbronn, et al. (green points), to those calculated by MCNP6 using the LAQGSM03.03 event generator using the GENXS heavy-ion extension (blue solid line).

1. Further Tests

We additionally tested this GENXS heavy-ion extension with several different event generators (CEM03.03, Bertini+Dresner+RAL, INCL+ABLA, and LAQGSM03.03). Results of this test appear in Fig. 37. Results are as we expect.

We also tested MCNP6 with the GENXS heavy-ion extension on a nucleus-induced reaction using the LAQGSM03.03 event generator. Results of this simulation compared with experimental data are seen in Fig. 38. Similar results are found in Example 6.5 of the MPI Testing Primer (Mashnik, 2013).

B. MCNP6 with the Light-Fragment Upgrades

The CEM03.03F LF upgrades discussed in this work were implemented into a working test version of MCNP6, which we call MCNP6-F. Two of the upgrades are always implemented in this model: the upgraded NASA-Kalbach inverse cross sections in the preequilibruim stage, and the new energy-dependent γ_j model. The other two upgrades (extension of preequilibrium emission to ^{28}Mg, and the extension of the coalescence model to ^{7}Be), both of which increase computation time, may be turned off if desired. A variable, called npreqtyp, was created to specify the number of preequilibrium particles considered for emission. It is now the twelfth option on the LCA Card. Its maximum (and default) value is 66, similar to the nevtype variable used for the evaporation stage. See Table I for a list of the 66 particles considered in the preequilibrium stage. In the old model, 6 preequilibrium particles were considered, and therefore a value of npreqtyp=6 turns off both the preequilibrium and coalescence extensions. The extended coalescence model is implemented for values of npreqtyp>6. MCNP6-F also includes the GENXS extension.

Basic testing and verification of MCNP6-F has been completed with the results being presented in the following section. In addition, MPI testing has been completed. Upon further testing, we anticipate these heavy-ion upgrades and the GENXS extension will be included in the next release of MCNP6.

1. Results

Double differential cross section spectra for several reactions are plotted in this section. Figs. 39–42 compare experimental data with results from CEM03.03F (blue solid lines), MCNP6-F with npreqtyp=66 (red dashed lines), and MCNP6 with the GENXS extension only (purple dash-dotted lines). MCNP6 with the GENXS extension only does not contain any of the four light-fragment upgrades discussed in this work (but contains the GENXS extension so that we can output double differential cross sections for light fragments). The new MCNP6-F with the light-fragment upgrades, in general, gives improved results compared to the unmodified

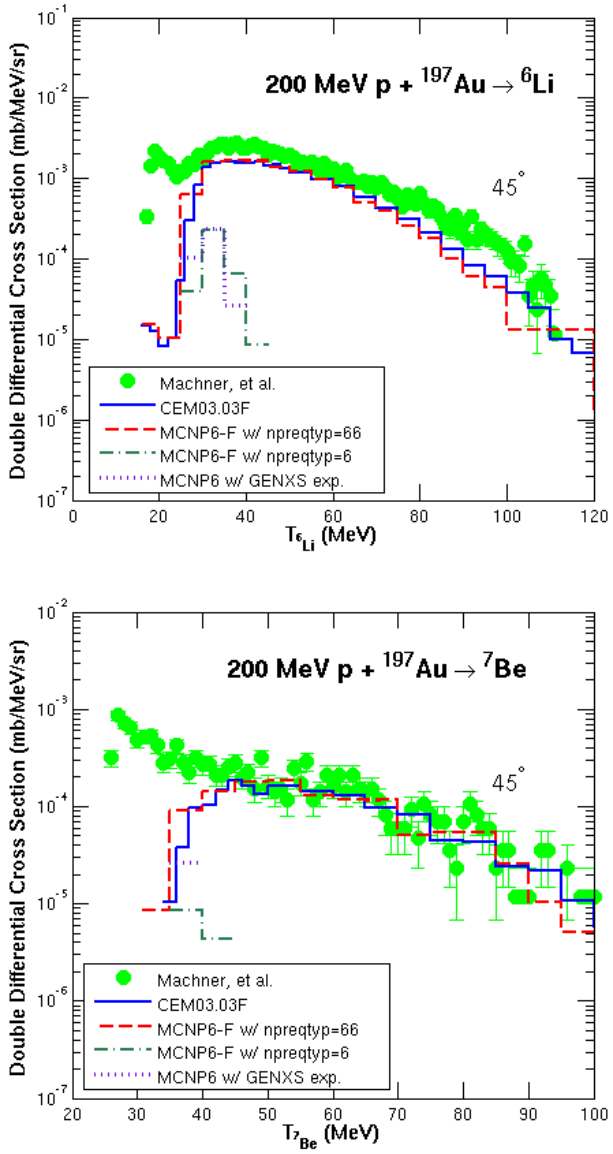

FIG. 39 Comparison of experimental data for 200 MeV p + ^{197}Au → ^{6}Li,^{7}Be at 45°, measured by Machner, et al. (Machner *et al.*, 2006) (green circles) to calculations from CEM03.03F (blue solid lines), MCNP6-F with npreqtyp=66 (red dashed lines), MCNP6-F with npreqtyp=6 (green dash-dotted lines), and MCNP6 with the GENXS extension only (purple dotted lines).

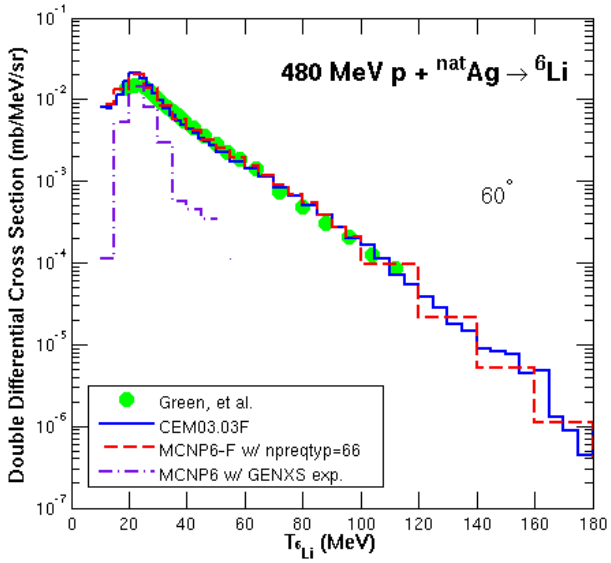

FIG. 40 Comparison of experimental data for 480 MeV p + ^{nat}Ag → ^{6}Li at 60°, measured by Green, et al. (Green *et al.*, 1984) (green circles) to calculated results from CEM03.03F (blue solid lines), MCNP6-F with npreqtyp=66 (red dashed lines), and MCNP6 with the GENXS extension only (purple dash-dotted lines).

MCNP6, most especially for heavy-cluster spectra.

Fig. 39 displays the results for 200 MeV p + ^{197}Au → ^{6}Li,^{7}Be at 45°, compared to experimental data by Machner, et al. (Machner *et al.*, 2006). These figures also contain spectra from MCNP6-F with npreqtyp=6; these results should be similar to MCNP6 with the GENXS extension only, as the only difference between the two is that MCNP6-F contains the improved inverse cross sections and the γ_j Model. These two figures show not only dramatically improved heavy-cluster production by MCNP6-F at high energies, but also improved production at relatively low energies around the preequilibrium peak. We believe this is due to the heavy target (gold) and therefore an increased ability to produce these low-energy heavy clusters from both the extended coalescence model and the extended preequilibrium model.

Fig. 40 shows the results for 480 MeV p + ^{nat}Ag → ^{6}Li at 60°, compared to experimental data measured by Green, et al. (Green *et al.*, 1984). MCNP6-F produces significantly improved results and matches the data reasonably well.

Fig. 41 illustrates the results for 1200 MeV p + ^{197}Au → ^{6}Li,^{7}Be at 20° with experimental data by Budzanowski, et al. (Budzanowski *et al.*, 2008). These figures provide additional evidence that MCNP6-F demonstrates increased production of heavy clusters in the mid- and high-energy regions compared to the original MCNP6. These reactions also highlight the need to improve the evaporation model. The peaks of the spectra are too high; these peaks are largely produced by evaporation. We hope to do this work in the future. We note a recent paper by A. Boudard et al. (Boudard *et al.*, 2013), which obtained similar results for heavy-cluster spectra from this reaction using INCL4.6 + ABLA07.

Fig. 42 demonstrates the results for 2500 MeV p + ^{nat}Ni → t, ^{7}Li at 100°, compared to experimental data measured by Budzanowski, et al. (Budzanowski *et al.*, 2010). The triton spectra again illustrate that MCNP6-F achieves increased production of heavy clusters without

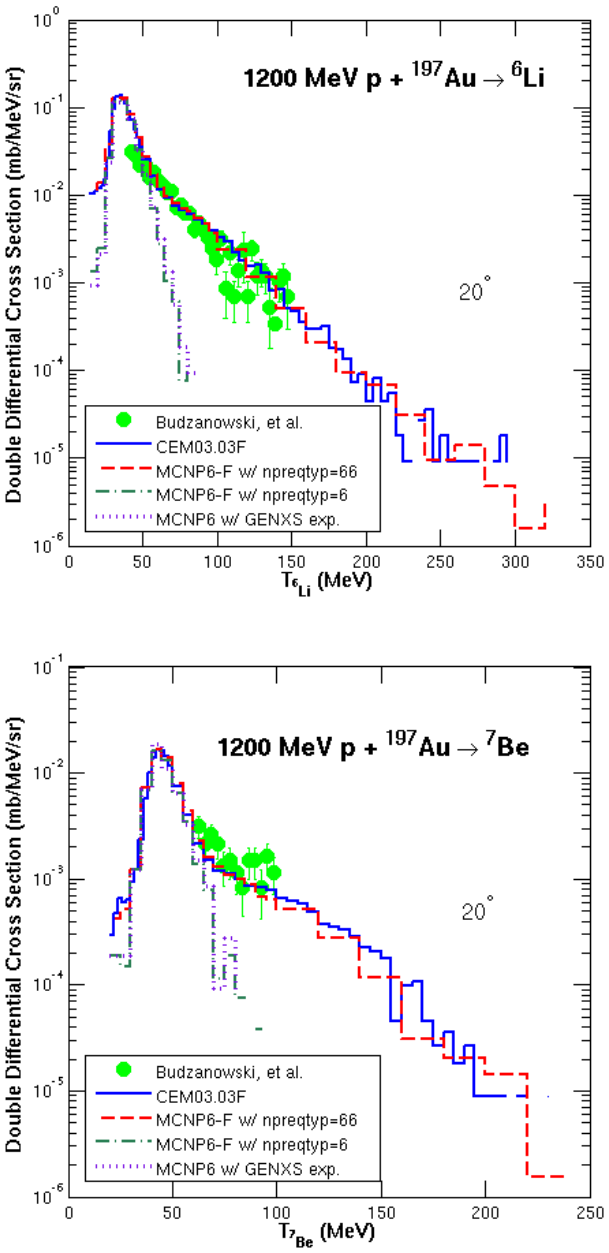

FIG. 41 Comparison of experimental data on 1200 MeV p + ^{197}Au → ^{6}Li,^{7}Be at 20°, measured by Budzanowski, et al. (Budzanowski *et al.*, 2008) (green circles) to calculated results by CEM03.03F (blue solid lines), MCNP6-F with npreqtyp=66 (red dashed lines), MCNP6-F with npreqtyp=6 (green dash-dotted lines), and MCNP6 with the GENXS extension only (purple dotted lines).

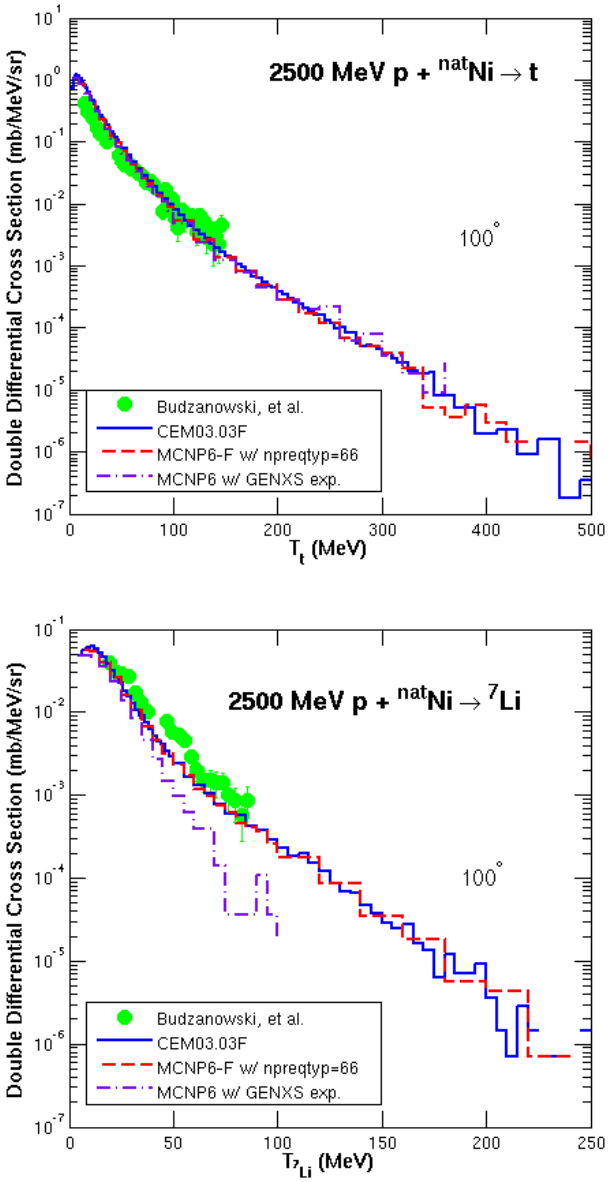

FIG. 42 Comparison of experimental data for 2500 MeV p + ^{nat}Ni → t,^{7}Li at 100°, measured by Budzanowski, et al. (Budzanowski *et al.*, 2010) (green circles) to calculated results from CEM03.03F (blue solid lines), MCNP6-F with npreqtyp=66 (red dashed lines), and MCNP6 with the GENXS extension only (purple dash-dotted lines).

destroying the established spectra of nucleons and light fragments with $A < 5$.

C. Summary

The goal of producing energetic light fragments in the CEM model, which has led to an improved model, CEM03.03F, has been successfully accomplished, by extending the modified exciton model and the coalescence model. Further improvment resulted from upgrading the inverse-cross-section model in the preequilibrium stage to the NASA-Kalbach hybrid model. We also created an empirical analytical model for γ_j which affords greater

flexibility and predictability. Finally, while energetic LF can be produced with Fermi breakup, especially for light targets, we did not find sufficient evidence to justify changing the Fermi breakup cut-off, A_{Fermi}, and have thus left it at $A_{Fermi} = 12$.

We have extensively tested CEM03.03F on proton-, neutron-, gamma-, and pion-induced reactions and have found, in general, better or no worse results compared to the standard CEM03.03. In the case of heavy-cluster production, the results of CEM03.03F generally far outperform those from CEM03.03. The computation time for CEM03.03F is about one-third longer than for CEM03.03.

We have also begun to extend the coalescence model in LAQGSM, and to incorporate the upgrades made to the MEM into LAQGSM as well. Preliminary results are promising.

In addition, we investigated the validity and performance of MCNP6, CEM, and LAQGSM in simulating fragmentation reactions at intermediate energies. We find that the fixed default versions of CEM03.03 and LAQGSM03.03 in MCNP6 provide reasonably good predictions for all reactions tested.

Finally, we have accomplished the goal of improving predictions of MCNP6 for the production of energetic heavy clusters. We have successfully implemented the following heavy-ion upgrades from CEM03.03F into a working version of MCNP6:

- Expanded preequilibrium emission to ^{28}Mg;
- Upgraded preequilibrium inverse cross sections to the NASA-Kalbach model;
- Extended the coalescence model to ^{7}Be;
- Developed a new, energy-dependent, γ_j model.

To allow analysis of heavier LF production, we extended the GENXS option in MCNP6 to include production cross sections for all isotopes. Preliminary results of the test of MCNP6-F are promising. Upon further testing of MCNP6-F, we anticipate the LF upgrades and GENXS extension will be included in the next release of MCNP6.

Goals for future work include upgrading the evaporation model used in CEM and LAQGSM, which includes implementing the NASA-Kalbach inverse cross sections into the evaporation stage, completing the LAQGSM coalescence model extension, and finishing integration of the preequilibrium upgrades from CEM03.03F into LAQGSM.

REFERENCES

Amelin, N., K. Gudima, and V. Toneev (1990), Soviet Journal of Nuclear Physics **51**, 327

Andersen, V., F. Ballarini, G. Battistoni, M. Campanella, M. Carboni, F. Cerutti, A. Empl, A. Fassò, A. Ferrari, E. Gadioli, M. Garzelli, K. Lee, A. Ottolenghi, M. Pellicioni, L. Pinsky, J. Ranft, S. Roesler, P. Sala, and T. Wilson (2004), Advances in Space Research **34**, 1302

Atchison, F. (2007), Nuclear Instruments and Methods in Physics Research B **259**, 909

Baktybaev, M., A. Duisebaev, B. Duisebaev, K. Ismailov, M. Itkis, K. Kadyrzhanov, R. Kalpakchieva, I. Kuznetsov, K. Kuterbekov, I. Kukhtina, S. Lukyanov, A. Mukhamedzhan, Y. Penionzhkevich, B. Sadykov, Y. Sobolev, and V. Ugryumov (2003), Physics of Atomic Nuclei **66**, 1615

Barashenkov, V. (1993), "Cross sections of interaction of particles and nuclei with nuclei (in Russian)," JINR, Dubna, Russia, tabulated data available at: www.nea.fr/html/dbdata/bara.html

Barashenkov, V., W. Gudowski, and A. Polanski (1990), "Integral high-energy nucleon-nucleus cross sections for mathematical experiments with electronuclear facilities," JINR Communication E2-99-207, JINR, Dubna, Russia, private communications from Drs. Alexander Polanski and Dick Prael to Stepan Mashnik

Barashenkov, V., A. Il'inov, and N. S. V. Toneev (1973), Uspekhi Fiziches-kikh Nauk **109**, 91

Barashenkov, V., and A. Polanski (1994), "Electronic guide for nuclear cross-sections," Joint Institute for Nuclear Research Communication E2-94-417, JINR, Dubna, Russia

Barashenkov, V., and V. Toneev (1972), Atomizdat

Beghian, L., F. Hofman, and S. Wilensky (1966), Neutron Cross-Section Technical Conference, Washington **2**, 726

Benecke, J., T. Chou, C. Yang, and E. Yen (1969), Physical Review **188**, 2159

Benlliure, J., P. Armbruster, M. Bernas, A. Boudard, J. Dufour, T. Enqvist, R. Legrain, S. Leray, B. Mustapha, F. Rejmund, K.-H. Schmidt, C. Stéphan, L. Tasaan-Got, and C. Volant (2001), Nuclear Physics A **683**, 513

Bernas, M., P. Armstrong, J. Benlliure, A. Boudard, E. Casarejos, S. Czajkowski, T. Enqvist, R. Legrain, S. Leray, B. Mustapha, P. Napolitani, J. Pereira, F. Rejmund, M.-V. Ricciardi, K.-H. Schmidt, C. Stéphan, J. Taieb, L. Tissan-Got, and C. Volant (2003), Nuclear Physics A **725**, 213, nucl-ex/0304003

Bertini, H. (1963), Physical Review **131**, 1801

Bertini, H. (1969), Physical Review **188**, 1711

Betak, E. (1976), Acta Physica Slovaka **26**, 21

Beyster, J., R. Henkel, R. Nobles, and J. Kister (1955), Physical Review **98**, 1216

Beyster, J., M. Walt, and E. Salmi (1956), Physical Review **104**, 1319

Blideanu, V., F. Lecolley, J. Lecolley, T. Lefort, N. Marie, A. Ataç and G. Ban, B. Bergenwall, J. Blomgren, S. Dangtip, K. Elmgren, P. Eudes, Y. Foucher, A. Guertin, F. Haddad, A. Hildebrand, C. Johansson, O. Jonsson, M. Kerveno, T. Kirchner, J. Klug, C. L. Brun, C. Lebrun, M. Louvel, P. Nadel-Turonski, L. Nilsson, N. Olsson, S. Pomp, A. Prokofiev, P.-U. Renberg, G. Rivière, I. Slypen, L. Stuttgé, U. Tippawan, and M. Österlund (2004), Physical Review C **70**, 014607

Bondorf, J., A. Botvina, A. Iljinov, I. Mishustin, and K. Sneppen (1995), Physics Reports **257**, 133

Bonner, T., and J. Slattery (1959), Physical Review **113**, 1088

Borning, A. (1987), "Computer system reliability and nuclear war," Foundation for Global Community

Boudard, A., J. Cugnon, J.-C. David, S. Leray, and D. Mancusi (2013), Physical Review C **87**, 014606

Boudard, A., J. Cugnon, S. Leray, and C. Volant (2002), Physical Review C **66**, 044615

Bubak, A., A. Budzanowski, D. Filges, F. Goldenbaum, A. Heczko, H. Hodde, L. Jarczyk, B. Kamys, M. Kistryn, S. Kistryn, S. Kliczewski, A. Kowalczyk, E. Kozik, P. Kulessa, H. Machner, A. Magiera, W. Migda, N. Paul, B. Piskor-Ignatowicz, M. Puchaa, K. Pysz, Z. Rudy, R. Siudak, M. Wojciechowski, and P. Wstner (2007), Physical Review C **76**, 014618

Budzanowski, A., M. Fidelus, D. Filges, F. Goldenbaum, H. Hodde, L. Jarczyk, B. Kamys, M. Kistryn, S. Kistryn, S. Kliczewski, A. Kowalczyk, E. Kozik, P. Kulessa, H. Machner, A. Magiera, B. Piskor-Ignatowicz, K. Pysz, Z. Rudy, R. Siudak, and M. Wojciechowski (2008), Physical Review C **78**, 024603

Budzanowski, A., M. Fidelus, D. Filges, F. Goldenbaum, H. Hodde, L. Jarczyk, B. Kamys, M. Kistryn, S. Kistryn, S. Kliczewski, A. Kowalczyk, E. Kozik, P. Kulessa, H. Machner, A. Magiera, B. Piskor-Ignatowicz, K. Pysz, Z. Rudy, R. Siudak, and M. Wojciechowski (2010), Physical Review C **82**, 034605

Carlson, R. (1996), Atomic Data and Nuclear Data Tables **63**, 93

Charity, R., L. Sobotka, J. Cibor, K. Hagel, M. Murray, J. B. Natowitz, R. Wada, Y. El Masri, D. Fabris, G. Nebbia, G. Viesti, M. Cinausero, E. Fioretto, G. Prete, A. Wagner, and H. Xu (2001), Physical Review C **63**, 024611, http://www.chemistry.wustl.edu/ rc/gemini/

Cline, C. (1972), Nuclear Physics A **193**, 417

Cooper, N. (2012), National Security Science , 12

Cugnon, J., A. Boudard, J.-C. David, A. Kelić-Heil, S. Leray, D. Mancusi, and M. V. Ricciardi (2011a), Journal of Physics: Conference Series **312**, 082019

Cugnon, J., A. Boudard, J.-C. David, A. Kelić-Heil, D. Mancusi, M. V. Ricciardi, and S. Leray (2011b), Proc. of the Tenth Int. Topical Meeting on Nuclear Applications of Accelerators (accApp), April 3-7, 2011, Knoxville, USA, 978-0-89448-706-4, 2012

Cugnon, J., C. Volant, and S. Vuillier (1997), Nuclear Physics A **620**, 475

David, J.-C. (2015), European Physical Journal A **51**, 157, arXiv:1505.0382

David, J.-C., A. Boudard, J. Cugnon, S. Leray, and D. Mancusi (2011), Rapport interne IRFU-11-249, ANDES (Accurate Nuclear Data for nuclear Energy Sustainability) EURATOM FP7 grant agreement No. 249671, Task T4.1 - Deliverable D4.1, FP7-ANDES - WP 4 Http://www-ist.cea.fr/publicea/exl-php/cadcgp.php

Degtjarev, J. (1966), Journal Nuclear Energy, Part A+B (Reactor Sci. Techn.) **20**, 818

Dostrovsky, I., Z. Fraenkel, and G. Friedlander (1959), Physical Review **116**, 683

El-Nagdy, M., A. Abdelsalam, Z. Abou-Moussa, and B. Badawy (2013), Canadian Journal of Physics **91**, 737

Ericson, T. (1960), Advances in Physics **9**, 425

F. Williams Jr., (1970), Physics Letters B **31**, 184

F. Williams Jr., (1971), Nuclear Physics A **161**, 231

Fermi, E. (1950), Progress of Theoretical Physics **5**, 570

Fidelus, M. (2010), "Model description of proton induced fragmentation of atomic nuclei," Ph.D. Thesis, Cracow

Filges, D., and F. Goldenbaum (2009), *Handbook of Spallation Research: Theory, Experiments and Applications* (WILEY-VCH Verlag GmbH & Co.) ISBN: 978-3-527-40714-9

Fomichev, A., V.Dushin, S. Soloviev, A. Fomichev, and S. Mashnik (2005), "Fission cross sections for ^{240}Pu, ^{243}Am, ^{209}Bi, ^{nat}W induced by neutrons up to 500 MeV measured relative to ^{235}U," LANL Report LA-UR-05-1533; V. G. Khlopin Radium Institute Preprint RI-262, St. Petersburg, Russia

Franz, J., P. Koncz, E. Roessle, C. Sauerwein, H. Schmitt, K. Schmoll, J. Eroe, Z. Fodor, J. Kecskemeti, Z. Kovacs, and Z. Seres (1990), Nuclear Physics A **510**, 774

Furihata, S. (2000), Nuclear Instruments and Methods in Physics Research B **171**, 252

Furihata, S. (2003), "Development of a generalized evaporation model and study of residual nuclei prodution," Ph.D. thesis, Tohoku University

Furihata, S., K. Nita, S. Meigo, Y. Ikeda, and F. Maekawa (2001), Japan Atomic Energy Research Institute

Golovchenko, A., J. Skvarč, N. Yasuda, M. Giacomelli, S. Tretyakova, R. Ilić, R. Bimbot, M. Toulemonde, and T. Murakami (2002), Physical Review C **66**, 014609

Goorley, T., M. James, T. Booth, F. Brown, J. Bull, L. J. Cox, J. Durkee, J. Elson, M. Fensin, R. A. Forster, J. Hendricks, H. G. Hughes, R. Johns, B. Kiedrowski, R. Martz, S. Mashnik, G. McKinney, D. Pelowitz, R. Prael, J. Sweezy, L. Waters, T. Wilcox, and T. Zukaitis (2012), Nuclear Technology **180**, 298

Green, R., R. Korteling, J. D'Auria, K. Jackson, and R. Helmer (1987), Physical Review C **35**, 1341

Green, R., R. Korteling, and K. Jackson (1984), Physical Review C **29**, 1806

Gudima, K., S. Mashnik, and A. Sierk (2001), "User manual for the code LAQGSM," LANL Report LA-UR-01-6804; http://lib-www.lanl.gov/lapubs/00818645.pdf

Gudima, K., S. Mashnik, and V. Toneev (1983), Nuclear Physics A **401**, 329

Gudima, K., G. Ososkov, and V. Toneev (1975), Yadernaya Fizika **21**, [Soviet Journal of Nuclear Physics 21 (1975) 139-143]

Hansen, D., A. Lühr, N. Sobolevsky, and N. Bassler (2012), Physics in Medicine & Biology **57**, 2393

Heilbronn, L., C. J. Zeitlin, Y. Iwata, T. Murakami, H. Iwase, T. Nakamura, T. Nunomiya, H. Sato, H. Yashima, R. M. Ronningen, and K. Ieki (2007), Nuclear Science and Engineering **157**, 142

Hultqvist, M., M. Lazzeroni, A. Botvina, I. Gudowska, N. Sobolevsky, and A. Brahme (2012), Physics in Medicine & Biology **57**, 4369

Iida, K., A. Kohama, and K. Oyamatsu (2007), Journal of the Physical Society of Japan **76**, 044201, arXiv:nucl-th/0601039

Ingemarsson, A., and M. Lantz (2003), Physical Review C **67**, 064605

Ingemarsson, A., J. Nyberg, P. Renberg, O. Sundberg, R. Carlson, A. Cox, A. Auce, R. Johansson, G. Tibell, D. Khoa, and R. Warner (2000), Nuclear Physics A **676**, 3

Jacak, B., G. Westfall, G. Crawley, D. Fox, C. Gelbke, and L. Harwood (1987), Physical Review C **35**, 1751

Junghans, A., M. de Jong, H.-G. Clerc, A. Ignatyuk, G. Kudyaev, and K.-H. Schmidt (1998), Nuclear Physics A **629**, 635

Kalbach, C. (1988), Physical Review C **37**, 2350

Kalbach, C. (1998), Journal of Physics G: Nuclear and Particle Physics **24**, 847

Kerby, L. (2015a), "An energy-dependent numerical model for

the condensation probability, γ_j," LANL Report, LA-UR-15-26648, submitted to Computer Physics Communications
Kerby, L. (2015b), "Precompound emission of energetic light fragments in spallation reactions," Ph. D. Thesis, University of Idaho
Kerby, L., and S. Mashnik (2014), "LANL fiscal year 2014 report," LANL Report LA-UR-14-27533, www.osti.gov/scitech/biblio/1162152
Kerby, L., and S. Mashnik (2015a), "An expanded coalescence model within the intranuclear cascade of CEM," LANL Report, LA-UR-15-20322
Kerby, L., and S. Mashnik (2015b), "A new model for the condensation probability, γ_j, in CEM," LANL Report, LA-UR-15-22370
Kerby, L., and S. Mashnik (2015c), Transactions **112**, 577
Kerby, L., and S. Mashnik (2015d), Nuclear Instruments and Methods B **356-357**, 135
Kerby, L., S. Mashnik, and J. Bull (2015), "MCNP6 GENXS option expansion to include fragment spectra of heavy ions," LANL Report, LA-UR-15-27858, summary accepted for presentation at PHYSOR 2016, Sun Valley, Idaho, USA, May 1-5, 2016
Kerby, L., S. Mashnik, and A. Sierk (2012), "Preliminary results of investigating precompound emission of light fragments in spallation reactions, summer 2012," LANL Report, LA-UR-12-24190
Kerby, L., S. Mashnik, and A. Sierk (2014a), Nuclear Data Sheets **118**, 316, arXiv:1303.4311
Kerby, L., S. Mashnik, and A. Tokuhiro (2014b), Transactions of the American Nuclear Society **110**, 465
Koi, T., and D. Wright (2013), "GEANT4 physics reference manual chapter 23 total reaction cross section in nucleusnucleus reactions," gentoo.osuosl.org/distfiles/PhysicsReferenceManual-4.10.0.pdf
Koning, A., S. Hilaire, and M. Duijvestijn (2004), "TALYS: Comprehensive nuclear reaction modeling," Proc. Int. Conf. on Nuclear Data for Sci. & Techn. (ND2004), September 26 - October 1, 2004, Santa Fe, NM, USA, edited by R. Haight, M. Chadwick, T. Kawano, and P. Talou, (AIP Conference Proceedings, Volume 769, Melville, New York, 2005), pp. 1154–1159
Konobeyev, A. Y., and U. Fischer (2014), "Status of evaluation of ^{9}Be DPA and Gas production cross-sections at neutron incident energies up to 200 MeV," presentation at the Fall 2014 Nuclear Data Week, 24-28 November 2014, NEA, Issy-le-Moulineaux, France; www.oecd-nea.org/dbdata/meetings/nov2014/
Konobeyev, A. Y., and Y. A. Korovin (1995), Kerntechnik **60**, 147
Kox, S., A. Gamp, C. Perrin, J. Arvieux, R. Bertholet, J. Bruandet, M. Buenerd, R. Cherkaoui, A. Cole, Y. El-Masri, N. Longequeue, J. Menet, F. Merchez, and J. Viano (1987), Physical Review C **35**, 1678
Krylov, A., M. Paraipan, N. Sobolevsky, G. Timoshenko, and V. Tret'yakov (2014), Physics of Particles and Nuclei Letters **11**, 549
Leray, S., A. Boudard, B. Braunn, J. Cugnon, J.-C. David, A. Leprince, and D. Mancusi (2014), Nuclear Data Sheets **118**, 312
Leray, S., J.-C. David, M. Khandaker, G. Mank, A. Mengoni, N. Otsuka, D. Filges, F. Gallmeier, A. Konobeyev, and R. Michel (2011), Journal of the Korean Physical Society **59** (2), 791
Lühr, A., D. Hansen, R. Teiwes, N. Sobolevsky, O. Jäkel, and N. Bassler (2012), Physics in Medicine & Biology **57**, 5169
Machner, H., D. Aschman, K. Baruth-Ram, J. Carter, A. Cowley, F. Goldenbaum, B. Nangu, J. Pilcher, E. Sideras-Haddad, J. Sellschop, F. Smit, B. Spoelstra, and D. Steyn (2006), Physical Review C **73**, 044606
MacReady, N. (2012), Journal of the National Cancer Institute **104** (9)
Mancusi, D., A. Boudard, J. Cugnon, J.-C. David, P. Kaitaniemi, and S. Leray (2014), Physical Review C **90**, 054602, arXiv:1407.7755v2
Mantzouranis, G., H. Weidenmüller, and D. Agassi (1976), Z. Phys. A **276**, 145
Mashnik, S. (2011a), "Validation and verification of MCNP6 against high-energy experimental data and calculations by other codes. I. The CEM testing primer," LANL Report LA-UR-11-05129, mcnp.lanl.gov
Mashnik, S. (2011b), "Validation and verification of MCNP6 against high-energy experimental data and calculations by other codes. II. The LAQGSM testing primer," LANL Report LA-UR-11-05627, mcnp.lanl.gov
Mashnik, S. (2011c), European Physical Journal - Plus **126**, 49, arXiv:1011.4978
Mashnik, S. (2013), "Validation and verification of MCNP6 against high-energy experimental data and calculations by other codes. III. The MPI testing primer," LANL Report LA-UR-13-26944, mcnp.lanl.gov
Mashnik, S. (2014), "MCNP6 simulation of reactions of interest to FRIB, medical, and space applications," LANL Report LA-UR-14-25095, arXiv:1407.2832
Mashnik, S., K. Gudima, M. Baznat, A. Sierk, R. Prael, and N. Mokhov (2005a), "CEM03.01 and LAQGSM03.01 versions of the improved Cascade-Exciton Model (CEM) and Los Alamos Quark-Gluon String Model (LAQGSM) codes," LANL Report LA-UR-05-2686, mcnp.lanl.gov
Mashnik, S., K. Gudima, N. Mokhov, and R. Prael (2007a), "LAQGSM03.03 upgrade and its validation," LANL Report LA-UR-07-6198, arXiv:0709.1736
Mashnik, S., K. Gudima, R. Prael, A. Sierk, M. Baznat, and N. Mokhov (2008), "CEM03.03 and LAQGSM03.03 event generators for the MCNP6, MCNPX, and MARS15 transport codes," Joint ICTP-IAEA Advanced Workshop on Model Codes for Spallation Reactions. Trieste, Italy, LANL Report LA-UR-08-2931
Mashnik, S., K. Gudima, A. Sierk, M. Baznat, and N. Mokhov (2005b), "CEM03.01 user manual," LANL Report LA-UR-05-7321, mcnp.lanl.gov
Mashnik, S., and L. Kerby (2014), Nuclear Instruments and Methods in Physics Research A **764**, 59, arXiv:1404.7820
Mashnik, S., and L. Kerby (2015), "MCNP6 simulation of light and medium nuclei fragmentation at intermediate energies," LANL Report, LA-UR-15-22811, presented at the 12th International Conference on Nucleus-Nucleus Collisions (NN2015), June 21-26, 2015, Catania, Italy
Mashnik, S., L. Kerby, and K. Gudima (2015), "Fragmentation of light nuclei at intermediate energies simulated with MCNP6," LANL Report, LA-UR-15-27417, presented at the Fifth International Conference on Nuclear Fragmentation From Basic Research to Applications (NUFRA2015), 4 – 11 October 2015, Kemer (Antalya), Turkey
Mashnik, S., R. Prael, and K. Gudima (2007b), "Implementation of CEM03.01 into MCNP6 and its verification and validation running through MCNP6. CEM03.02 upgrade," LANL Research Note X-3-RN(U)-07-03, LANL Report LA-

UR-06-8652, mcnp.lanl.gov/
Mashnik, S., and A. Sierk (2012), "CEM03.03 user manual," LANL Report LA-UR-12-01364, mcnp.lanl.gov
Mashnik, S., A. Sierk, O. Bersillon, and T. Gabriel (1998a), Nuclear Instruments and Methods in Physics Research A **414**, 68, lANL Report LA-UR-97-97-2905, mcnp.lanl.gov
Mashnik, S., A. Sierk, and K. Gudima (2002), "Complex particle and light fragment emission in the Cascade-Exciton Model of nuclear reactions," LANL Report LA-UR-02-5185, invited talk presented at the 12th Biennial Topical Meeting of the Radiation Protection and Shielding Division (RPSD) of the American Nuclear Society, April 14-17, 2002, Santa Fe, NM; E-print: nucl-th/0208048
Mashnik, S., A. Sierk, and K. Gudima (2006), "Complex particle and light fragment emission in the Cascade-Exciton Model of nuclear reactions," LANL Report LA-UR-02-5185, and private communication with Dr. K. Gudima
Mashnik, S., A. Sierk, K. Gudima, and M. Baznat (2010), LANL Report LA-UR-10-00510, viewgraphs of the invited talk presented at the Second Advanced Workshop on Model Codes for Spallation Reactions, 8-11 February 2010, CEA-Saclay, France, http://nds121.iaea.org/alberto/mediawiki-1.6.10/index.php/Benchmark:2ndWorkProg
Mashnik, S., A. Sierk, K. V. Riper, and W. Wilson (1998b), "Production and validation of isotope production cross section libraries for neutrons and protons to 1.7 GeV," LANL Report LA-UR-98-6000, in: Proc. SARE-4, Knoxville, TN, September 13-16, 1998 (ORNL, 1999, pp. 151-162); arXiv:nucl-th/9812071; our T-16 Library "T-16 Lib" is updated permanently when new experimental data became available to us
Mashnik, S., and S. Smolyansky (1996), JINR Preprint E2-94-353, Dubna, 1994, 24 pp.; Proc. Int. Study Center in Nonlinear Science *Dynamics of Transport in Fluids, Plasmas and Charged Beams*, Villa Gualino, Torino, Italy, June-September, 1994, Eds. G. Maino and M. Ottaviani, Singapore: World Scientific, 1996, pp. 137–159
Mashnik, S., and V. Toneev (1974), JINR Communication **P4-8417**
Mazarakis, M., and W. Stephens (1973), Physical Review C **7**, 1280
Meier, M., W. Amian, C. Goulding, G. Morgan, and C. Moss (1992), Nuclear Science and Engineering **110**, 289
Meier, M., D. Clark, C. Goulding, J. McClelland, G. Morgan, C. Moss, and W. Mian (1989), Nuclear Science and Engineering **102**, 310
Mocko, M. (2006), "Rare isotope production," Ph. D. thesis, Michigan State University
Mocko, M., M. B. Tsang, L. Andronenko, M. Andronenko, F. Delaunay, M. Famiano, T. Ginter, V. Henzl, D. Henzlová, H. Hua, S. Lukyanov, W. G. Lynch, A. M. Rogers, M. Steiner, A. Stolz, O. Tarasov, M.-J. van Goethem, G. Verde, W. S. Wallace, and A. Zalessov (2006), Physical Review C **74**, 054612
Morrison, G. (1956), Physica (Utrecht) **22**, 1135
Nakamoto, T., K. Ishibashi, N. Matsufuji, N. Shigyo, K. Maehata, H. Arima, S. Meigo, H. Takada, S. Chiba, and M. Numajiri (1997), Journal of Nuclear Science and Technology **34**, 860
Nakamura, T., and L. Heilbronn (2006), *Handbook on Secondary Particle Production and Transport by High-Energy Heavy Ions* (World Scientific, Singapore)
Ogawa, T., T. Sato, S. Hashimoto, and K. Niita (2013), Nuclear Instruments and Methods in Physics Research A **723**, 36
Pasechnik, M. (1955), 1st UN Conf. Peaceful Uses Atomic Energy, Geneva **2**, 3
Polf, J., and K. Parodi (2015), Physics Today **68**, 28
Poze, K., and N. Glazkov (1956), Soviet Physics - JETP **3**, 745
Prael, R. (2011), "Tally edits for the MCNP6 GENXS option," LANL Report, LA-UR-11-02146
Prael, R., A. Ferrari, R. Tripathi, and A. Polanski (1998a), "Comparison of nucleon cross section parametrization methods for medium and high energies," LANL Report LA-UR-98-5813, proc. Forth Int. Workshop on Simulating Accelerator Radiation Environments (SARE-4), Hyatt Regency, Knoxville, TN, September 13-16, 1998, edited by Tony A. Gabriel, Oak Ridge National Laboratory (1999) pp. 171
Prael, R., A. Ferrari, R. Tripathi, and A. Polanski (1998b), "Plots supplemental to: Comparison of nucleon cross section parametrization methods for medium and high energies," LANL Report LA-UR-98-5843
Pshenichnov, I., A. Botvina, I. Mishustin, and W. Grainer (2010), Nuclear Instruments and Methods in Physics Research B **268**, 604
Rejmund, F., B. Mustapha, P. Armbruster, J. Benlliure, M. Bernas, A. Boudard, J. Dufour, T. Enqvist, R. Legrain, S. Leray, K.-H. Schmidt, C. Stéphan, J. Taieb, L. Tassan-Got, and C. Volant (2001), Nuclear Physics A **683**, 540
Ribansky, I., and P. Oblozinsky (1973), Physics Letters **45B**
Ribansky, I., P. Oblozinsky, and E. Betak (1973), Nuclear Physics A **205**, 545
Ronen, Y. (2012), Physica Scripta **86**, 065203
Sato, T., K. Niita, N. Matsuda, S. Hashimoto, Y. Iwamoto, S. Noda, T. Ogawa, H. Iwase, H. Nakashima, T. Fukahori, K. Okumura, T. Kai, S. Chiba, T. Furuta, and L. Sihver (2013), Journal of Nuclear Science and Technology **50**, 913
Schulz, H., G. Röpke and K. Gudima, and V. Toneev (1983), Physics Letters **134B**, 458
Schumacher, R., G. Adams, D. Ingham, J. Matthews, W. Sapp, R. Turley, R. Owens, and B. Roberts (1982), Physical Review C **25**, 2269
Shen, W., B. Wang, J. Feng, W. Zhan, Y. Zhu, and E. Feng (1989), Nuclear Physics A **491**, 130
Sihver, L., A. Kohama, K. Iida, S. Hashimoto, H. Iwase, and K. Niita (2014a), Nuclear Instruments and Methods in Physics Research B **334**, 34
Sihver, L., M. Lantz, and A. Kohama (2014b), Physical Review C **89**, 067602
Sihver, L., M. Lantz, T. Böhlen, A. Mairani, A. Cerutti, and A. Ferrari (2012a), "A comparison of total reaction cross section models used in FLUKA, GEANT4, and PHITS," IEEE Aerospace Conference, dOI: 10.1109/AERO.2012.6187014
Sihver, L., M. Lantz, M. Takechi, A. Kohama, A. Ferrari, F. Cerutti, and T. Sato (2012b), Advances in Space Research **49**, 812
Sihver, L., C. Tsao, R. Silberberg, T. Kanai, and A. Barghouty (1993), Physical Review C **47**, 1225
Singleterry, R. (2012), "Space travel and the long tent pole," presentation at LANL, San Ildefonso Auditory, and private communication from Dr. Singleterry, 2012
Souza, S., B. Carlson, R. Donangelo, W. Lynch, and M. Tsang (2013), Physical Review C **88**, 014607
Strizhak, V. (1957), Soviet Physics - JETP **4**, 769
Taieb, J., K.-H. Schmidt, L. Tissan-Got, P. Armstrong,

J. Benlliure, M. Bernas, A. Boudard, E. Casarejos, S. Czajkowski, T. Enqvist, R. Legrain, S. Leray, B. Mustapha, M. Pravikoff, F. Rejmund, C. Stéphan, C. Volant, and W. Wlazlo (2003), Nuclear Physics A **724**, 413

Takechi, M., M. Fukuda, M. Mihara, K. Tanaka, T. Chinda, T. Matsumasa, M. Nishimoto, R. Matsumiya, Y. Nakashima, H. Matsubara, K. Matsuta, T. Minamisono, T. Ohtsubo, T. Izumikawa, S. Momota, T. Suzuki, T. Yamaguchi, R. Koyama, W. Shinozaki, M. Takahashi, A. Takizawa, T. Matsuyama, S. Nakajima, K. Kobayashi, M. Hosoi, T. Suda, M. Sasaki, S. Sato, M. Kanazawa, and A. Kitagawa (2009), Physical Review C **79**, 061601

Tarrío, D., L. Tassan-Got, L. Audouin, B. Berthier, I. Duran, L. Ferrant, S. Isaev, C. L. Naour, C. Paradela, C. Stephan, D. Trubert, U. Abbondanno, G. Aerts, F. Álvarez-Velarde, S. Andriamonje, J. Andrzejewski, P. Assimakopoulos, G. Badurek, P. Baumann, F. F. Belloni, E. Berthoumieux, F. Calviño, M. Calviani, D. Cano-Ott, R. Capote, C. Carrapiço and A. Carrillo de Albornoz, P. Cennini, V. Chepel, E. Chiaveri, N. Colonna, G. Cortes, A. Couture, J. Cox, M. Dahlfors, S. David, I. Dillmann, R. Dolfini, C. Domingo-Pardo, W. Dridi, C. Eleftheriadis, M. Embid-Segura, A. Ferrari, R. Ferreira-Marques, L. Fitzpatrick, H. Fraisl-Koelbl, K. Fujii, W. Furman, I. Goncalves, E. González-Romero, A. Goverdovski, F. Gramegna, E. Griesmayer, C. Guerrero, F. Gunsing, B. Haas, R. Haight, M. Heil, A. Herrera-Martinez, M. Igashira, E. Jericha, Y. Kadi, F. Käppeler, D. Karadimos, D. Karamanis, M. Kerveno, V. Ketlerov, P. Koehler, V. Konovalov, E. Kossionides, M. Krtička, C. Lampoudis, H. Leeb, C. Lederer, A. Lindote, I. Lopes, R. Losito, M. Lozano, S. Lukic, J. Marganiec, L. Marques, S. Marrone, T. Martínez, C. Massimi, P. Mastinu, E. Mendoza, A. Mengoni, P. M. Milazzo, C. Moreau, M. Mosconi, F. Neves, H. Oberhummer, S. O'Brien, M. Oshima, J. Pancin, C. Papachristodoulou, C. Papadopoulos, N. Patronis, A. Pavlik, P. Pavlopoulos, L. Perrot, M. T. Pigni, R. Plag, A. Plompen, A. Plukis, A. Poch, J. Praena, C. Pretel, J. Quesada, T. Rauscher, R. Reifarth, M. Rosetti, C. Rubbia, G. Rudolf, P. Rullhusen, J. Salgado, C. Santos, L. Sarchiapone, R. Sarmento, I. Savvidis, G. Tagliente, J. L. Tain, L. Tavora, R. Terlizzi, G. Vannini, P. Vaz, A. Ventura, D. Villamarin, V. Vlachoudis, R. Vlastou, F. Voss, S. Walter, H. Wendler, M. Wiescher, and K. Wisshak (2011), Physical Review C **83**, 044620, n_TOF Collaboration

Taylor, H., and O. Lönsjö and T. Bonner (1955), Physical Review **100**, 174

Toneev, V., and K. Gudima (1983), Nuclear Physics **A400**, 173c

Townsend, L., and J. Wilson (1988), Physical Review C **37**, 892

Tripathi, R., F. Cucinotta, and J. Wilson (1996), Nuclear Instruments and Methods in Physics Research B **117**, 347

Tripathi, R., F. Cucinotta, and J. Wilson (1997), Nuclear Instruments and Methods in Physics Research B **129**, 11

Tripathi, R., F. Cucinotta, and J. Wilson (1999), Nuclear Instruments and Methods in Physics Research B **155**, 349

Tsang, H., G. Srinivasan, and N. Azziz (1990), Physical Review C **42**, 1598

Ugryumov, V., I.Kuznetsov, K.Basybekov, E. Bialkowski, A. Budzanowski, A. Duysebaev, B. Duysebaev, T. Zholdybaev, K. M. Ismailov, K. Kadyrzhanov, R. Kalpakchieva, A. Kugler, I. Kukhtina, V. Kushniruk, K. Kuterbekov, A. Mukhambetzhan, Y. Penionzhkevich, B. Sadykov, I. Skwirczynska, and Y. Sobolev (2004), Nuclear Physics A **734**, E53

Ugryumov, V., I. Kuznetsov, E. Bialkowski, A. Kugler, K. Kuterbekov, I. Kuhtina, V. Kushniruk, V. Lyapin, V. Maslov, Y. Penionzhkevich, Y. Sobolev, W. Trzaska, G. Tjurin, S. Khlebnikov, and S. Yamaletdinov (2005), Physics of Atomic Nuclei **68**, 16

Uozumi, Y., P. Evtoukhovitch, H. Fukuda, M. Imamura, H. Iwamoto, V. Kalinikov, W. Kallies, N. Khumutov, T. Kin, N. Koba, Y. Koba, N. Kuchinski, A. Moisenko, D. Mzavia, M. Nakano, V. Samoilov, Z. Tsamalaidze, G. Wakabayashia, and Y. Yamashita (2007), Nuclear Instruments and Metods in Physics Research A **571**, 743

Venables, W., D. Smith, and the R Core Team (2015), "An introduction to R. Notes on R: A programming environment for data analysis and graphics version 3.2.0," cran.r-project.org/doc/manuals/r-release/R-intro.pdf

Walt, M., and J. Beyster (1955), Physical Review **98**, 677

Warner, R., R. Patty, P. Voyles, A. Nadasen, F. Becchetti, J. Brown, H. Esbensen, A. Galonsky, J. Kolata, J. Kruse, M. Lee, R. Ronningen, P. Schwandt, J. von Schwarzenberg, B. Sherrill, K. Subotic, J. Wang, and P. Zecher (1996), Physical Review C **54**, 1700

Wellisch, H., and D. Axen (1996), Physical Review C **54**, 1329

Wu, J., and C. Chang (1978), Physical Review C **17**, 1540

Yariv, Y. (2008), "ISABEL — INC model for high-energy hadron-nucleus reactions," Proc. Joint ICTP-IAEA Advanced Workshop on Model Codes for Spallation Reactions, ICTP Trieste, Italy, 4-8 February 2008, iNDC(NDS)-0530 Distr. SC, IAEA, Vienna, August 2008, pp. 15–28

Yariv, Y., and Z. Frankel (1979), Physical Review C **20**, 2227

Yariv, Y., and Z. Frankel (1981), Physical Review C **24**, 488

Zeitlin, C., S. Guetersloh, L. Heilbronn, J. Miller, A. Fukumura, Y. Iwata, and T. Murakami (2007), Physical Review C **76**, 014911